INVESTIGATION OF BUCKLING, POST-BUCKLING BEHAVIOUR OF
VARIABLE STIFFNESS COMPOSITE PLATES

A THESIS SUBMITTED TO
THE GRADUATE SCHOOL OF NATURAL AND APPLIED SCIENCES
OF
MIDDLE EAST TECHNICAL UNIVERSITY

BY

UTKU KAAN CÖMERT

IN PARTIAL FULFILLMENT OF THE REQUIREMENTS
FOR
THE DEGREE OF MASTER OF SCIENCE
IN
MECHANICAL ENGINEERING

AUGUST 2022

Approval of the thesis:

INVESTIGATION OF BUCKLING, POST-BUCKLING BEHAVIOUR OF VARIABLE STIFFNESS COMPOSITE PLATES

submitted by **UTKU KAAN CÖMERT** in partial fulfillment of the requirements for the degree of **Master of Science** in **Mechanical Engineering, Middle East Technical University** by,

Prof. Dr. Halil Kalıpçılar
Dean, Graduate School of **Natural and Applied Sciences**   _____

Prof. Dr. M. A. Sahir Arıkan
Head of the Department, **Mechanical Engineering**   _____

Prof. Dr. Haluk Darendeliler
Supervisor, **Mechanical Engineering**   _____

Examining Committee Members:

Prof. Dr. Süha Oral
Mechanical Engineering, METU   _____

Prof. Dr. Haluk Darendeliler
Mechanical Engineering, METU   _____

Prof. Dr. Suat Kadıoğlu
Mechanical Engineering, METU   _____

Prof. Dr. Serkan Dağ
Mechanical Engineering, METU   _____

Prof. Dr. Can Çoğun
Mechatronics Engineering, Çankaya University   _____

Date: 31.08.2022

I hereby declare that all information in this document has been obtained and presented in accordance with academic rules and ethical conduct. I also declare that, as required by these rules and conduct, I have fully cited and referenced all material and results that are not original to this work.

Name Last name : Utku Kaan Cömert

Signature :

ABSTRACT

INVESTIGATION OF BUCKLING, POST-BUCKLING BEHAVIOUR OF VARIABLE STIFFNESS COMPOSITE PLATES

Cömert, Utku Kaan
Master of Science, Mechanical Engineering
Supervisor : Prof. Dr. Haluk Darendeliler

August 2022, 103 pages

In this thesis, buckling and post-buckling behaviour of variable stiffness (VS) composite plates are investigated. VS plates are designed by using quadratic Bezier curves to define fiber paths and a script is written for this purpose. Manufacturing limitations and defects are included into the simulations. In the analyses, Finite Element Method (FEM) is used to solve linear and nonlinear buckling with Hashin failure criterion. The plates constructed by using fiber paths with linear and nonlinear angle variation are simulated and the method is validated with tests from literature. Optimization cycles are run to optimize the buckling load of variable stiffness plates with a central hole for different plates. Post-buckling behaviour of plates with optimum angle configurations are investigated by considering progressive failure. It is observed that nonlinear angle variation can enlarge the design space and improve buckling load. For the first ply failure loads, an improvement is also observed for plates with quadratic Bezier curve fiber paths.

Keywords: Variable Stiffness, Bezier, Buckling, Post-buckling, Progressive Failure

ÖZ

DEĞİŞKEN KATILIKLI KOMPOZİT PLAKALARIN BURKULMA, BURKULMA SONRASI DAVRANIŞLARININ İNCELENMESİ

Cömert, Utku Kaan
Yüksek Lisans, Makina Mühendisliği
Tez Yöneticisi: Prof. Dr. Haluk Darendeliler

Ağustos 2022, 103 sayfa

Bu tezde, değişken katılıklı (DK) kompozit plakaların burkulma ve burkulma sonrası davranışları incelenmiştir. DK kompozit plakalar, fiber dizilimini tanımlamak için ikinci dereceden Bezier eğrileri kullanılarak tasarlanmış ve bu amaçla bir komut dosyası yazılmıştır. Üretim sınırlamaları ve kusurları simülasyonlara dahil edilmiştir. Analizlerde doğrusal ve doğrusal olmayan burkulmayı Hashin kırılma kriteri ile çözmek için Sonlu Elemanlar Yöntemi (FEM) kullanılmıştır. Merkezinde bir delik olan, doğrusal ve doğrusal olmayan açı değişimine sahip fiber dizilimleri kullanılarak oluşturulan plakalar simüle edilmiştir ve kullanılan çözüm yöntemi, literatürdeki testlerle doğrulanmıştır. Burkulma yükünü optimize etmek için optimizasyon döngüleri çalıştırılmıştır. Optimum açı konfigürasyonlarına sahip plakaların burkulma sonrası davranışları, ilerlemeli hasar dikkate alınarak incelenmiştir. Doğrusal olmayan açı değişiminin, tasarım alanını genişletebileceği ve burkulma yükünü artırabileceği gözlemlenmiştir. İkinci dereceden Bezier eğrisi fiber dizilimine sahip plakalar için de ilk tabaka kırılma yüklerinde iyileşme gözlemlenmiştir.

Anahtar Kelimeler: Değişken Katılık, Bezier, Burkulma, Burkulma Sonrası, Hasar

To My Beloved Family

ACKNOWLEDGMENTS

TABLE OF CONTENTS

LIST OF TABLES

TABLES

LIST OF FIGURES

FIGURES

LIST OF ABBREVIATIONS

ABBREVIATIONS

FRP : Fiber Reinforced Polymer

VS : Variable Stiffness

VSP : Variable Stiffness Plate

LAV : Linear Angle Variation

NAV : Nonlinear Angle Variation

AFP : Automated Fiber Placement

CDM : Continuous Damage Modeling

ATL : Automated Tape Layering

FSDT : First-order Shear Deformation Theory

CLPT : Classical Laminated Plate Theory

CS : Constant Stiffness

LIST OF SYMBOLS

SYMBOLS

θ	Fiber Orientation Angle
T_i	Fiber Orientation Angle
E_1	Longitudinal Elastic Modulus
E_2	Transverse Elastic Modulus
ν_{12}	Poisson's Raito
G_{12}	Shear Modulus
ε_1	Strain in Fiber Direction
ε_2	Strain in Direction Perpendicular to Fiber
γ_{12}	Shear Strain in Local Coordinate System
σ_1	Normal Stress in Fiber Direction
σ_2	Normal Stress in Direction Perpendicular to Fiber
τ_{12}	Shear Stress in Local Coordinate System
Q_{ij}	Reduced Stiffness Matrix
$\overline{Q_{ij}}$	Transformed Reduced Stiffness Matrix
T_{ij}	Transformation Matrix
u	Displacement in Fiber Direction
v	Displacement in Direction Perpendicular to Fiber
φ	Shifting Angle
N_{CP}	Performance Constant
R_c	Radius of Curvature
X_T	Tensile Strength in Longitudinal Direction
X_C	Compression Strength in Longitudinal Direction
Y_T	Tensile Strength in Longitudinal Direction
Y_C	Compression Strength in Longitudinal Direction
S	In-Plane Shear Strength

G_{1+} Energy Dissipation Rates per Unit Area for Fiber Tension

G_{1-} Energy Dissipation Rates per Unit Area for Fiber Compression

G_{2+} Energy Dissipation Rates per Unit Area for Matrix Tension

G_6 Energy Dissipation Rates per Unit Area for Matrix Compression

CHAPTER 1

INTRODUCTION

1.1   Background and Motivation

1.1.1   Composite Materials

Composites are defined as a combination of two or more materials in macroscopic scale [1]. The benefit of this combination is that the improved material properties can be achieved where combined materials cannot yield these properties individually. Because of their adjustable physical properties, composite materials are used widely in industry to expand the design space for application where commonly used materials cannot provide the desired properties. Compared to traditional materials such as steel, aluminum and titanium, composites provide lightweight solutions with improved strength properties. Enhanced stiffness and fatigue life can be obtained with composite material compared to its constituents [1].

Composite materials widely used in plate and shell forms which are susceptible to buckling. Under certain loads, composite parts could buckle due to unstable nature. Therefore, failure of these parts could be because of buckling and post-buckling behaviours. Investigation of buckling and postbuckling with progressive failure is one of the steps while designing these parts.

Composite materials can be classified under several categories. Different types of composite parts can be produced for different applications. In the scope of this thesis, fiber reinforced polymers (FRP) will be investigated.

1.1.2   Fiber Reinforced Polymers

Fiber reinforced polymers are built by placing fibers in a matrix. Long fibers provide a stiffer and stronger solution compared to the bulk form of the same material, depending on the form [1]. Reason for this result is that, in fibers, the crystals are aligned along the fiber axis when bulk material has more imperfections such as dislocations. Therefore, fibers are closer to a perfect structure than bulk form which leads to better mechanical properties [1]. Fibers can be made out of different materials such as e-glass, s-glass, carbon, beryllium, boron, graphite etc. However, fibers by themselves do not determine the characteristics of the composite since they are submerged into a matrix material. Matrix binds the fibers. It supports the fibers, conducts the stress between them. Metals, polymers, ceramics or carbon can be used as matrix material.

Implementation of FRPs into engineering solutions has increased in the last several decades because of their advantages over standard materials in several aspects such as structural properties and weight. In contrast to metals, fiber reinforced composite designs have wider range of options. This situation leads to lesser parts to be designed and manufactured which helps to reduce weight and cost. Even though the design potential is broader than standard materials, more conservative solutions are chosen due to uncertainties and lack of required technology [2].

1.2   Objective of Thesis

Most of the studies conducted on this concept cover the linear angle variation. However, using nonlinear angle variation could offer a wider design space by increasing the number of configurations with improved performance. Also, including the real-life concerns such as manufacturing limits and defects could improve the maturity of the design.

1.3   Scope of the Thesis

In this thesis study, buckling and post-buckling behaviours of variable stiffness plates with circular cut-out are investigated under end-shortening compression load by considering progressive failure. Manufacturing limits and defects are included into the analyses. Test cases in the literature are used to validate the analysis method and optimization cycles are conducted to find the optimum configurations for buckling load. These configurations are analyzed for post-buckling with progressive failure by using Hashin's failure criterion and continuous damage modeling (CDM). All analyses are conducted by using ANSYS Mechanical APDL by integrating a Python script.

1.4   Outline of the Thesis

In Chapter 1, composite structures and variable stiffness concept are introduced as well as the manufacturing technology with its limits and defects.

In Chapter 2, previous studies on variable stiffness composites are reviewed.

In Chapter 3, the theory of composite structures is explained. First-order Shear Deformation theory is presented.

In Chapter 4, the theory behind the variable stiffness composites is explained and methodology to build variable stiffness plates is described for both linear and nonlinear angle variations.

In Chapter 5, two test cases conducted by using constant stiffness plate and linear angle variation plate to observe bucking and post-buckling behaviour are described and validation studies for the method of this thesis are presented.

In Chapter 6, an angle configuration is selected for variable stiffness plates and buckling and post-buckling with progressive failure responses are investigated.

3

In Chapter 7, the previously validated method is used for further cases, and optimization cycles for linear and nonlinear angle variation is conducted. The optimum design points for buckling loading are compared. Also, post-buckling analyses are conducted by considering progressive failure with Hashin's failure criterion of the optimum configurations.

CHAPTER 2

LITERATURE SURVEY

2.1 Early Studies on Variable Stiffness Concept

Throughout the years, FRPs have been used with straight fibers. The most commonly used orientations are 0°, 45° and 90° [3]. 0° and 90° plies provide higher strength in axial and transverse loadings respectively while 45° plies are better for improving buckling behaviour of the plate [3].

Biggers and Srinivasan [4] used straight fibers to improve buckling capacity of a composite plate by placing 0° fibers at edges of the plate which are parallel to the loading. This method helps to redistribute the loading by manipulating the stiffness in local scale.

Another study conducted by Crothers et al. [5] showed that tailoring the fibers in a way that the fibers follows the path of principal stress trajectories where stress concentration is higher around the cut-outs could minimize the stress concentration since the stiffness near the cut-out is adjusted and tensile strength is improved.

Hyer and Lee [6] showed that deviating the fiber orientation from position to position could improve buckling performance. By using a sensitivity analysis and a gradient-search method, fiber orientations on determined location over the plate have been modified differently from the constant orientation concept and buckling performance has been increased.

Tatting et al. [7] explained that the VS composite plates perform better than the CS composite plates in buckling loading while having holes. Plates have been manufactured and tested to show that the fiber tailoring could improve the performance of composites.

Huang and Haftka [8] optimized the fiber orientations around the critical areas such as hole, on a single layer of multilayer laminate. As a result, load-carrying capacity of the laminate has been increased without changing the overall stiffness.

Wu et al. [9] worked on VSPs to investigate the impact of fiber tailoring on post-buckling behaviour. This study shows that the VSPs perform substantially better compared to straight fiber plates. Furthermore, combining straight fibers with variable angle fibers at the outer faces, could improve the pre-buckling strength.

Arranz et al. [10] analyzed grid-stiffened curvilinear fiber composite panels to observe their buckling response and optimized the configuration for buckling load while considering gaps between courses.

Coşkun et al. [11] showed that the optimum configuration of VSP for buckling loading increased the buckling load compared to the quasi-isotropic plate of the same size. Also, plate stiffness is reduced for the same configuration compared to quasi-isotropic plates.

2.2   Studies on Curvilinear Fiber Path Definition

Method for defining fiber angle is the first step to investigate before going into more detailed studies. There are different methods to configure the fiber angle of a ply. It can be grouped into two categories; linear angle variation, nonlinear angle variation.

Reynaldo [2] constructed the variable stiffness composites by designing the plates with curvilinear fiber paths. The stiffness varies over the plate spatially based on local fiber orientation. Linear angle variation is constructed by formulating the fiber angle over a curvilinear fiber depending on a single axis (properly located x axis is the common choice). Most of the studies conducted on VSPs use this method.

Nonlinear angle variation, on the other hand, enlarges the design space for possible configurations of VSPs. Different methods for defining the fiber curve can be used to achieve a nonlinear angle variation. One of these studies has been conducted by

Wu et al. [12] by using Lagrange interpolation and Control Points. Opposite to linear angle variation where only one axis can be selected for curve definition, two different axes can be used for curve definition. Predefined reference points on the plane can be used with specified fiber orientations and a double series of higher order polynomials is used for interpolating the positions between reference points. At the end, Lagrange polynomials has been used for nonlinear angle variation of fiber directions.

Nagendra et al. [13] used non-uniform rational B-splines (NURBS) by interpolating between control points to define a nonlinear angle variation curve.

Defining the fiber angles with a nonlinear function is another method for nonlinear angle variation. Parnas et al. [14] used Bezier curves and cubic polynomials to determine the fiber angles and bicubic Bezier surfaces for layer thicknesses to minimize the weight.

Fiber paths with constant curvature are formulated by Blom et al. [15] to eliminate the manufacturing limitations.

Alhajahmad et al. [16] used Lobatto-Legendre polynomials to define the fiber paths to design structures with improved load-carrying capacity.

CHAPTER 3

THEORY OF COMPOSITE LAMINATES

For orthotropic materials, there are nine elastic constants for three dimensional space. In composite material problems, constant count is reduced to four since the composite materials are orthotropic and the extension-shear coupling is not considered. Therefore, a laminate can be determined by four elastic constants [2]; longitudinal elastic modulus, E_1, transverse elastic modulus, E_2, Poisson's ratio, v_{12}, and in-plane shear modulus, G_{12}. However, transverse stress components can induce failures because FRPs are weak in the transverse direction. In the First-Order Shear Deformation Theory (FSDT), transverse shear stress components are not neglected [17] and more elastic constants, first transverse shear modulus, G_{13}, and second transverse shear modulus, G_{23}, are added.

Composite laminates are constructed by stacking several layers with desired fiber orientation. Generally, thickness of laminates are considerably small compared to their planar dimensions. Therefore, laminates can be studied as plates. In this thesis, FSDT will be used.

3.1   First-Order Shear Deformation Theory

In Classical Laminated Plate Theory (CLPT), it is assumed that the Kirchoff hypothesis holds; transverse normals remain straight after deformation, transverse normals remain normal to midsurface after deformation, and transverse normals do not elongate.

In FSDT, Kirchhoff hypothesis in CLPT which states that the transverse normals remain perpendicular to the midplane is relaxed. Therefore, the transverse shear effect is included into the plate theory [17].

3.1.1   Displacement and Strain Relations

The displacements of FSDT are written as [17]:

$$u(x, y, z, t) = u_0(x, y, t) + z\phi_x(x, y, t) \tag{3.1}$$

$$v(x, y, z, t) = v_0(x, y, t) + z\phi_y(x, y, t) \tag{3.2}$$

$$w(x, y, z, t) = w_0(x, y, t) \tag{3.3}$$

where ϕ_x and ϕ_y denote the rotations of a transverse normal about y and x axes, respectively and formulated as:

$$\phi_x = \frac{\partial u}{\partial z} \qquad \phi_y = \frac{\partial v}{\partial z} \tag{3.4}$$

Undeformed and deformed geometries of an edge of a plate under the assumptions of FSDT can be seen in Figure 3.1:
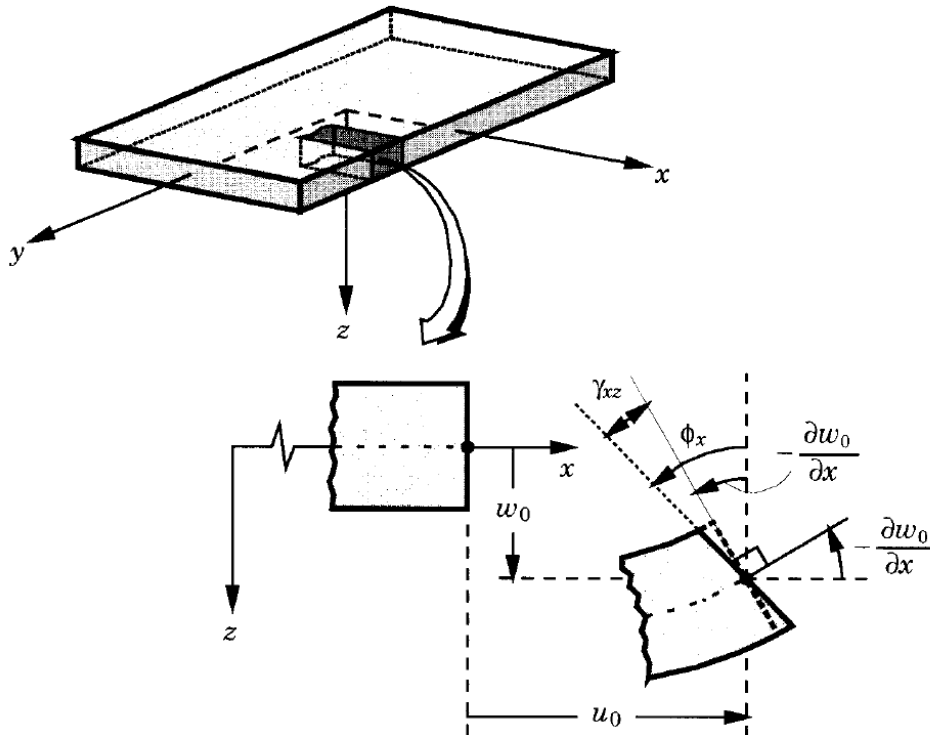
Figure 3.1. Undeformed and Deformed Geometries for FSDT [17]

10

Then, strains can be calculated as [17]:

$$
\begin{bmatrix} \varepsilon_{xx} \\ \varepsilon_{yy} \\ \gamma_{xy} \\ \gamma_{xz} \\ \gamma_{yz} \end{bmatrix} = \begin{bmatrix} \dfrac{\partial u_0}{\partial x} + \dfrac{1}{2}\left(\dfrac{\partial w_0}{\partial x}\right)^2 + z\dfrac{\partial \phi_x}{\partial x} \\[2mm] \dfrac{\partial v_0}{\partial y} + \dfrac{1}{2}\left(\dfrac{\partial w_0}{\partial y}\right)^2 + z\dfrac{\partial \phi_y}{\partial y} \\[2mm] \dfrac{\partial u_0}{\partial y} + \dfrac{\partial v_0}{\partial x} + \dfrac{\partial w_0}{\partial x}\dfrac{\partial w_0}{\partial y} + z\dfrac{\partial \phi_x}{\partial y} + z\dfrac{\partial \phi_y}{\partial x} \\[2mm] \dfrac{\partial w_0}{\partial x} + \phi_x \\[2mm] \dfrac{\partial w_0}{\partial y} + \phi_y \end{bmatrix} \tag{3.5}
$$

3.1.2   Lamina Constitutive Equations

Lamina is the building block of a laminate. The stress-strain relation for orthotropic lamina can be written as [17]:

$$
\begin{bmatrix} \sigma_1 \\ \sigma_2 \\ \sigma_6 \end{bmatrix} = \begin{bmatrix} Q_{11} & Q_{12} & 0 \\ Q_{12} & Q_{22} & 0 \\ 0 & 0 & Q_{66} \end{bmatrix} \begin{bmatrix} \varepsilon_1 \\ \varepsilon_2 \\ \varepsilon_6 \end{bmatrix} \tag{3.6}
$$

$$
\begin{bmatrix} \sigma_4 \\ \sigma_5 \end{bmatrix} = \begin{bmatrix} Q_{44} & 0 \\ 0 & Q_{55} \end{bmatrix} \tag{3.7}
$$

where Q_{ij} is defined as reduced stiffness and can be expressed by using elastic constants as [17]:

$$
Q_{11} = \frac{E_1}{1 - \nu_{12}\nu_{21}} \tag{3.8}
$$

$$
Q_{22} = \frac{E_2}{1 - \nu_{12}\nu_{21}} \tag{3.9}
$$

$$
Q_{12} = \frac{\nu_{12}E_2}{1 - \nu_{12}\nu_{21}} \tag{3.10}
$$

$$
Q_{66} = G_{12} \tag{3.11}
$$

$$Q_{44} = G_{23} \tag{3.12}$$

$$Q_{55} = G_{13} \tag{3.13}$$

A laminate consists of several laminae and the given equation is for the lamina coordinate system, $(1 - 2)$. If the laminate is made of laminae of same material, coordinate system transformation can be used to establish the stress-strain relation of the laminate in global coordinate system, $(x - y)$ as [17]:

$$\begin{bmatrix} \sigma_{xx} \\ \sigma_{yy} \\ \sigma_{xy} \end{bmatrix} = \begin{bmatrix} \overline{Q}_{11} & \overline{Q}_{12} & \overline{Q}_{16} \\ \overline{Q}_{12} & \overline{Q}_{22} & \overline{Q}_{26} \\ \overline{Q}_{16} & \overline{Q}_{26} & \overline{Q}_{66} \end{bmatrix} \begin{bmatrix} \varepsilon_{xx} \\ \varepsilon_{yy} \\ \gamma_{xy} \end{bmatrix} \tag{3.14}$$

$$\begin{bmatrix} \sigma_{yz} \\ \sigma_{xz} \end{bmatrix} = \begin{bmatrix} \overline{Q}_{44} & \overline{Q}_{45} \\ \overline{Q}_{45} & \overline{Q}_{55} \end{bmatrix} \begin{bmatrix} \gamma_{yz} \\ \gamma_{xz} \end{bmatrix} \tag{3.15}$$

where $[\overline{Q}]$ is calculated by using the given equation [17]:

$$[\overline{Q}] = [T]^{-1}[Q][T]^{-T} \tag{3.16}$$

The transformation matrix $[T]$ is related to θ, the orientation angle of the lamina since the transformation matrix converts the local coordinate system $(1 - 2)$ to the global coordinate system $(x - y)$.

3.1.3 Laminate Constitutive Equations

The force and moment resultants related to the lamina strains are defined as [17]:

$$\begin{bmatrix} N_{xx} \\ N_{yy} \\ N_{xy} \end{bmatrix} = \int_{-\frac{h}{2}}^{\frac{h}{2}} \begin{bmatrix} \sigma_{xx} \\ \sigma_{yy} \\ \sigma_{xy} \end{bmatrix} dz \tag{3.17}$$

$$\begin{bmatrix} M_{xx} \\ M_{yy} \\ M_{xy} \end{bmatrix} = \int_{-\frac{h}{2}}^{\frac{h}{2}} \begin{bmatrix} \sigma_{xx} \\ \sigma_{yy} \\ \tau_{xy} \end{bmatrix} z dz \tag{3.18}$$

$$\begin{bmatrix} \widehat{N}_{nn} \\ \widehat{N}_{ns} \end{bmatrix} = \int_{-\frac{h}{2}}^{\frac{h}{2}} \begin{bmatrix} \widehat{\sigma}_{nn} \\ \widehat{\sigma}_{ns} \end{bmatrix} dz \tag{3.19}$$

$$\begin{bmatrix} \widehat{M}_{nn} \\ \widehat{M}_{ns} \end{bmatrix} = \int_{-\frac{h}{2}}^{\frac{h}{2}} \begin{bmatrix} \hat{\sigma}_{nn} \\ \hat{\sigma}_{ns} \end{bmatrix} z dz \tag{3.20}$$

$$\begin{bmatrix} I_0 \\ I_1 \\ I_2 \end{bmatrix} = \int_{-\frac{h}{2}}^{\frac{h}{2}} \begin{bmatrix} 1 \\ z \\ z^2 \end{bmatrix} \rho_0 dz \tag{3.21}$$

$$\hat{Q}_n = \int_{-\frac{h}{2}}^{\frac{h}{2}} \hat{\sigma}_{nz} dz \tag{3.22}$$

Where N_{ij} is in-plane force resultant, M_{ij} is moment resultant, Q_n is transverse force resultant and I_i is mass moment of inertia. Force and moment diagrams are given in Figure 3.2:
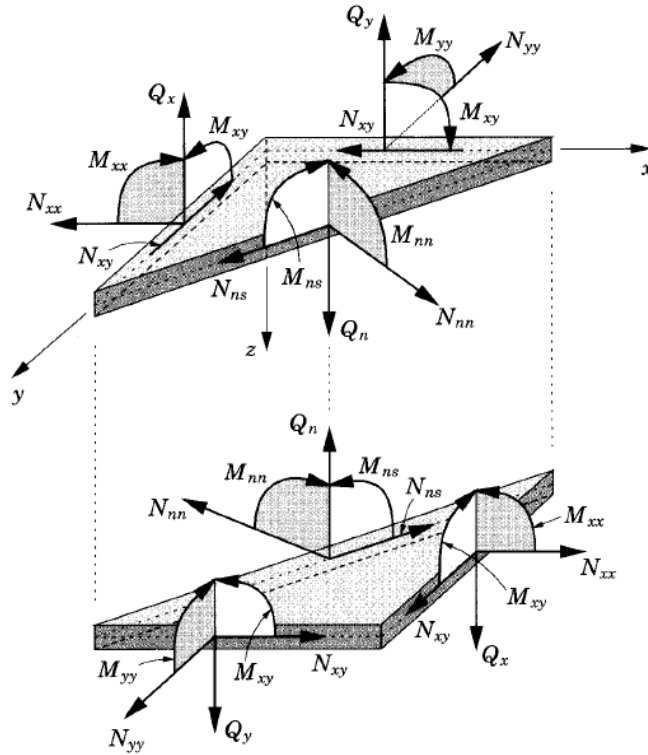

Figure 3.2. Force and Moment Resultants on a Plate Element [17]

If these resultants from (3.17) to (3.22) are integrated over the laminate, resultants for laminate can be found as [17]:

$$
\begin{bmatrix} N_{xx} \\ N_{yy} \\ N_{xy} \end{bmatrix} = \sum_{k=1}^{N} \int_{z_k}^{z_{k+1}} \begin{bmatrix} \sigma_{xx} \\ \sigma_{yy} \\ \sigma_{xy} \end{bmatrix} dz
$$

$$
= \sum_{k=1}^{N} \int_{z_k}^{z_{k+1}} \begin{bmatrix} \overline{Q_{11}} & \overline{Q_{12}} & \overline{Q_{16}} \\ \overline{Q_{12}} & \overline{Q_{22}} & \overline{Q_{26}} \\ \overline{Q_{16}} & \overline{Q_{26}} & \overline{Q_{66}} \end{bmatrix} \begin{bmatrix} \varepsilon_{xx} \\ \varepsilon_{yy} \\ \gamma_{xy} \end{bmatrix} dz
$$

(3.23)

$$
\begin{bmatrix} N_{xx} \\ N_{yy} \\ N_{xy} \end{bmatrix} = \begin{bmatrix} A_{11} & A_{12} & A_{16} \\ A_{12} & A_{22} & A_{26} \\ A_{16} & A_{26} & A_{66} \end{bmatrix} \begin{bmatrix} \dfrac{\partial u_0}{\partial x} + \dfrac{1}{2}\left(\dfrac{\partial w_0}{\partial x}\right)^2 \\[2mm] \dfrac{\partial v_0}{\partial y} + \dfrac{1}{2}\left(\dfrac{\partial w_0}{\partial y}\right)^2 \\[2mm] \dfrac{\partial u_0}{\partial y} + \dfrac{\partial v_0}{\partial x} + \dfrac{\partial w_0}{\partial x}\dfrac{\partial w_0}{\partial y} \end{bmatrix}
$$

(3.24)

$$
+ \begin{bmatrix} B_{11} & B_{12} & B_{16} \\ B_{12} & B_{22} & B_{26} \\ B_{16} & B_{26} & B_{66} \end{bmatrix} \begin{bmatrix} \dfrac{\partial \phi_x}{\partial x} \\[2mm] \dfrac{\partial \phi_y}{\partial y} \\[2mm] \dfrac{\partial \phi_x}{\partial y} + \dfrac{\partial \phi_y}{\partial x} \end{bmatrix}
$$

$$
\begin{bmatrix} M_{xx} \\ M_{yy} \\ M_{xy} \end{bmatrix} = \sum_{k=1}^{N} \int_{z_k}^{z_{k+1}} \begin{bmatrix} \sigma_{xx} \\ \sigma_{yy} \\ \sigma_{xy} \end{bmatrix} z\,dz
$$

$$
= \sum_{k=1}^{N} \int_{z_k}^{z_{k+1}} \begin{bmatrix} \overline{Q_{11}} & \overline{Q_{12}} & \overline{Q_{16}} \\ \overline{Q_{12}} & \overline{Q_{22}} & \overline{Q_{26}} \\ \overline{Q_{16}} & \overline{Q_{26}} & \overline{Q_{66}} \end{bmatrix} \begin{bmatrix} \varepsilon_{xx} \\ \varepsilon_{yy} \\ \gamma_{xy} \end{bmatrix} z\,dz
$$

(3.25)

$$
\begin{bmatrix} M_{xx} \\ M_{yy} \\ M_{xy} \end{bmatrix} = \begin{bmatrix} B_{11} & B_{12} & B_{16} \\ B_{12} & B_{22} & B_{26} \\ B_{16} & B_{26} & B_{66} \end{bmatrix} \begin{bmatrix} \dfrac{\partial u_0}{\partial x} + \dfrac{1}{2}\left(\dfrac{\partial w_0}{\partial x}\right)^2 \\[2mm] \dfrac{\partial v_0}{\partial y} + \dfrac{1}{2}\left(\dfrac{\partial w_0}{\partial y}\right)^2 \\[2mm] \dfrac{\partial u_0}{\partial y} + \dfrac{\partial v_0}{\partial x} + \dfrac{\partial w_0}{\partial x}\dfrac{\partial w_0}{\partial y} \end{bmatrix}
$$

(3.26)

$$
+ \begin{bmatrix} D_{11} & D_{12} & D_{16} \\ D_{12} & D_{22} & D_{26} \\ D_{16} & D_{26} & D_{66} \end{bmatrix} \begin{bmatrix} \dfrac{\partial \phi_x}{\partial x} \\[2mm] \dfrac{\partial \phi_y}{\partial y} \\[2mm] \dfrac{\partial \phi_x}{\partial y} + \dfrac{\partial \phi_y}{\partial x} \end{bmatrix}
$$

$$\begin{bmatrix} Q_y \\ Q_x \end{bmatrix} = K \sum_{k=1}^{N} \int_{z_k}^{z_{k+1}} \begin{bmatrix} \sigma_{yz} \\ \sigma_{xz} \end{bmatrix} dz \qquad (3.27)$$

$$\begin{bmatrix} Q_y \\ Q_x \end{bmatrix} = K \begin{bmatrix} A_{44} & A_{15} \\ A_{45} & A_{55} \end{bmatrix} \begin{bmatrix} \dfrac{\partial w_0}{\partial y} + \phi_y \\ \dfrac{\partial w_0}{\partial x} + \phi_x \end{bmatrix} \qquad (3.28)$$

where A_{ij} is extensional stiffness, D_{ij} is bending stiffness and B_{ij} is bending-extensional coupling stiffness and defined as [17]:

$$A_{ij} = \sum_{k=1}^{N} \overline{Q_{\iota J}}(z_{k+1} - z_k) \qquad (3.29)$$

$$B_{ij} = \frac{1}{2} \sum_{k=1}^{N} \overline{Q_{\iota J}}({z_{k+1}}^2 - {z_k}^2) \qquad (3.30)$$

$$D_{ij} = \frac{1}{3} \sum_{k=1}^{N} \overline{Q_{\iota J}}({z_{k+1}}^3 - {z_k}^3) \qquad (3.31)$$

and K is the shear correction factor. It is taken as $5/6$ [18].

3.2   Buckling of Composite Laminate Plate

Buckling causes the plate to deform in out-of-plane direction. This deformation, also called buckling mode, is observed in the form of sine waves. Based on the geometry of the plate, the buckling mode could be in the shape of half sine wave or its multiples [1]. Buckling of a plate can be seen in Figure 3.3 where N is compressive loading and $\overline{N}$ is buckling load.

To explain the buckling behaviour further, load-displacement plot is presented in Figure 3.4. Buckling is an unstable condition. Plate deforms in the direction of compressive load. If the plate did not have any imperfection, an in-plane deformation would occur. However, this is not the case for real application. Therefore, displacement bifurcates after a critical load and buckling occurs.
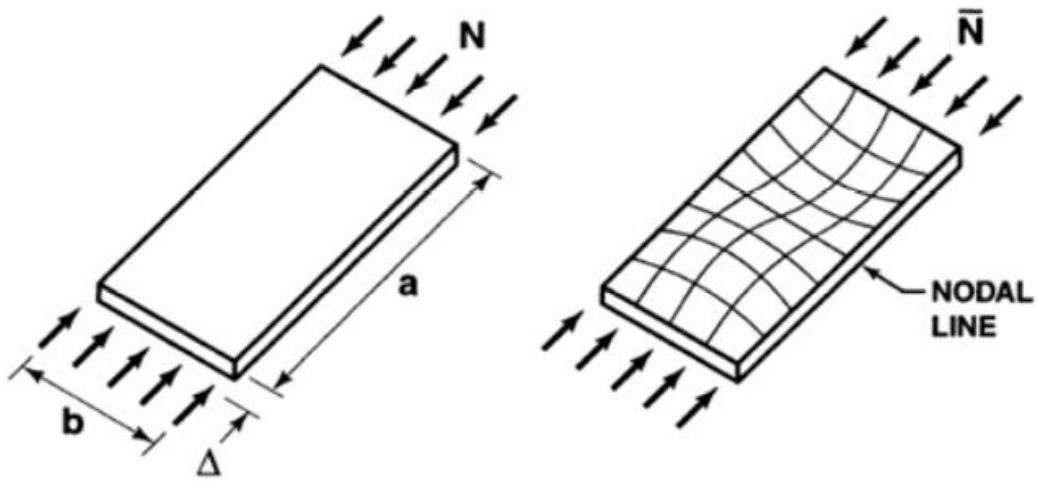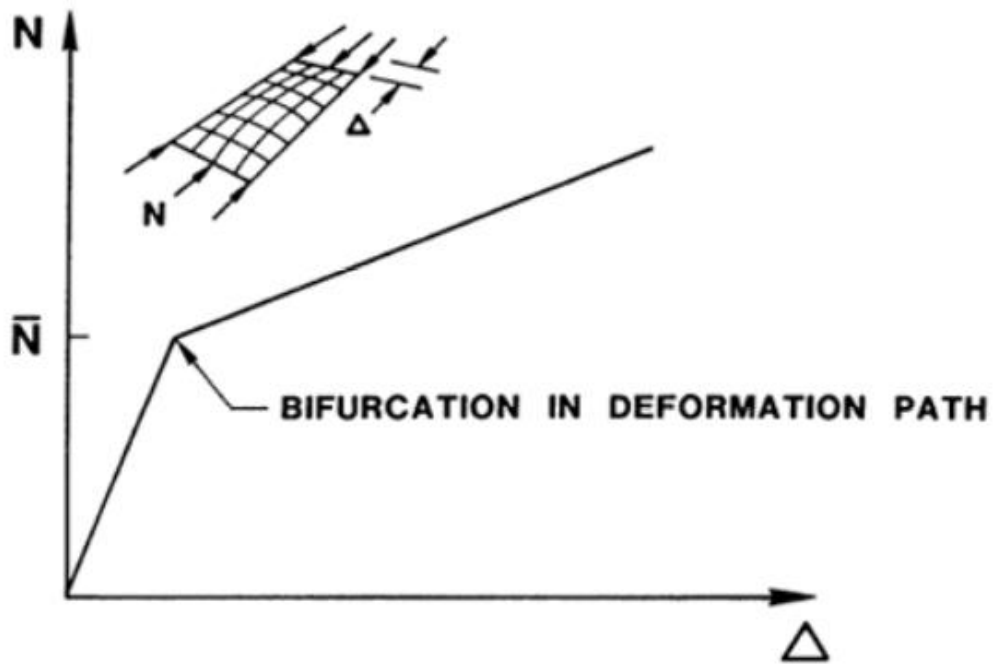
Figure 3.3. Buckling of a Plate [1]

Figure 3.4. Load-Displacement Plot of Plate [1]

The buckling governing equation for plate with simply supported edges can be written as [17]:

$$D_{11} \frac{\partial^4 w}{\partial x^4} + 4D_{16} \frac{\partial^4 w}{\partial x^3 \partial y} + 2(D_{11} + 2D_{66}) \frac{\partial^4 w}{\partial x^2 \partial y^2}$$
$$+ 4D_{26} \frac{\partial^4 w}{\partial x \partial y^3} + D_{22} \frac{\partial^4 w}{\partial y^4} + \bar{N}_{xx} \frac{\partial^2 w}{\partial x^2} = 0 \tag{3.32}$$

and boundary conditions are:

$$if \ 0 \leq x \leq a$$
$$\partial w = 0 \quad \frac{\partial M}{\partial x} = -D_{11} \frac{\partial^2 w}{\partial x^2} - D_{12} \frac{\partial^2 w}{\partial y^2} - 2D_{16} \frac{\partial^2 w}{\partial x \partial y} = 0 \tag{3.33}$$

$$if \ 0 \leq y \leq b$$
$$\partial w = 0 \quad \frac{\partial M}{\partial x} = -D_{12} \frac{\partial^2 w}{\partial x^2} - D_{22} \frac{\partial^2 w}{\partial y^2} - 2D_{26} \frac{\partial^2 w}{\partial x \partial y} = 0 \tag{3.34}$$

In this equation, stiffnesses, D_{ij}, are function of orientation angle, θ. Orientation angle is function of position, x and y.

3.3 Failure of Laminates

When the plate is loaded with compressive forces, after a point, the plate starts to fail at the post-buckling region. This point is the first ply failure point. Then, the damage starts to progress. To predict the damage, a failure criterion and damage model should be defined for the model. In this analysis Hashin's failure criterion is used to determine failure and continuous damage modeling to observe damage progress. Hashin's failure criterion calculates the damage index to determine whether the stress levels are high enough to cause the failure. Hashin's failure criteria for fiber and matrix are given in following equations [19]:

ξ_{fiber}

$$= \begin{cases} \left(\dfrac{\sigma_x}{\sigma_{xt}^f}\right)^2 + \dfrac{\sigma_{xy}{}^2 + \sigma_{xz}{}^2}{\sigma_{xy}^{f\ 2}} & if\ \sigma_x > 0 \\[2em] \left(\dfrac{\sigma_x}{\sigma_{xc}^f}\right)^2 & if\ \sigma_x \le 0 \end{cases} \qquad (3.35)$$

ξ_{matrix}

$$= \begin{cases} \left(\dfrac{\sigma_y + \sigma_z}{\sigma_{yt}^f}\right)^2 + \dfrac{\sigma_{yz}{}^2 - \sigma_y \sigma_z}{\sigma_{yz}^{f\ 2}} + \dfrac{\sigma_{xy}{}^2 + \sigma_{xz}{}^2}{\sigma_{xy}^{f\ 2}} & if\ \sigma_y + \sigma_z > 0 \\[2em] \dfrac{1}{\sigma_{yc}^f}\left(\left(\dfrac{\sigma_{yc}^f}{2\sigma_{yz}^f}\right)^2 - 1\right)(\sigma_y + \sigma_z) + \left(\dfrac{\sigma_y + \sigma_z}{2\sigma_{yz}^f}\right)^2 \\[1.5em] \quad + \dfrac{\sigma_{yz}{}^2 - \sigma_y \sigma_z}{\sigma_{yz}^{f\ 2}} + \dfrac{\sigma_{xy}{}^2 + \sigma_{xz}{}^2}{\sigma_{xy}^{f\ 2}} & if\ \sigma_y + \sigma_z \le 0 \end{cases} \qquad (3.36)$$

When stress levels reach the limit, the plate starts to fail from that point. This causes loss of stiffness at that location and after some time, the stiffness reduces to zero. At this stage, the element fails. To degrade the stiffness, continuous damage modeling is used. Fracture toughness values are used for this method and element stiffnesses are degraded accordingly.

CHAPTER 4

VARIABLE STIFFNESS LAMINATE DEFINITION

4.1 Terminology for FRPs

Conventional fiber reinforced composite lamina consists of stiff fibers submerged into a matrix material. Fibers can be laid in desired orientation to achieve required strength properties. Orientation is expressed by using lamina coordinate system as shown in Figure 4.1.
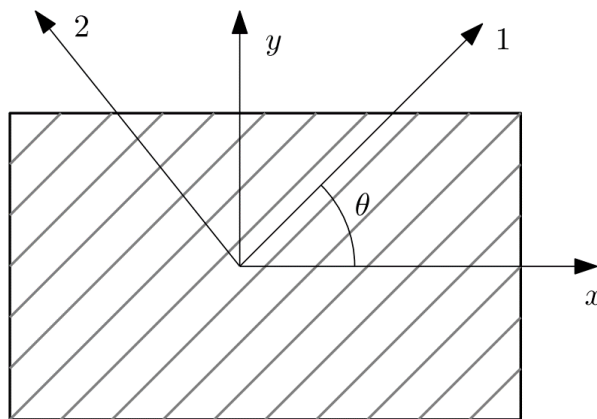
Figure 4.1. FRP Lamina [20]

The global coordinate system is shown as $x - y$ directions in two-dimensional space where $1 - 2$ directions indicate the orientation of a single lamina or ply. The 1 direction is parallel to the fiber direction where the direction 2 is perpendicular to the direction 1. Directional material properties are defined according to the lamina coordinate system. External loads are applied to the composite part by using a global coordinate system. The angle between global x coordinate and ply coordinate 1 is the fiber orientation angle, θ.

Several plies are combined into a single part called laminate. Plies with different fiber orientations can be used in a laminate with a specific stacking order to achieve desired structural properties. Laminate properties are usually adjusted by changing this specific stacking order (changing orientations of the fibers in ply, changing the number of plies to be laid) or material. Therefore, design space is limited by orientation angle, laminate thickness, and material. To achieve orthotropic material properties over the laminate, stacking order should satisfy the symmetry and balanced conditions [21].

A symmetric laminate consists of the two symmetric stacking orders combined to each other at the midplane of the laminate [22]. To clarify, the laminate can be divided into two equal parts at the midplane and the stacking order of one sublaminate should be the symmetric of the other sublaminate with respect to the midplane. On the other hand, unsymmetric laminate does not satisfy this condition. Its laminae are not symmetric with respect to midplane. The symmetric and unsymmetric conditions can be seen in Figure 4.2
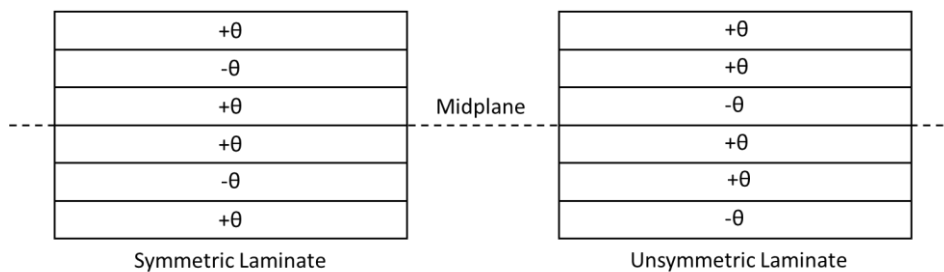

Figure 4.2. Symmetric and Unsymmetric Laminate

In a balanced laminate, there are equal numbers of plies with opposite signs of fiber orientation angles to balance each other. That means, there should be a $-\theta$ ply in the laminate when there is a $+\theta$ ply independent of the location [22]. For the unbalanced laminate, some plies do not have their opposite signed ply in the laminate. The balanced and unbalanced conditions can be seen in Figure 4.3.
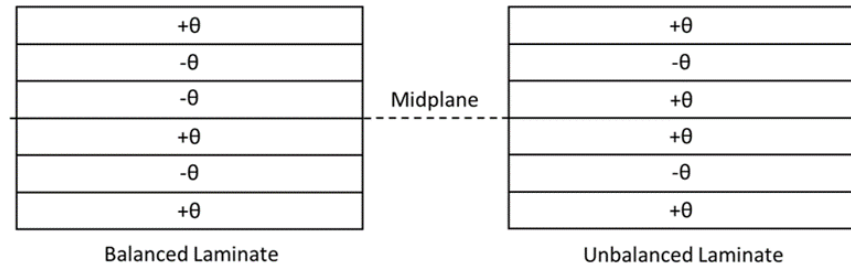
20

Figure 4.3. Balanced and Unbalanced Laminate

Layers of a laminate can be oriented such that its behaviour is close to a isotropic material. Quasi-isotropic laminate acts as an in-plane isotropic material. To explain it further, extensional stiffness matrix, $[A_{ij}]$, of the laminate is isotropic which means extension and shear are uncoupled ($A_{16} = A_{26} = 0$). The components of this matrix are independent of laminate orientation [23]. One example of this type of laminates is $[45/0/-45/90]_{2s}$.

4.2   Variable Stiffness Composites

As mentioned previously, the design space for composite parts is limited when using the traditional methods. Fiber angle is constant throughout a single ply and different plies are combined to achieve optimal results. However, another method to enlarge the design space is to vary the ply properties based on the position. This is called the Variable Stiffness (VS) method and composites manufactured with this method can be named as Variable Stiffness Composites.

Ply properties can be changed continuously by varying the fiber orientation angle over the ply. This operation is called steering the fiber. With this method, desired structural property can be achieved at required positions over the plate. Therefore, unnecessary ply stacking can be decreased which leads to weight reduction and efficiency. Variable stiffness concept can be seen in Figure 4.4.
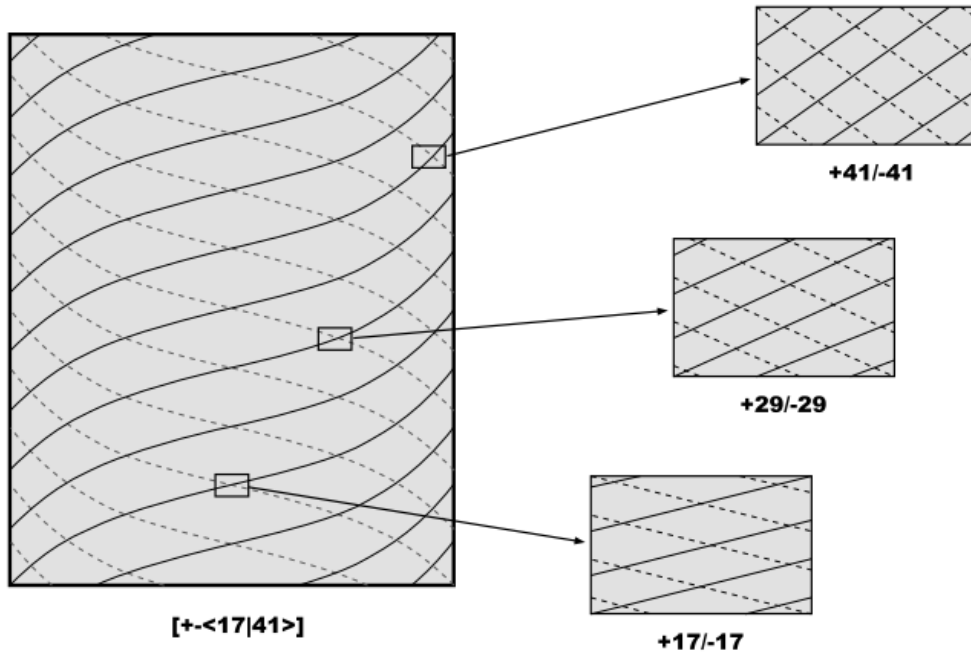
Figure 4.4. Variable Stiffness Fiber Paths [24]

VSPs can be built by changing the fiber angle continuously from point to point. The angle variation is derived by mathematical equations and the fiber angle variation can be linear or nonlinear depending on the position.

Linear angle variation (LAV) method determines the fiber angles based on the position by varying the angles equally at equal distances i.e., angle variation is constant. However, in the nonlinear angle variation (NAV) method, fiber angles do not change by a constant value, instead the angle difference between two positions is different from any other two points. Angle variation of these two methods for an arbitrary case can be seen in Figure 4.5.

Variable Stiffness (VS) laminates can be constructed by different types of curvilinear fiber paths. Generally, two main parameters are used to define the fiber path which are inlet angle, T_0, and exit angle, T_1. The main purpose to define the fiber path as a curvilinear path is to vary the fiber angle over the plate. Based on the desired inlet and exit angle, fiber orientation angles between inlet and exit can be calculated with selected curve type. Curvilinear fiber path definition is illustrated in Figure 4.6.
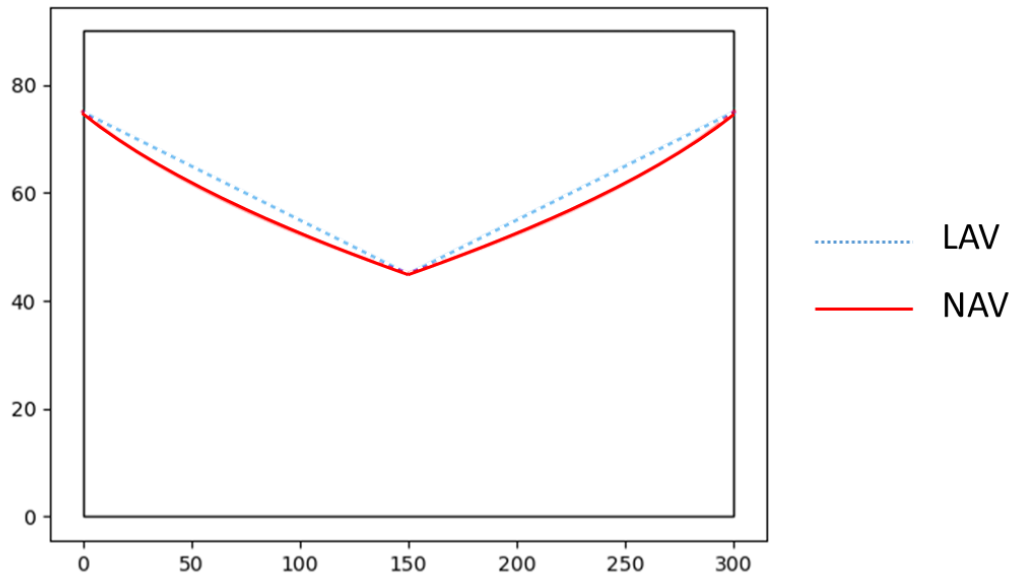
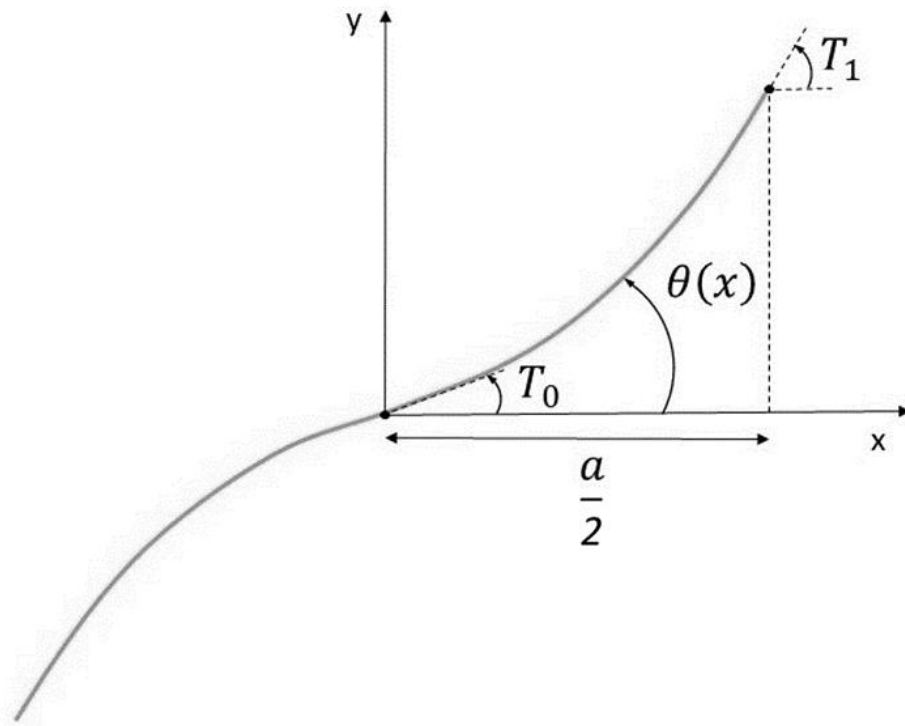Figure 4.5. Angle Variations of LAV and NAV Methods

Figure 4.6. Curvilinear Fiber Path Definition [10]

Linear angle variation (LAV) method is achieved by varying the fiber orientation angle of the reference path over a selected axis linearly. The inlet angle, T_0, is located at a fixed position (generally at the geometric center of ply) and exit angle, T_1, at the edge of the ply on the given axis. With the following equation [25]:

$$\theta(x) = 2(T_1 - T_0)\frac{x}{a} + T_0 \qquad (4.1)$$

fiber orientation can be determined at desired location where a is the length of the ply at the selected axis. With this method, fiber orientation angles are defined as a function of the x coordinate. This means, y coordinate does not contribute to the angle variation and it is also a function of x. The ply is antisymmetric with respect to the y coordinate. Angles at the negative side of the x axis can be calculated by multiplying the first term of the function by -1. The ply constructed with LAV curve is denoted as $< T_0 | T_1 >$. The local coordinate system, $x' - y'$, is coincident with the global coordinate system. However, it can be rotated with respect to global coordinate system with an angle ϕ to define a generalized fiber path formulation. LAV can be seen in Figure 4.7.
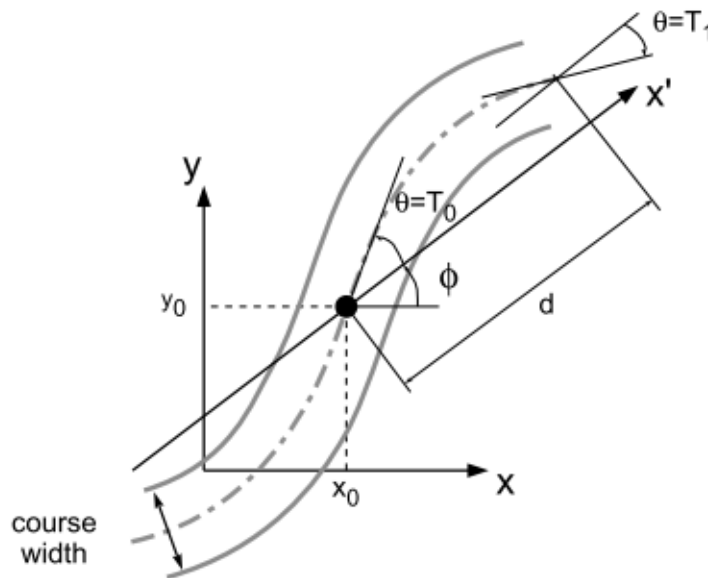

Figure 4.7. Fiber Path with Linear Angle Variation (LAV) [24]

24

Then the equation (4.1) is modified as:

$$\theta(x') = \phi + 2(T_1 - T_0)\frac{x'}{d} + T_0 \tag{4.2}$$

and the ply configuration is denoted as $\phi < T_0|T_1 >$. Once the reference path has been defined, a single course can be calculated by shifting the reference path perpendiculary. At last, the whole ply can be obtained by shifting in the desired direction.

Nonlinear angle variation, on the other hand, enlarges the design space for possible configurations of VSPs. Different methods for defining the fiber curve can be used to achieve a nonlinear angle variation. Since the derivative of a curve's equation is angle variation, an equation with its first derivative have a nonlinear function can be used for defining fiber path. Bezier curves are one of these. In this thesis, quadratic Bezier curves are used for defining the NAV fiber path.

Bezier Curve is defined with control points. Number of control points, N_{CP}, can be 2 or more. This number also defines the order of the Bezier Curve. Order can be calculated with following equation as:

$$Order = N_{CP} - 1 \tag{4.3}$$

With this equation, it can be seen that there should be 3 control points to define a quadratic Bezier curve. Control points are denoted as $P_1(x_1, y_1)$, $P_2(x_2, y_2)$, and $P_3(x_3, y_3)$. Position of any point on Bezier curve is calculated with following equation as:

$$P = (1 - t)^2 P_1 + 2(1 - t)t P_2 + t^2 P_3 \tag{4.4}$$

where $P(x, y)$ is the position of desired point and t is a parameter between 0 and 1. Depending on the positions of control points, different curves can be generated. The equations of x and y can be extracted from Equation (4.4) as:

$$x = (1-t)^2 x_1 + 2(1-t)tx_2 + t^2 x_3 \tag{4.5}$$

$$y = (1-t)^2 y_1 + 2(1-t)ty_2 + t^2 y_3 \tag{4.6}$$

The control point P_1 is fixed at the center of the plate. The x coordinate of the control point P_3 is fixed at the edge of plate. However, the location of the control point P_2 can be selected freely. Therefore, for a given set of inlet and exit angles, different curves can be built. By changing the position of P_2 value and constructing different curves, radius of curvature of the curve can be changed. This helps to build fiber paths with desired radius of curvature within the limits of manufacturing. Radius of curvature is calculated by selecting 3 consecutive points on the Bezier curve and building a circle with these points. Equation of a circle in general form is defined with (4.7):

$$x^2 + y^2 + 2ax + 2by + c = 0 \tag{4.7}$$

In this equation, there are 3 unknown parameters. With 3 known points, this equation can be converted to 3 linear equations and solved with inverse matrix method as:

$$\begin{bmatrix} 2x_1 & 2y_2 & 1 \\ 2x_2 & 2y_2 & 1 \\ 2x_3 & 2y_3 & 1 \end{bmatrix} \begin{bmatrix} a \\ b \\ c \end{bmatrix} = \begin{bmatrix} -(x_1{}^2 + y_1{}^2) \\ -(x_2{}^2 + y_2{}^2) \\ -(x_3{}^2 + y_3{}^2) \end{bmatrix} \tag{4.8}$$

and center location and radius of the circle (radius of curvature) can be found as:

$$x_c = -a \tag{4.9}$$

$$y_c = -a \tag{4.10}$$

$$R_c = \sqrt{a^2 + b^2 - c} \tag{4.11}$$

From equations (4.5), (4.6) and (4.9), the reference curve for fiber path can be constructed within the limits of manufacturing.

4.3   Manufacturing Technology and Defects

In early stages of composite manufacturing, fibers were constructed by hand-layup method, which requires a technician to place the fibers by hand over a mold. Quality of the final product was highly dependent on the skill level of the technician and every product was not exactly the same. This human factor was affecting the part and it required a great workload.

With the technological developments, automated methods were developed such as Automated Tape Laying (ATL) and Automated Fiber Placement (AFP). In ATL, a robotic head is fed with prepreg fiber tapes to lay down the unidirectional composite tape on the surface (Figure 4.8). Lukaszewicz et al. [26] said that this technology could decrease the wastage of material and reduce errors on the final product. Furthermore, Postier [27] showed that the production time could be reduced 65% with less wastage.
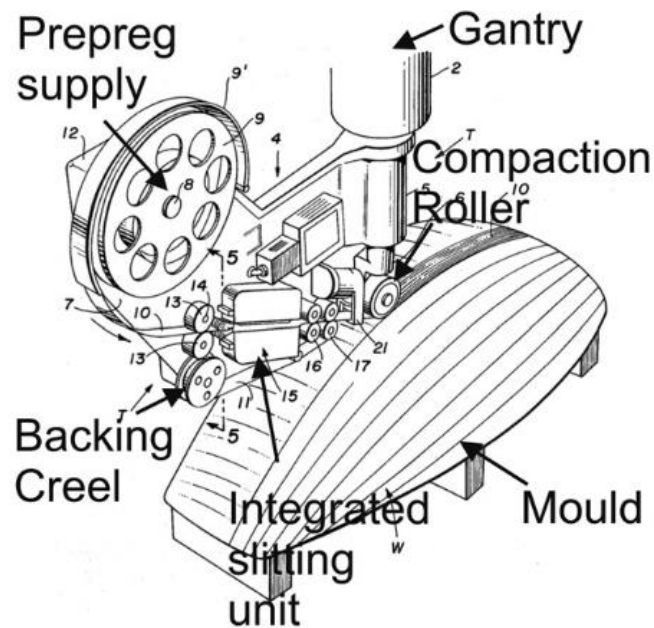

Figure 4.8. ATL Machine [28]

ATL technology is developed further to AFP technology (Figure 4.9). AFP allows to feed the tape in a way that the tape can be cut into strips, called tows, and delivered with desired speeds to required locations. With this new technology, more complex shapes could be produced [29].
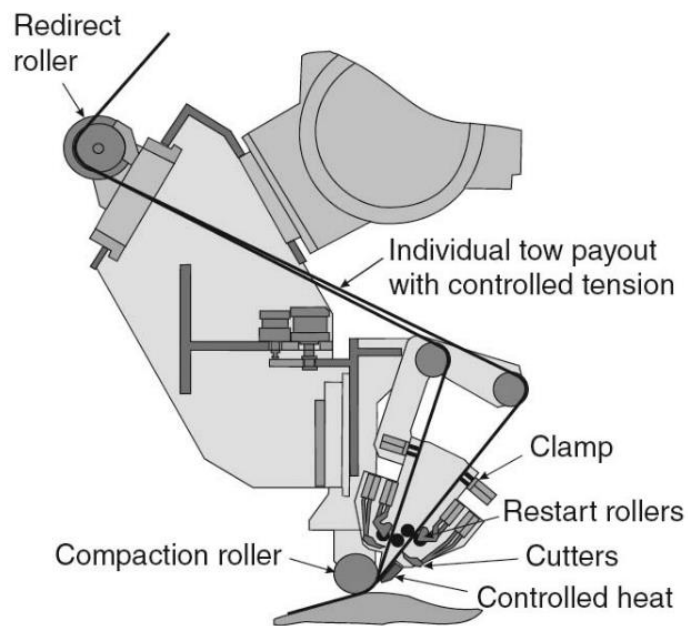

Figure 4.9. AFP Machine [30]

Automated fiber placement technology is a developing method to create composite parts with tow winding [31]. Within the limitations of AFP, fibers can be altered in desired manner to achieve the desired conditions without human interaction [32]. An AFP machine delivers a band of fibers, called course, onto the mold structure via a roller head controlled by a robotic arm. This course consists of several subunits called tows. Tows could be explained as a bundle of fibers. There are some typical tow widths used widely in industry such as 3.175 mm, 6.35 mm and 12.7 mm [15]. AFP machine could deliver several tows at the same time as a full course or could stop, cut, or restart some of the tows at speeds up to 1m/s to achieve the desired product.

AFP machine contains a high accuracy robotic arm to move the tow placement head via computer control. It can help the designer to construct more complex geometries

where traditional methods cannot achieve [33]. With AFP technology, parts could be produced faster and more precisely because of computer controlled manufacturing. Operation of an AFP machine can be seen in Figure 4.10.
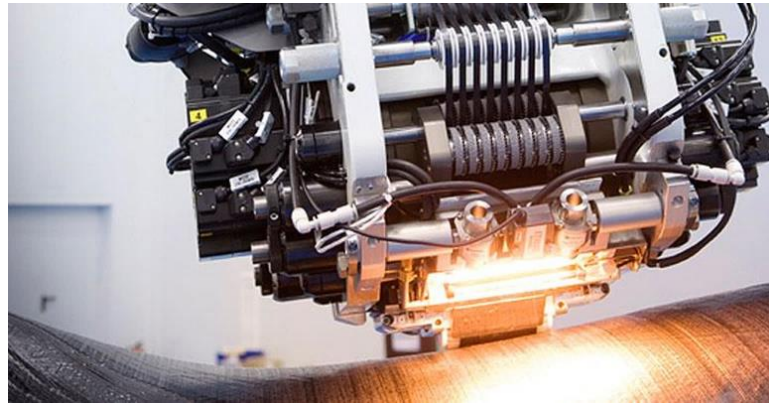

Figure 4.10. Automated Fiber Placement Machine [34]

AFP machine produces a single ply of VSP in two ways. These are parallel method and shifting method. If courses are laid down parallel to each other without any gaps or overlaps, this procedure is called the parallel method. With the parallel method, an ideal VSP ply can generated. However, this method has a drawback. In every course laid down with parallel method, the curvature of the centerlines is different. Therefore, inner courses will have small curvatures which are beyond the minimum limit of the AFP machine. Below this limit, courses start to wrinkle. The limit changes based on the material and feed rate of tows. Most of the time, it is between 400 mm and 1000 mm [35]. Parallel method can be seen in Figure 4.11.
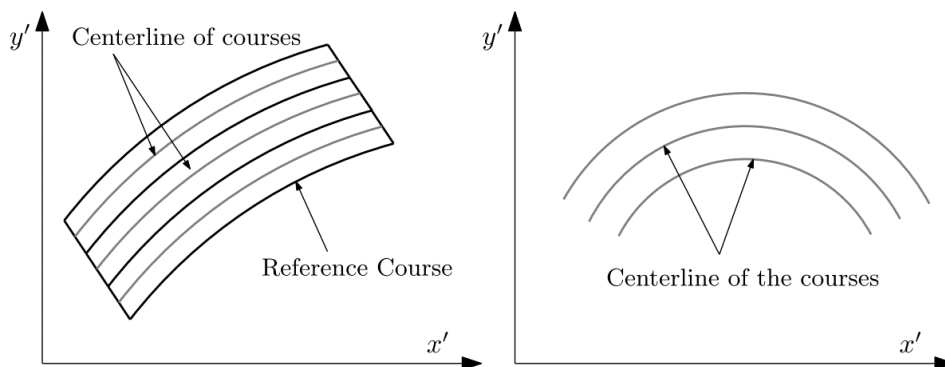

Figure 4.11. Parallel Method [20]

29

The second method is to shift the roller head in the direction of one of the axes to lay down courses with the same centerline configurations. With this method, curvature of the centerlines does not change from course to course, which guarantees the elimination of wrinkling due to the small radius of curvature. Shifting method can be seen in Figure 4.12. However, this method creates another problem with manufacturing. Since the edges of courses do not coincide with each other, courses could be overlapping each other or leaving gaps between them. These defects are called manufacturing defects and affect the performance of the final parts. Therefore, they should be considered during the design phase. Manufacturing defects can be seen in Figure 4.13.
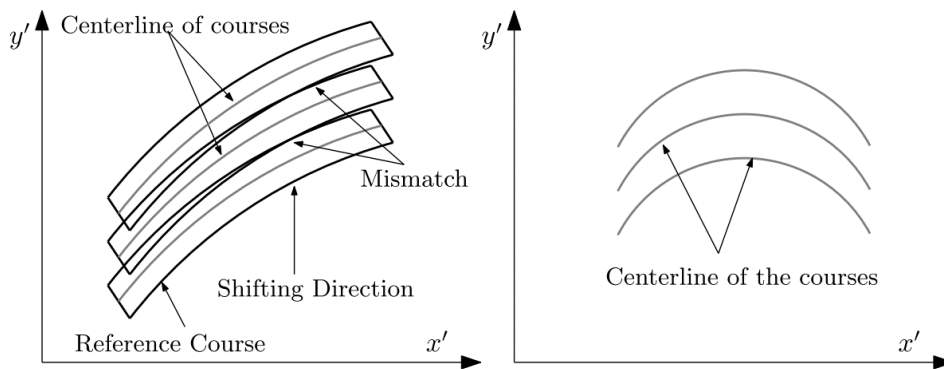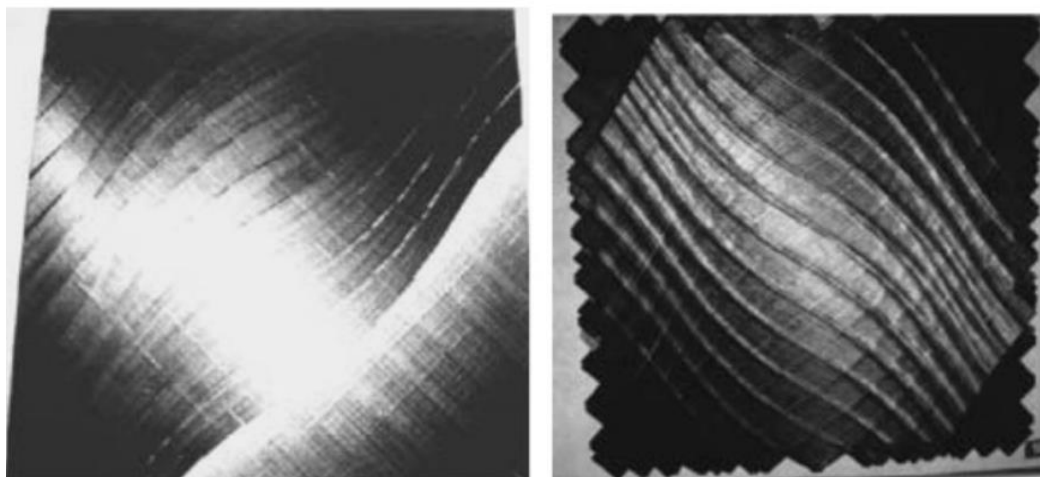

Figure 4.12. Shifting Method [20]

Figure 4.13. Manufacturing Defects (Gaps and Overlaps) [36]

In the scope of this thesis, overlapped condition will be investigated. Courses with the same curvature coincides during the manufacturing process. In these regions, courses overlaps eachother and thickness build-ups occur. To avoid this situation, courses could be shifted with more distance between them [37]. However, increased shifting distance creates gaps between the courses. These gaps are resin rich pockets and could lead to failures more likely [38]. Therefore, design with overlaps are more preferable than one with gaps. Gap and overlap conditions are illustrated in Figure 4.14.
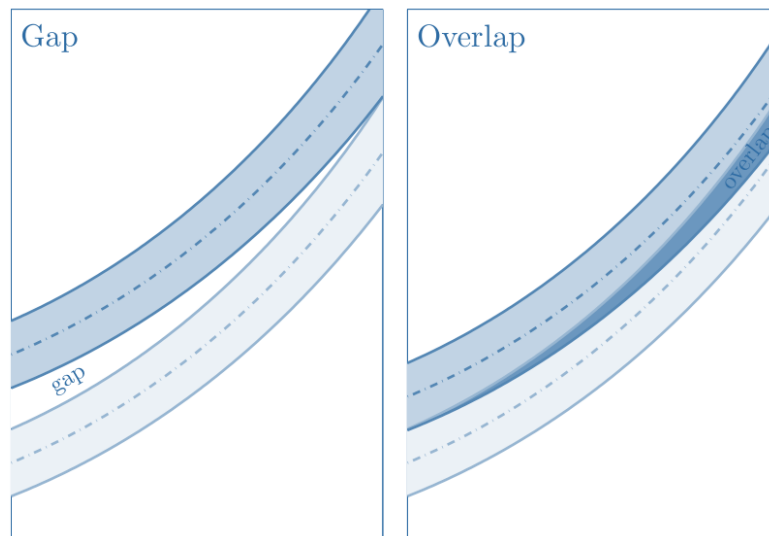

Figure 4.14. Gap and Overlap Conditions [39]

CHAPTER 5

VALIDATION WITH TEST

In this chapter, previous test studies conducted by Namdar and Darendeliler [21] and Jegley et al. [36] and are presented. In the studies, a constant stiffness plate and a linear angle variation laminate with specified angle configuration have been designed and tested, respectively.

5.1 Constant Stiffness Plate Test

5.1.1 Experimental Setup

The tested composite plate consists of 16 layers. It is a rectangular plate with its dimensions as 460 mm in height and 350 mm in width. Angle configuration for the plate is $[45/-45/0/45/90/90/-45/0]_s$. Plate geometry is given in Figure 5.1 and the experimental setup can be seen in Figure 5.2.

The plate has been connected to the test bench with clamps. At Edge 1 and Edge 2, the plate is fixed with potted ends. Therefore, the tested plate height is reduced to 400 mm due to potted ends. At 10 mm distance from Edge 3 and Edge 4, the plate is held with knife edges.

The plate is made from AS4/8552 carbon-epoxy material. Its layer thickness is 0.184 mm. The material properties are given in Table 5.1. In the analysis, values of G_{13} and G_{23} are taken as equal to G_{12}. Also, values ν_{13} and ν_{23} are taken as equal to ν_{12}.

Table 5.1 Material Properties of AS4/8552 [21]

| Parameter	Description	Value	Unit
E_1	Elastic Modulus in Longitudinal Direction	130	GPa
E_2	Elastic Modulus in Transverse Direction	8.5	GPa
G_{12}	Shear Modulus	4.2	GPa
ν_{12}	Poisson's Ratio	0.35	-
X_T	Tensile Strength in Longitudinal Direction	1530	MPa
X_C	Compression Strength in Longitudinal Direction	770	MPa
Y_T	Tensile Strength in Transverse Direction	64	MPa
Y_C	Compression Strength in Transverse Direction	175	MPa
S_L	Shear Strength	95	MPa
G_{1+}	Fiber Tension	49.5	J/mm^2
G_{1-}	Fiber Compression	12.5	J/mm^2
G_{2+}	Matrix Tension	1.3	J/mm^2
G_6	Matrix Compression	9.5	J/mm^2
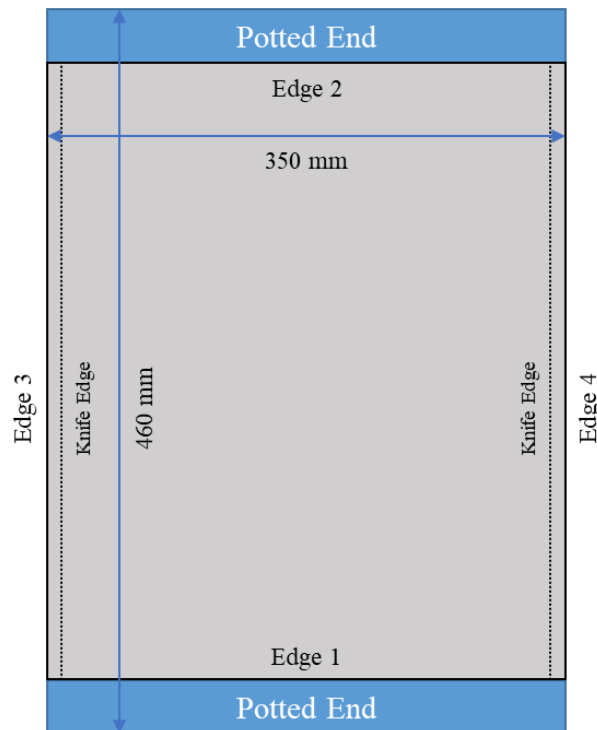
Figure 5.1. Plate Geometry of Constant Stiffness Plate

Figure 5.2. Experimental Setup of Constant Stiffness Plate

5.1.2   Numerical Results (FEA)

For numerical calculations, a commercial finite element software (ANSYS Mechanical APDL) has been used. SHELL181 with Fully Integration element is used with 3 mm maximum element edge. The material is AS4/8552. The finite element model can be seen in Figure 5.3.

To insert the fiber orientation angles, shell definitions have been made. The angle configuration is given in the previous section. The boundary conditions can be seen in Table 5.2.
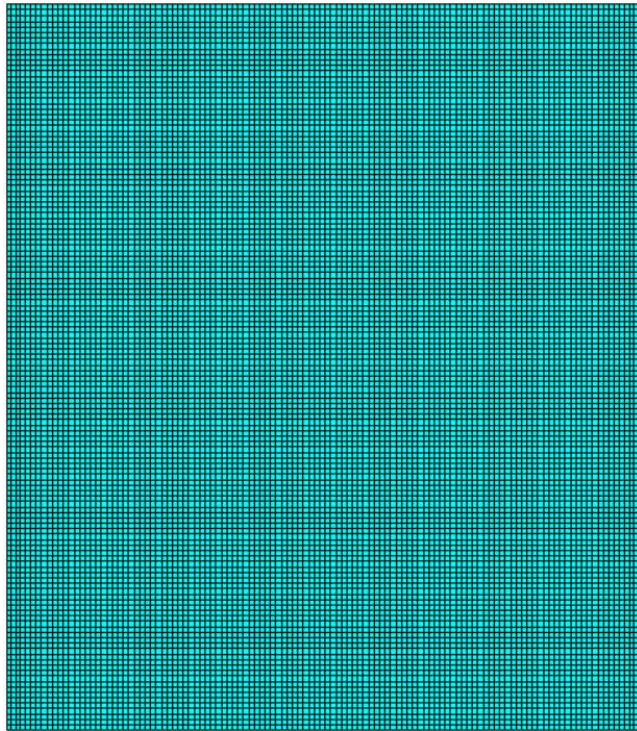
Figure 5.3. Finite Element Model of Constant Stiffness Plate

Table 5.2 Boundary Conditions for FEA

Edge	*Boundary Conditions*
Edge 1	$u_x = u_y = u_z = \theta_x = \theta_y = \theta_z = 0$
Edge 2	$u_x = u_z = \theta_x = \theta_y = \theta_z = 0$
Edge 3	At Knife Edge, $u_z = 0$
Edge 4	At Knife Edge, $u_z = 0$

5.1.3 Results

5.1.3.1 Buckling Results

To solve the buckling problem, a linear buckling solution has been made in the FEA software. The buckling load is found as 22.21 kN. The buckling mode is given below in Figure 5.4:
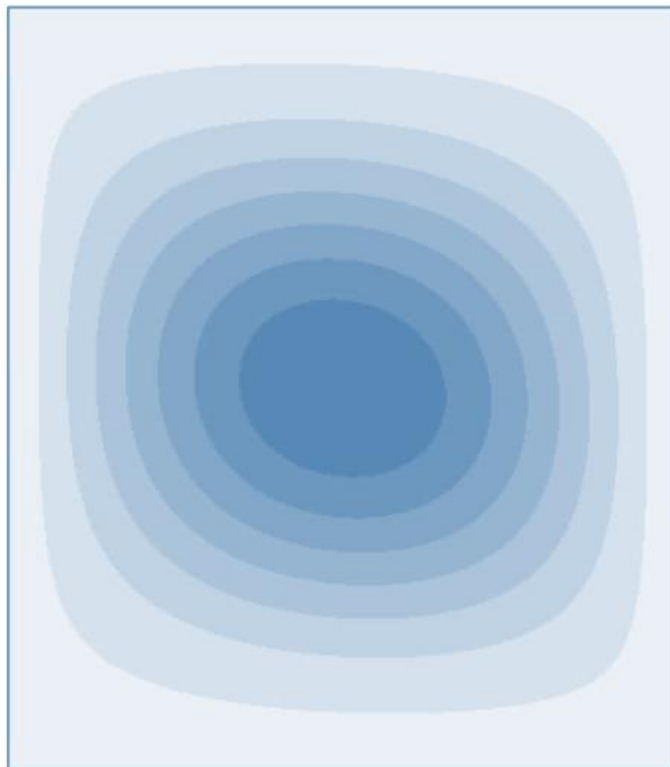
Figure 5.4. First Buckling Mode of Constant Stiffness Plate

5.1.3.2 Post-buckling Results with Progressive Failure

To determine the post-buckling behaviour of the composite plate, a non-linear static analysis is performed. The more detailed explanation of this analysis can be found in section 5.2.3.2. The post-buckling analysis results and experimental results are given in Table 5.3:

37

Table 5.3 First Ply Failure Results of Constant Stiffness Plate

Case	First Ply Failure Load (kN)
Test Results (2 Specimens Average)	81.2
Numerical Result	87.8
Difference (%)	8.1

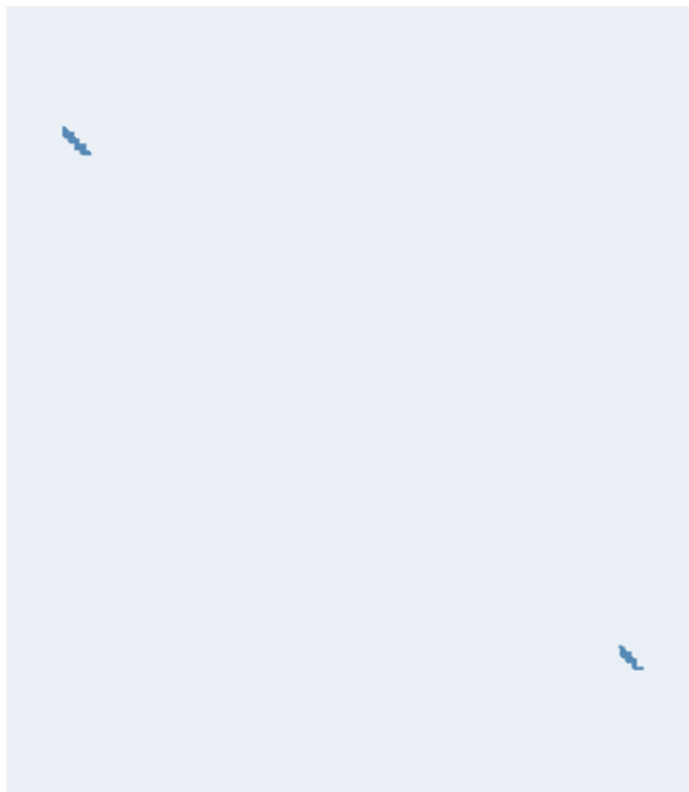The first ply failure plot of the plate is given in Figure 5.5:

Figure 5.5. First Ply Failure Plot of Constant Stiffness Plate

5.2   Variable Stiffness Plate Test

The quadratic Bezier curves are used in this thesis. These curves are flexible and linear angle variation curves can be achieved by modifying the position of P_2.

By using the test results, analysis method and script can be validated for further analysis where test set-up is not available.

5.2.1   Experimental Setup

The laminate used for the test has been built by 20 layers and is a rectangular plate with its dimensions as 508 mm in height, 381 mm in width. There is a circular cut-out (hole) in the middle of the plate of diameter 76.2 mm (1/5 of plate width). The plate geometry is given in Figure 5.6:
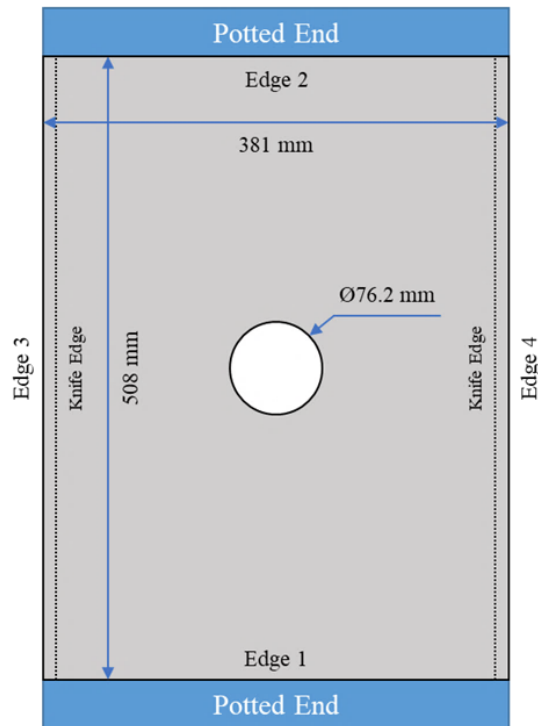

Figure 5.6. Plate Geometry of Variable Stiffness Plate

The plate has been connected to the test bench with clamps. At Edge 1 and Edge 2, the plate is fixed with potted ends. At 5 mm distance from Edge 3 and Edge 4, the plate is held with knife edges.

Material used for building the laminate is AS4/977-3 carbon-epoxy system. For elastic properties, this material data [24] has been used given in Table 5.4. In the

analysis, values of G_{13} and G_{23} are taken as equal to G_{12}. Also, values v_{13} and v_{23} are taken as equal to v_{12}.

Table 5.4 Elastic Properties of AS4/977-3 [24]

Parameter	Description	Value	Unit
E_1	Elastic Modulus in Longitudinal Direction	129.8	GPa
E_2	Elastic Modulus in Transverse Direction	9.2	GPa
G_{12}	Shear Modulus	5.1	GPa
v_{12}	Poisson's Ratio	0.36	-

In the scope of this test, the plate has been loaded until the failure. Therefore, strength data of the material system should be used in the analysis. This data has been found from [24] and given in Table 5.5.

Table 5.5 Strength Properties of AS4/977-3 [24]

Parameter	Description	Value	Unit
X_T	Tensile Strength in Longitudinal Direction	2070	MPa
X_C	Compression Strength in Longitudinal Direction	1160	MPa
Y_T	Tensile Strength in Transverse Direction	29	MPa
Y_C	Compression Strength in Transverse Direction	157.9	MPa
S_L	Shear Strength	91	MPa

After reaching the strength limit, the part starts to fail progressively. During the progress, strain energy is released by the part. After depleting all the energy, part fails. Strain energy release rate per unit area is found from experiment. It is also called fracture toughness. G_{2+} and G_6 values are determined for IM7/977-2 by using interlaminar test methods by Reeder [40]. G_{1+} and G_{1-} values are determined by Camanho [41] for IM7/8552. Energy dissipation rates per unit area are given in Table 5.6:

Table 5.6 Energy Dissipation Rates per Unit Area of AS4/977-3 [41]

Parameter	Description	Value	Unit
G_{1+}	Fiber Tension	81.5	J/mm^2
G_{1-}	Fiber Compression	106.3	J/mm^2
G_{2+}	Matrix Tension	0.31	J/mm^2
G_6	Matrix Compression	1.68	J/mm^2

The layup selected for the test plate is determined by Tatting et al. by considering the buckling behaviour. Based on the optimization, the optimum layup satisfying the best buckling result is $[\pm45/\pm< 45|60 >_2/\pm< 30|15 >/\pm< 45|60 >]_s$. The manufacturing limit for the turning radius of the AFP machine head is 635 mm. Therefore, the angle variation between inlet and exit angles are constrained by 15°. Also, outermost plies are covered with straight plies to prevent manufacturing defects at these plies. To minimize the thickness build-up due to overlapped plies and avoid resin-rich gaps to coincide due to tow-dropped plies, plies with the same configuration are staggered with respect to each other. The experimental setup can be seen in Figure 5.7.
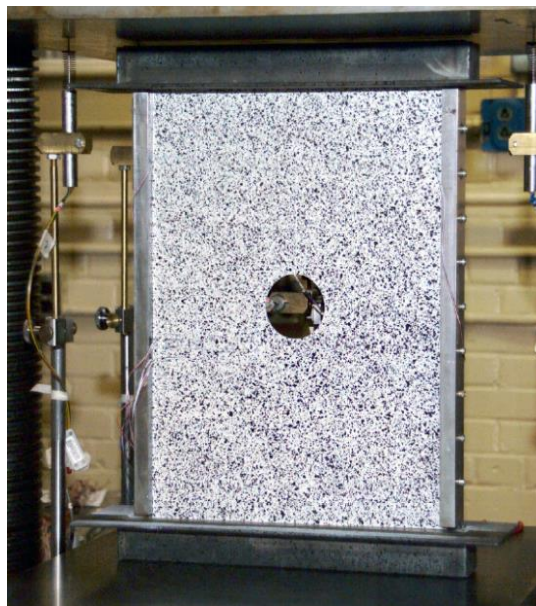
Figure 5.7. Experimental Setup of Variable Stiffness Plate [24]

5.2.2 Numerical Calculations (FEA)

The plate has been modeled in a commercial finite element analysis software (ANSYS Mechanical APDL) to simulate the experiment and an analysis methodology has been built for further cases. The purpose of the test is to validate the analysis methodology.

SHELL181 with Fully Integration element is used with 3 mm maximum element edge. The material is AS4/977-3. The finite element model is given in Figure 5.8.

Input parameters are fed into ANSYS Mechanical APDL and these parameters pass into a developed Python Script. Fiber orientations for each element is calculated by this script. Then, point cloud to assign fiber angles are read by ANSYS Mechanical APDL and shell definitions are made.
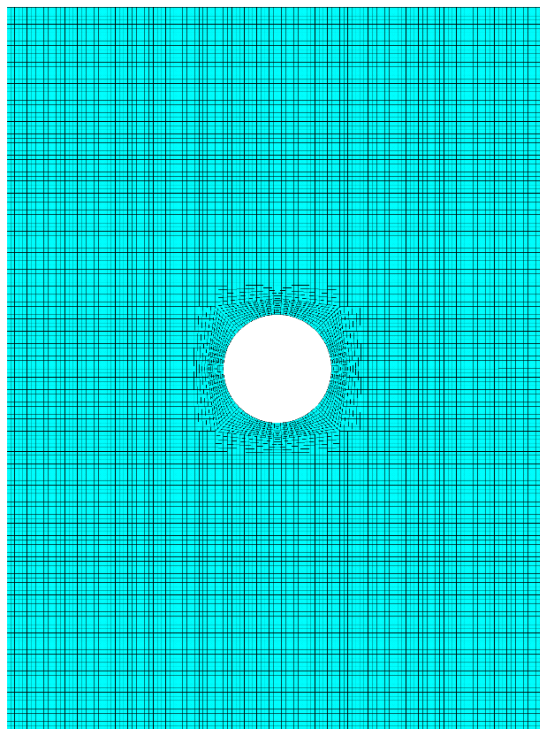
Figure 5.8. Finite Element Model of Variable Stiffness Plate

The number of the plies used for production is 20 for the plate. However, due to overlapped regions, which is a manufacturing defect, the maximum thickness of the

plate could rise to the thickness of 32 plies. Therefore, laminate thickness varies along the plate. Thickness build-up is mostly at the left and right edges of the plate due to increasing fiber orientation angle. Layer count distribution of the plate is given in Figure 5.9.

If the manufacturing conditions are considered, the plies are laid down onto the tool surface one by one. Therefore, the bottom surface is completely flat, and the free surface is not uniform due to thickness build-up of overlapped courses. To model this effect in finite element analysis, the reference surfaces of shell elements which contain the nodes have been shifted. To effectively consider the unsymmetrical loading effect and possible bending loads, reference surface of shell elements with minimum thickness kept at midsurface and reference surfaces of elements with greater thickness are shifted to same level of the shell element with minimum thickness. The methodology is illustrated in Figure 5.10.
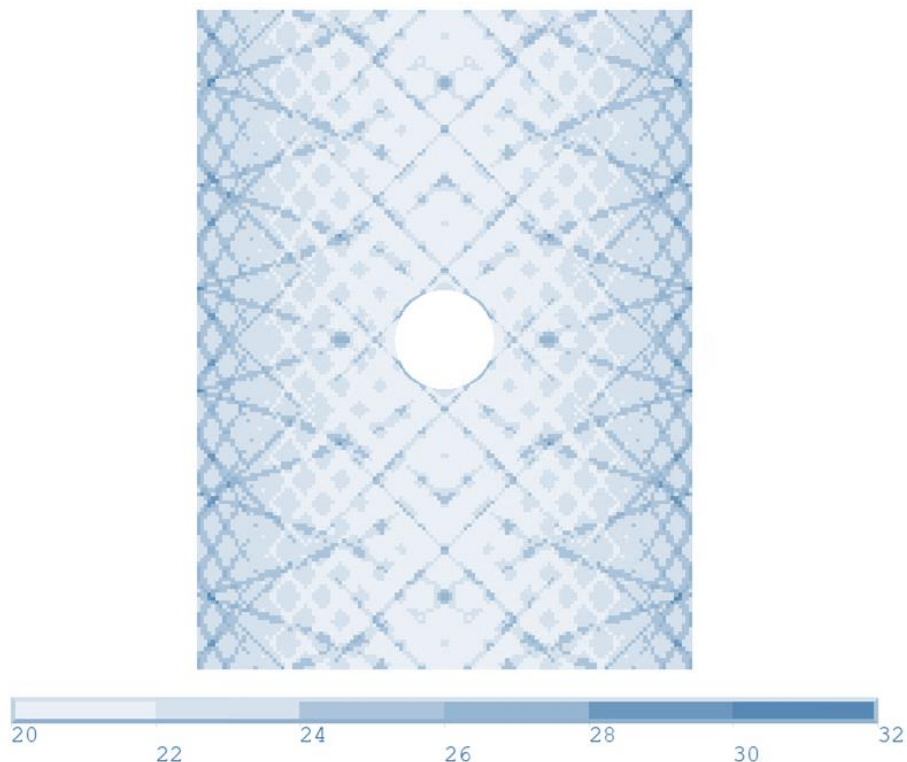
Figure 5.9. Layer Count Distribution

Figure 5.10. Middle Plane Offset Method

Boundary conditions for the analysis have been defined by considering the test conditions. In the previous section, experimental setup has been explained and shown in Figure 5.7. Upper and lower edges are clamped to the test bench. At the left and right edges, the plate has been held with knife edge clamps at 5 mm distance from the edges. Boundary conditions given in Table 5.7.

Table 5.7 Boundary Conditions for FEA

Edge	*Boundary Conditions*
Edge 1	$u_x = u_y = u_z = \theta_x = \theta_y = \theta_z = 0$
Edge 2	$u_x = u_z = \theta_x = \theta_y = \theta_z = 0$
Edge 3	At Knife Edge, $u_z = 0$
Edge 4	At Knife Edge, $u_z = 0$

5.2.3 Results

5.2.3.1 Buckling Results

Firstly, a linear eigenvalue buckling problem has been solved via FEA and the first two modes have been calculated. Unit end-shortening displacement load has been applied at Edge 1. First and second mode shapes are given in Figure 5.11.
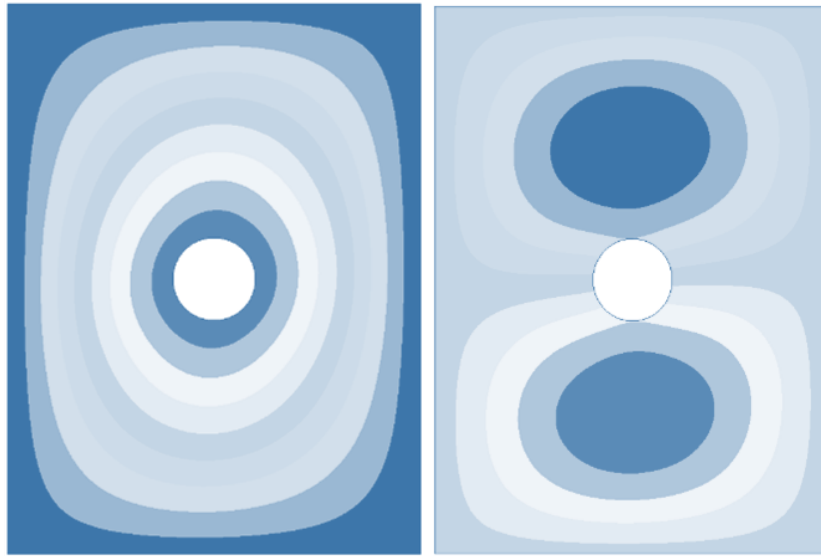
Figure 5.11. First and Second Buckling Modes

In the test, 3 specimens have been tested. Average buckling load from these 3 specimens have been calculated. Buckling result from numerical solution and experiment are given in Table 5.8.

Table 5.8 Buckling Results for VS Test Case

Case	*Buckling Load (kN)*
Test Results (3 Specimens Average)	27.3
Numerical Result	25.6
Difference (%)	6.6

Experimental results are quite close to the numerical results which can validate the analysis method for the buckling response.

5.2.3.2   Post-buckling Results with Progressive Failure

The nonlinear buckling analysis is conducted after solving a linear eigenvalue buckling problem. A perfect structure does not buckle under the compression load. However, there is not any perfect structure in nature which leads to buckling.

Therefore, an imperfection should be embedded into the finite element model. The buckling modes have been applied to the finite element model to create initial imperfections to cause the plate to buckle. Namdar and Darendeliler [21] applied the imperfections such that the amplitudes of these two mode shapes were 0.1 to 5 % of the total plate thickness. The positions of the corresponding nodes of the finite element model have been modified accordingly. The boundary condition is the same as in the linear eigenvalue buckling problem.

After a post-buckling analysis with progressive failure, first ply failure load has been calculated for this laminate. Experiment results and numerical results are given in Table 5.9.

Table 5.9 First Ply Failure Results of Variable Stiffness Plate

Case	First Ply Failure Load (kN)
Test Results (3 Specimen Average)	112.3
Numerical Result	115.3
Difference (%)	2.7

End shortening displacement is close to the test measurements as shown in Figure 5.12. The unknowns about the test setup such as manufacturing defects, curing process, test bench calibration could be the reason for this difference. The maximum difference between test result and numerical calculation is less than 10% for end-shortening displacement.

Then results show that the accuracy of analysis methodology is sufficiently enough to model actual behaviour. Therefore, this method could be used for other cases where experimental study is not available.

The progressive failure results of the plate in FEA is given in Figure 5.13.
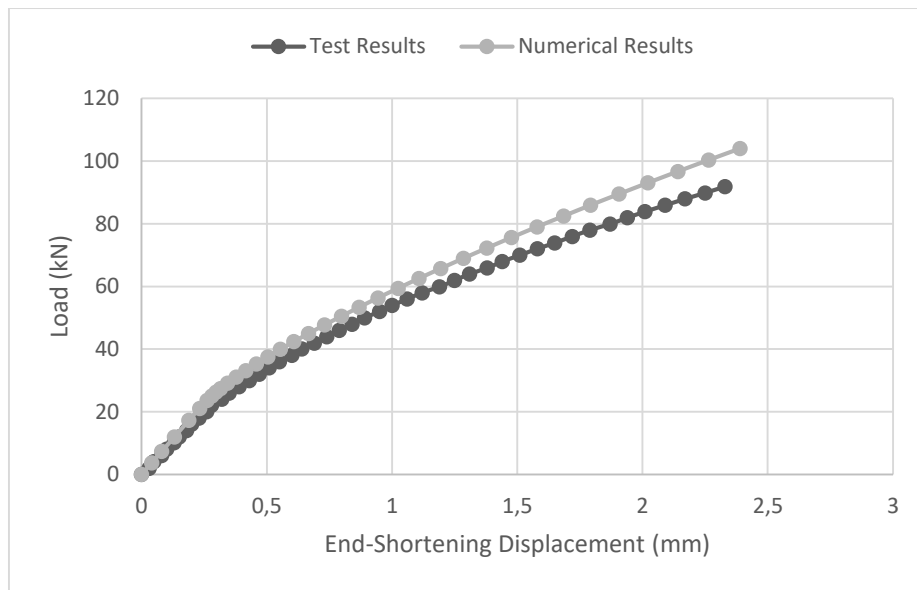
Figure 5.12. End-Shortening Displacement
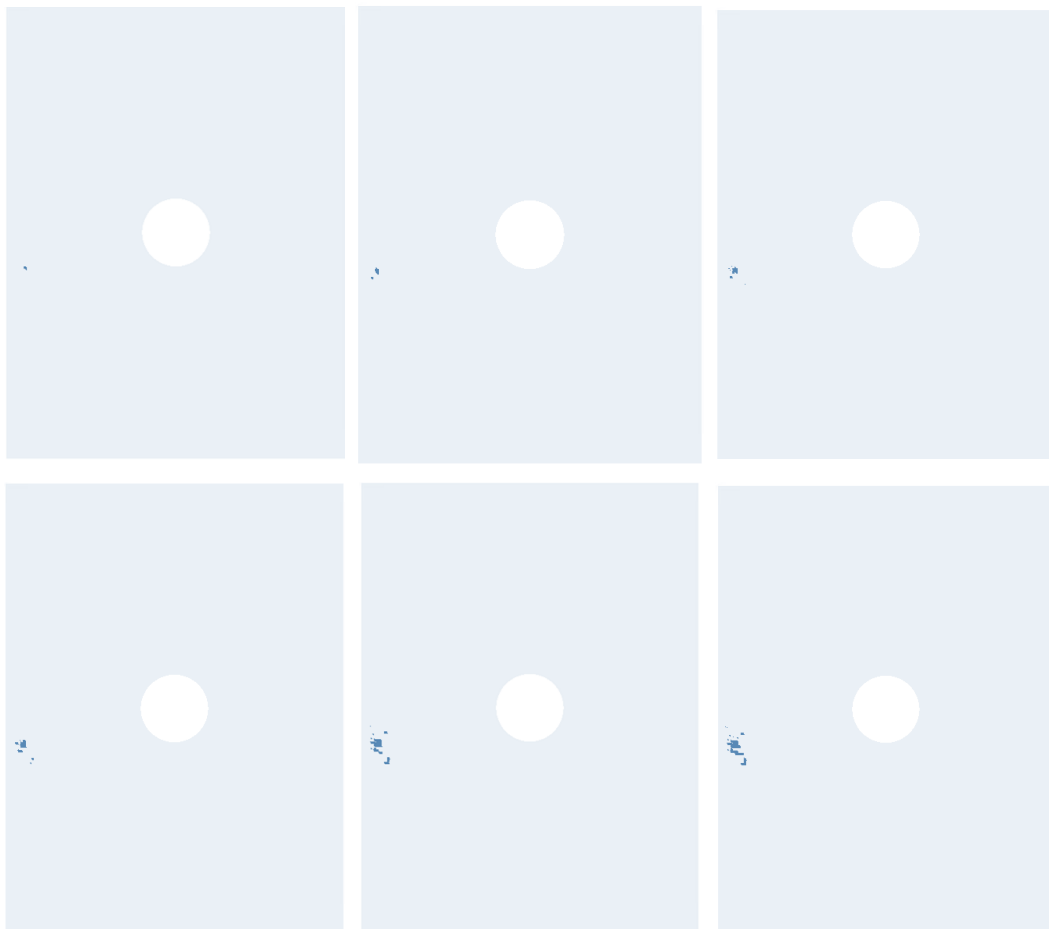
Figure 5.13. Progressive Failure of Test Plate

CHAPTER 6

BUCKLING AND POST-BUCKLING OF AN ARBITRARY VARIABLE STIFFNESS PLATE WITH PROGRESSIVE FAILURE

In this chapter, buckling and post-buckling analyses are carried out of a selected configuration variable stiffness plate with progressive failure. The selected configuration is $[\pm< 45|75 >]_{8s}$. Results of this configuration are compared with a quasi-isotropic plate with the configuration of $[45/0/-45/90]_{2s}$. These calculations have been conducted for 3 different cases. Cases are defined based on the geometry of the plate as:

- Case I: $b/a = 1$, $a = 300\ mm, b = 300\ mm$
- Case II: $b/a = 1.5$, $a = 300\ mm, b = 450\ mm$
- Case III: $b/a = 2$, $a = 300\ mm, b = 600\ mm$

where a is plate width and b is plate height. Plate has a hole at the geometric center with diameter, $D_h = a/5 = 60\ mm$. Plate geometry can be seen in Figure 6.1.

2 types of laminates have been constructed as linear angle variation and nonlinear angle variation. To model the laminates, a commercial finite element software, ANSYS Mechanical APDL, has been used with Python Script to calculate fiber paths. For the FEA, element edge size is 3 mm and element type is SHELL181 with Fully Integration. AS4/977-3 carbon-epoxy material is used. Boundary conditions for the model are selected as considering the actual test conditions and given in Table 5.7.
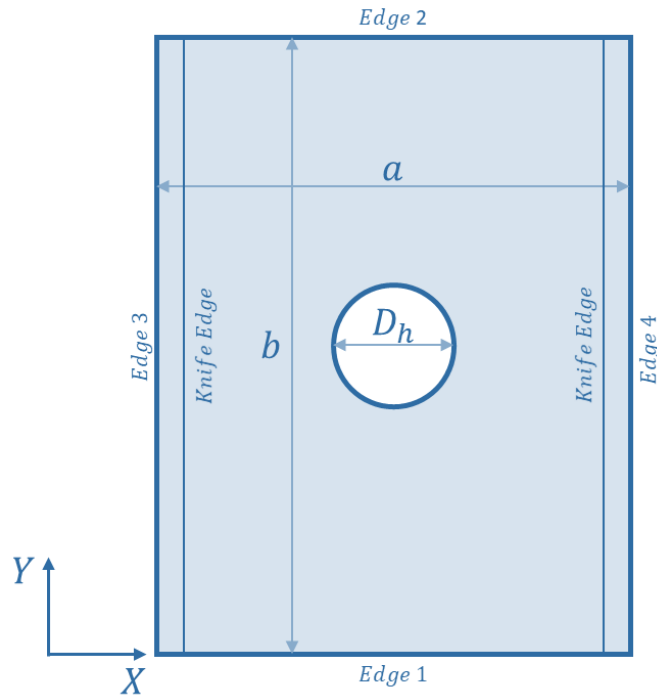
Figure 6.1. Plate Geometry

6.1 Buckling Analysis

6.1.1 Case I

In this case, plate geometry is square, and its edges are 300 mm in length ($a = 300\ mm$, $b = 300\ mm$). The inlet and exit angle have been used to define the laminate as $(\pm < T_1|T_2 >)_{8s}$. Total of 16 plies have been used to construct the laminate. It is a balanced and symmetric laminate. Analyses have been run for both linear angle variation and nonlinear angle variation (quadratic Bezier) as explained in the previous section. Numerical results are given in

Table 6.1. LAV and NAV plates perform better than the quasi-isotropic plate by 6.24 and 4.78 times respectively. Also, LAV achieves higher buckling load than NAV plate by 25%.

50

Table 6.1 Buckling Results of Case I for $[\pm < 45|75 >]_{8s}$

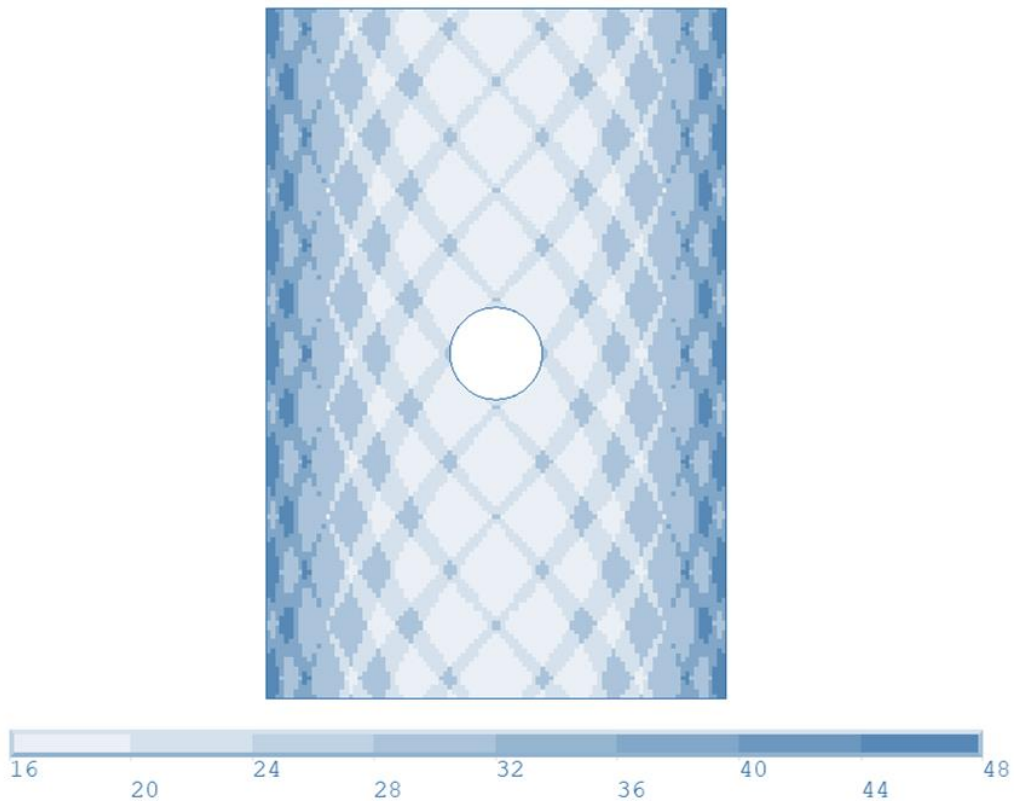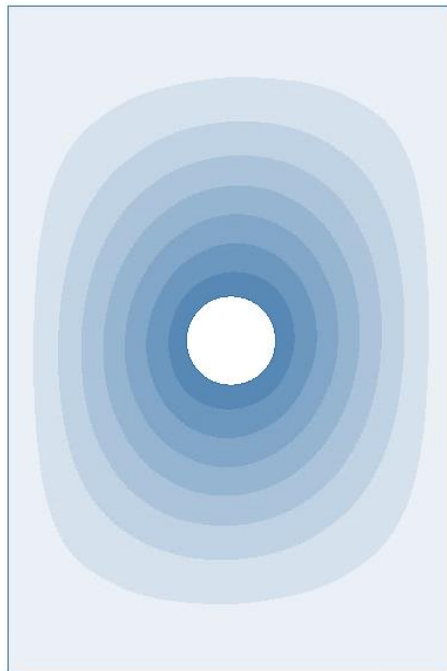| Case	N_{buck} (kN)
LAV	65.9
NAV	52.6
Quasi-Isotropic	9.1
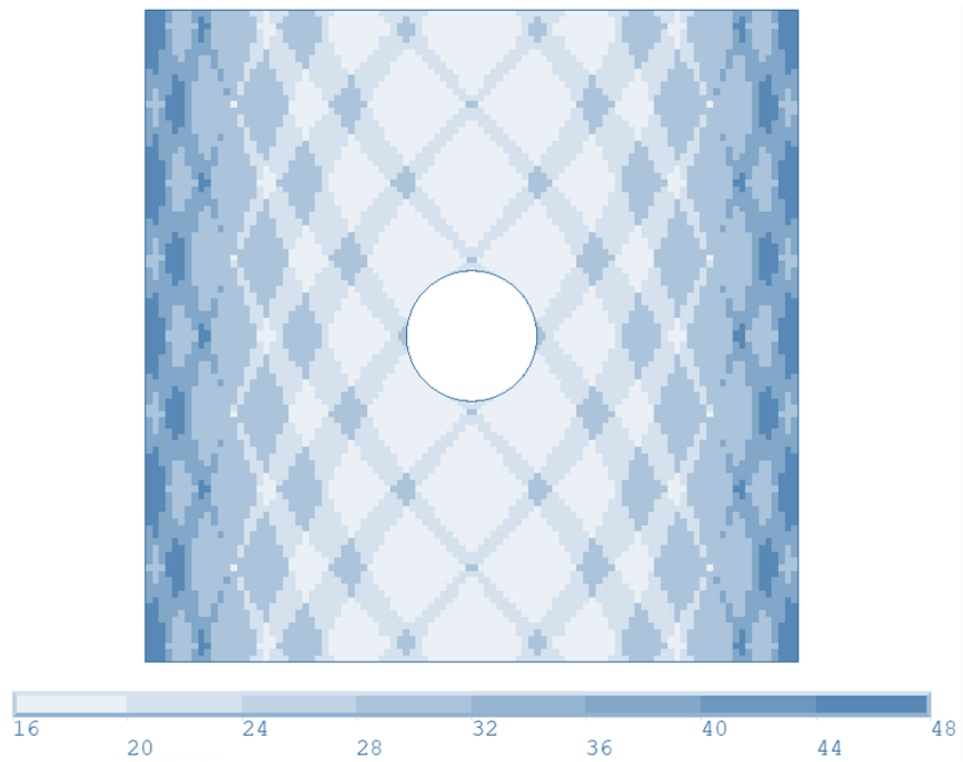
Figure 6.2. Thickness Distribution of Case I – LAV

51
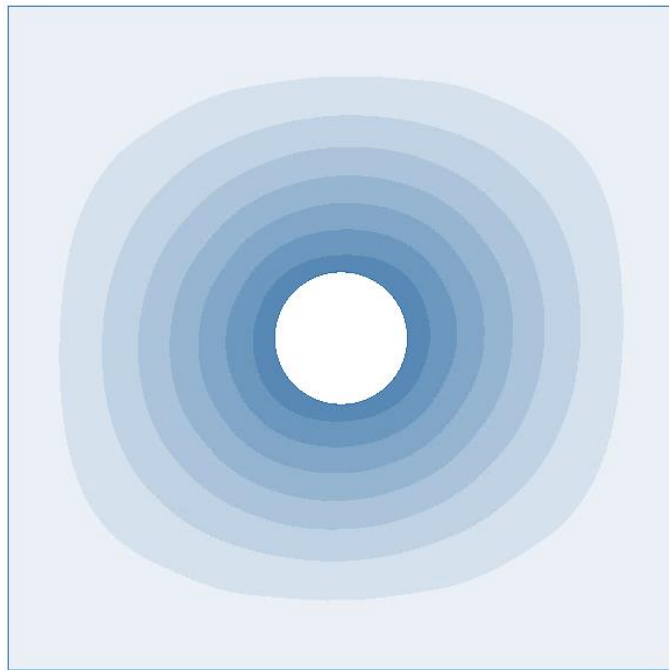
Figure 6.3. First Buckling Mode of Case I – LAV
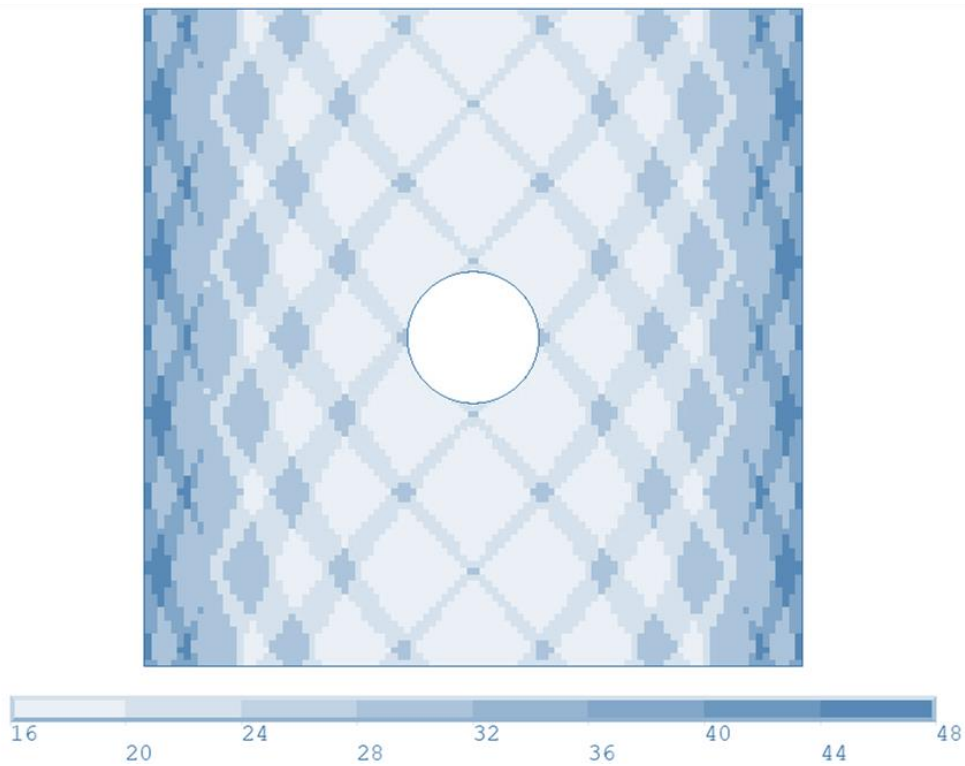
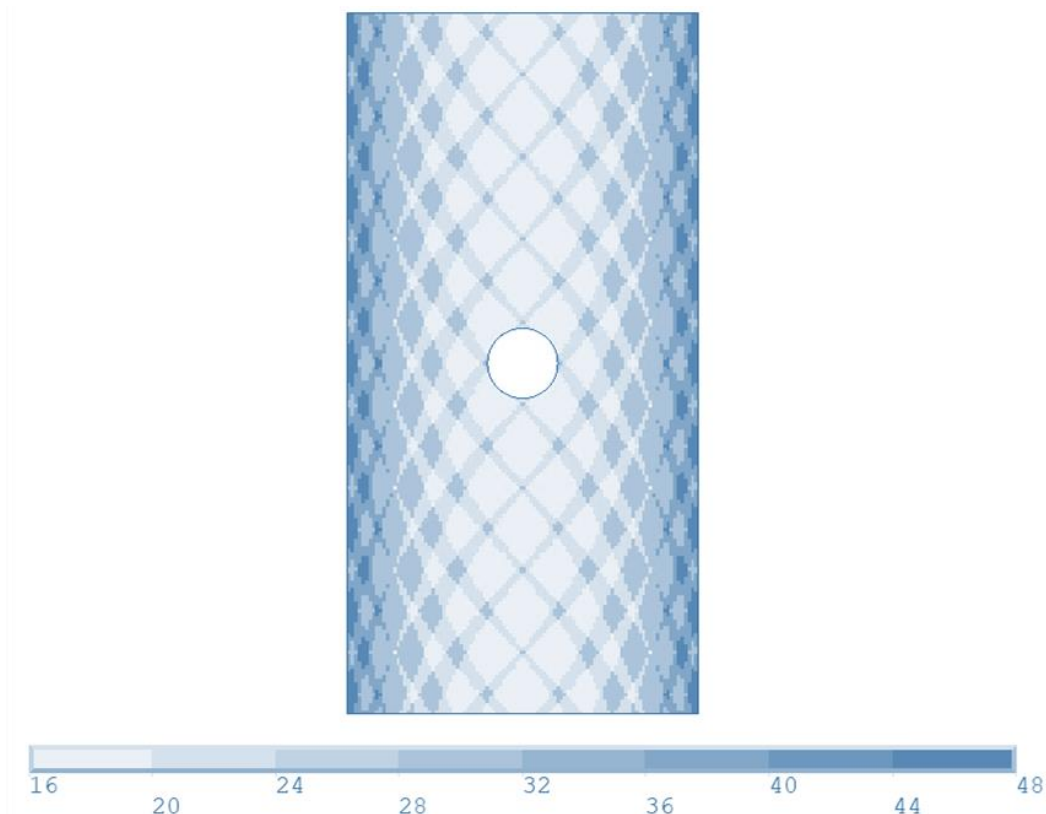Figure 6.4. Thickness Distribution of Case I – NAV
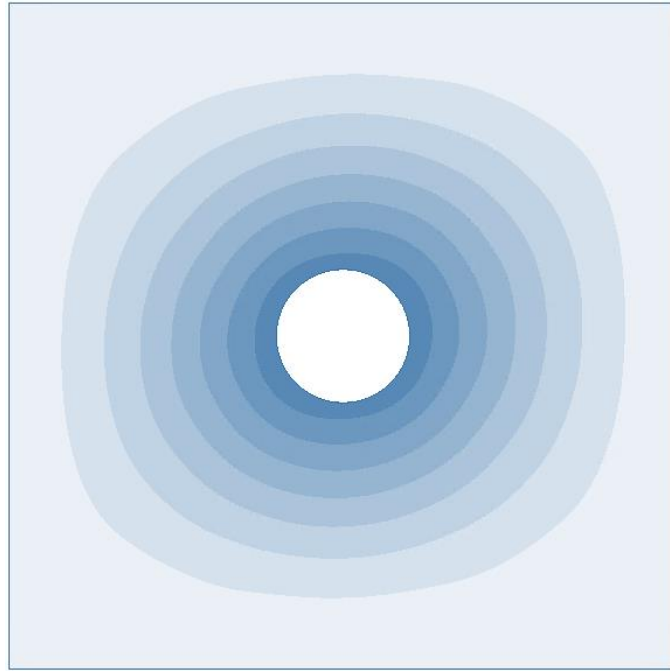
Figure 6.5. First Buckling Mode of Case I – LAV

6.1.2   Case II

In this case, height to width ratio is taken as 1.5. Therefore, the dimensions for the plate are 300 mm x 450 mm. Buckling results are found as in Table 6.2.

Table 6.2 Buckling Results of Case II for $[\pm < 45|75 >]_{8s}$

Case	N_{buck} (kN)
LAV	58.5
NAV	49.6
Quasi-Isotropic	8.4

As in Case I, VS plates perform better under the buckling loading than the quasi-isotropic plate. Buckling loads for LAV and NAV are 6.96 and 5.91 times of the quasi-isotropic plate. In addition, LAV configuration achieves higher buckling load than NAV plate by 18%.
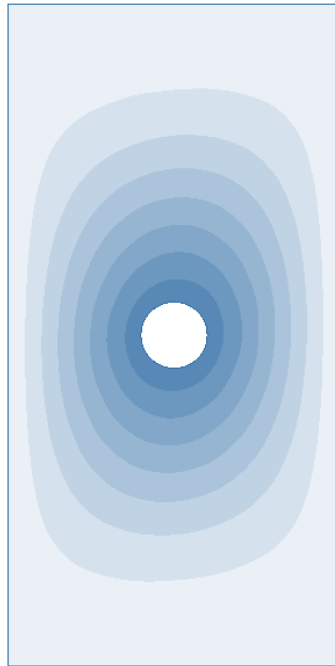
Figure 6.6. Thickness Distribution of Case II – LAV

Figure 6.7. First Buckling Mode of Case II – LAV
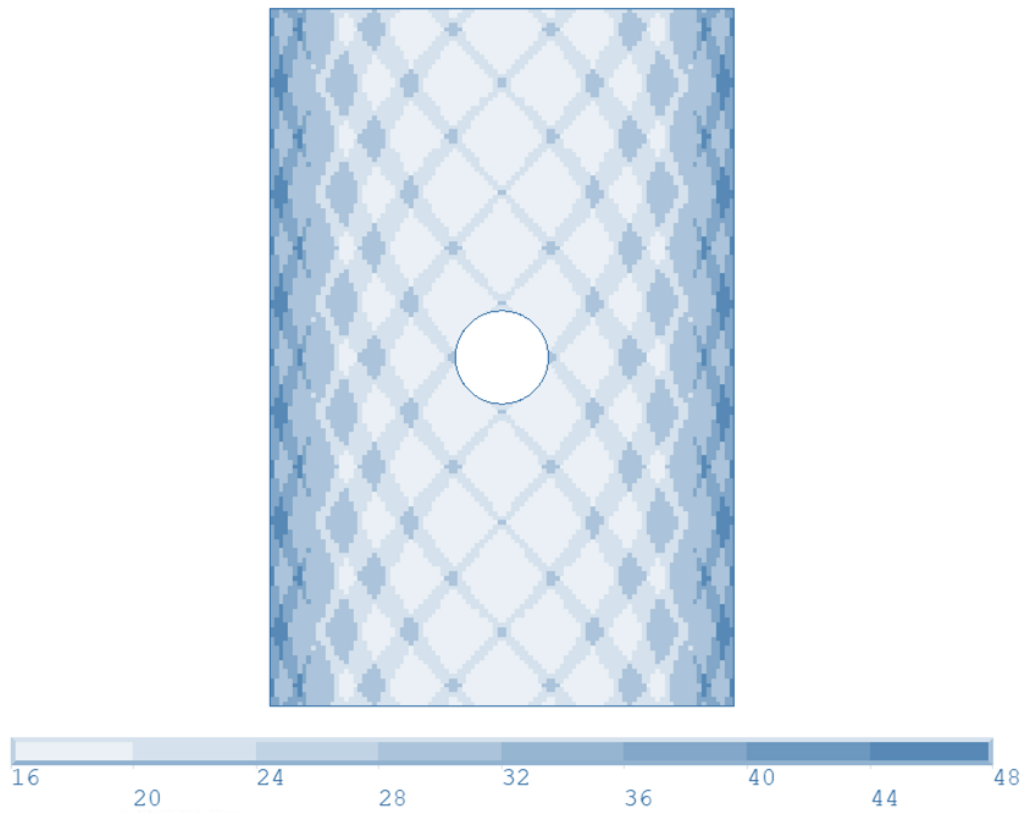
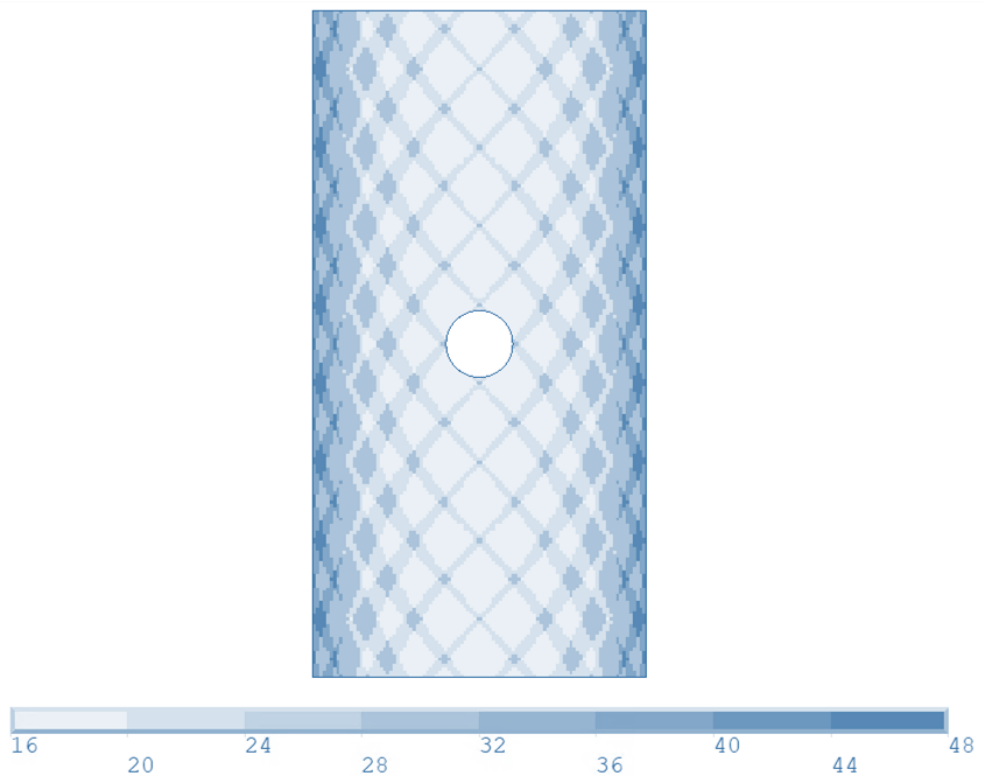Figure 6.8. Thickness Distribution of Case II – NAV
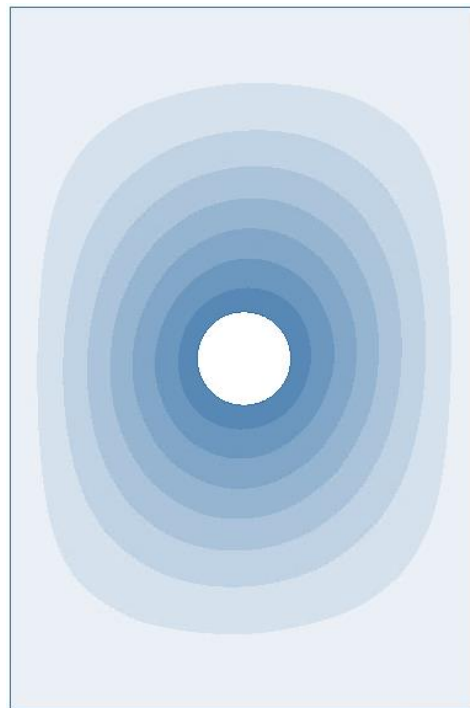
Figure 6.9. First Buckling Mode of Case II – NAV

6.1.3   Case III

For the last case, plate geometry is selected as 300 mm x 600 mm. Its height to width ratio is increased to 2. Buckling results of this case is given in Table 6.3.

Table 6.3 Buckling Results of Case II for $[\pm<45|75>]_{8s}$

Case	N_{buck} (kN)
LAV	66.7
NAV	60.6
Quasi-Isotropic	8.2

As a result, LAV and NAV configuration performs better than the quasi-isotropic plate by 8.13 and 7.39 times. Also, LAV plate outperforms the NAV plate by 10%.

Figure 6.10. Thickness Distribution of Case III – LAV

Figure 6.11. First Buckling Mode of Case III – LAV

Figure 6.12. Thickness Distribution of Case III – NAV
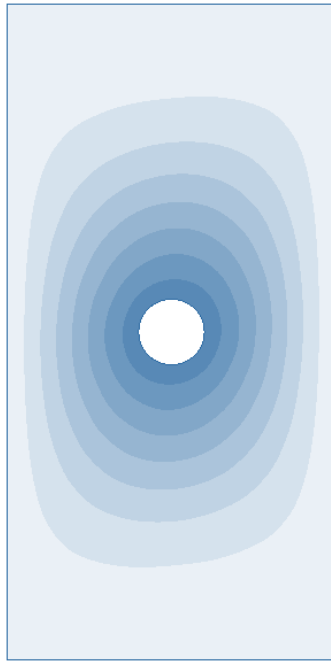
Figure 6.13. First Buckling Mode of Case III – NAV

6.2 Post-Buckling Results with Progressive Failure

In this section, post-buckling analysis of previously calculated variable stiffness laminates in 6.1. Post-buckling analysis is run by using the same finite element model by enabling large deformation and nonlinear analysis options. Analysis method is explained in 5.2.3.2.

6.2.1 Case I

The first case was the plate with dimensions of 300x300 mm. Angle configuration was $[\pm< 45|75 >]_{8s}$ for both LAV and NAV plates. Results are given in

Table 6.4.

VS concept improves the first ply failure greatly compared to quasi-isotropic configuration. The LAV and NAV configurations fail at loads 3.79 and 3.38 times higher than the quasi-isotropic configuration. Also, LAV outperforms the NAV by

58

12.2% in first ply failure load. Failure of the plates for LAV and NAV are given in Figure 6.14 and Figure 6.15, respectively.

Table 6.4 First Ply Failure Loads of Case I for $[\pm< 45|75 >]_{8s}$

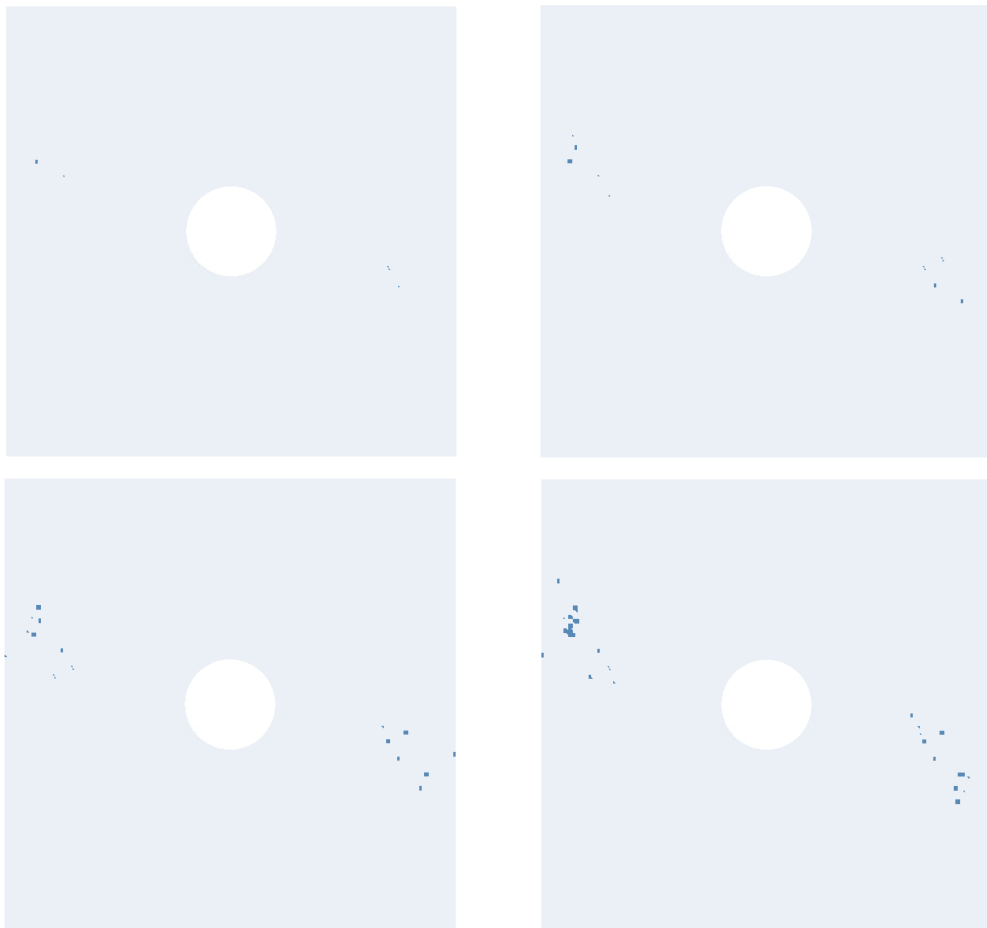| Case	N_{fpf} (kN)
LAV	218.6
NAV	194.9
Quasi-Isotropic	57.6

Figure 6.14. Progressive Failure of Case I for $[\pm< 45|75 >]_{8s}$ – LAV
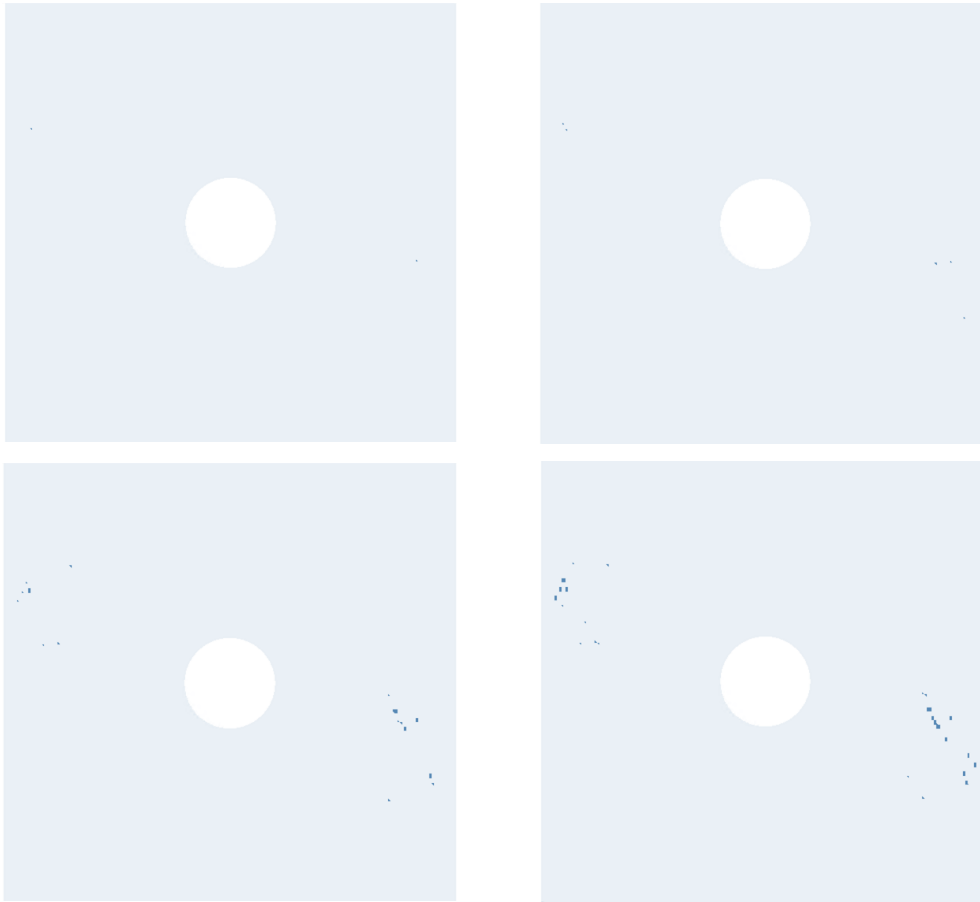
Figure 6.15. Progressive Failure of Case I for $[\pm < 45|75 >]_{8s} - \text{NAV}$

6.2.2   Case II

In this case, aspect ratio is taken as 1.5 which makes the dimensions for the plate is 300 mm x 450 mm. Results are given in Table 6.5:

Table 6.5 First Ply Failure Loads of Case II for $[\pm < 45|75 >]_{8s}$

Case	N_{fpf} (kN)
LAV	208.6
NAV	187.2
Quasi-Isotropic	53.7

LAV and NAV plates exhibit better post-buckling performance compared to quasi-isotropic. First ply failure load of LAV configuration is 3.88 times of the first ply failure load of quasi-isotropic configuration. For NAV, it is 3.49 times. Also, LAV configuration performs better than the NAV configuration by 11.43%. Failure of the plates for LAV and NAV are given in Figure 6.16 and Figure 6.17, respectively.
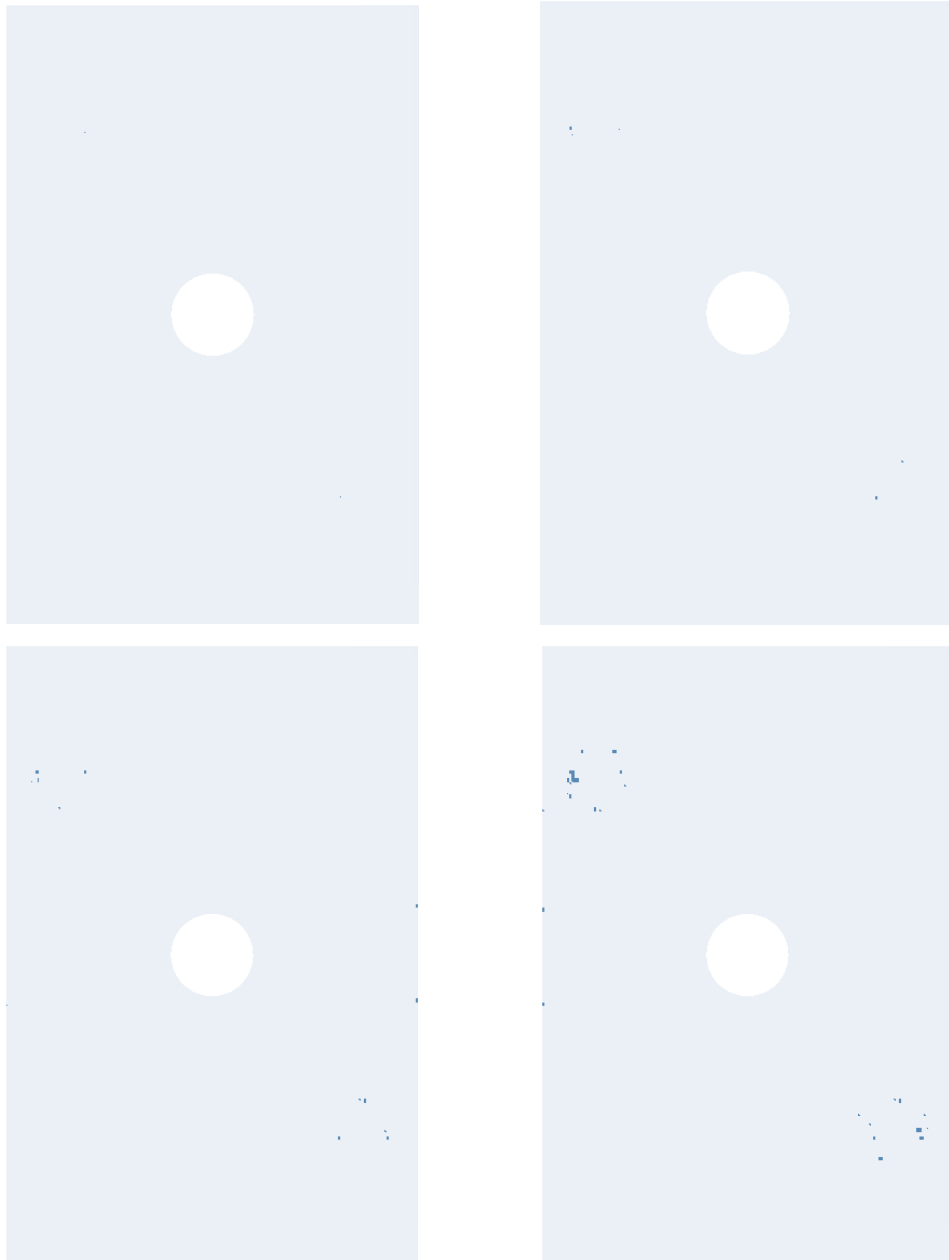

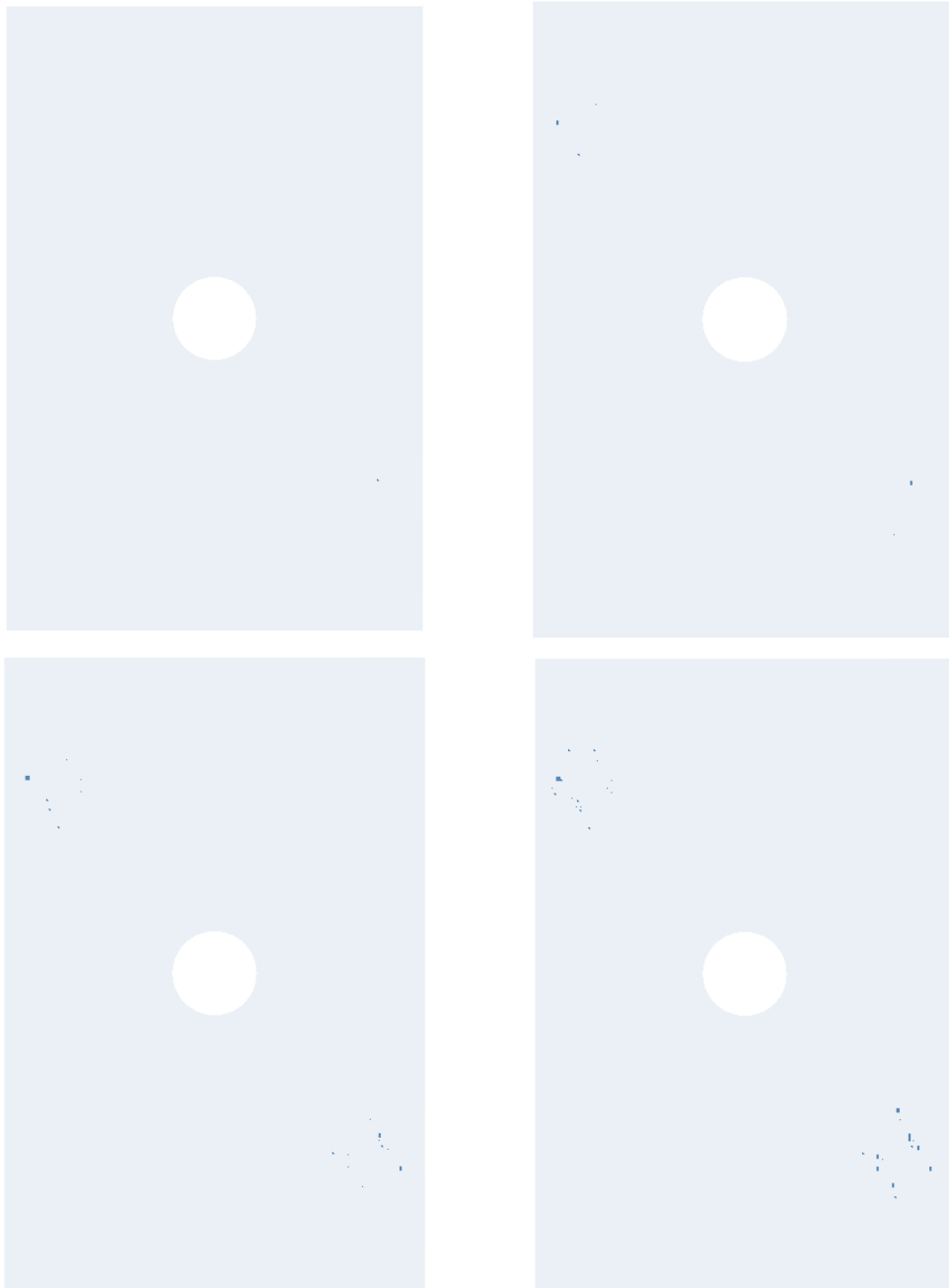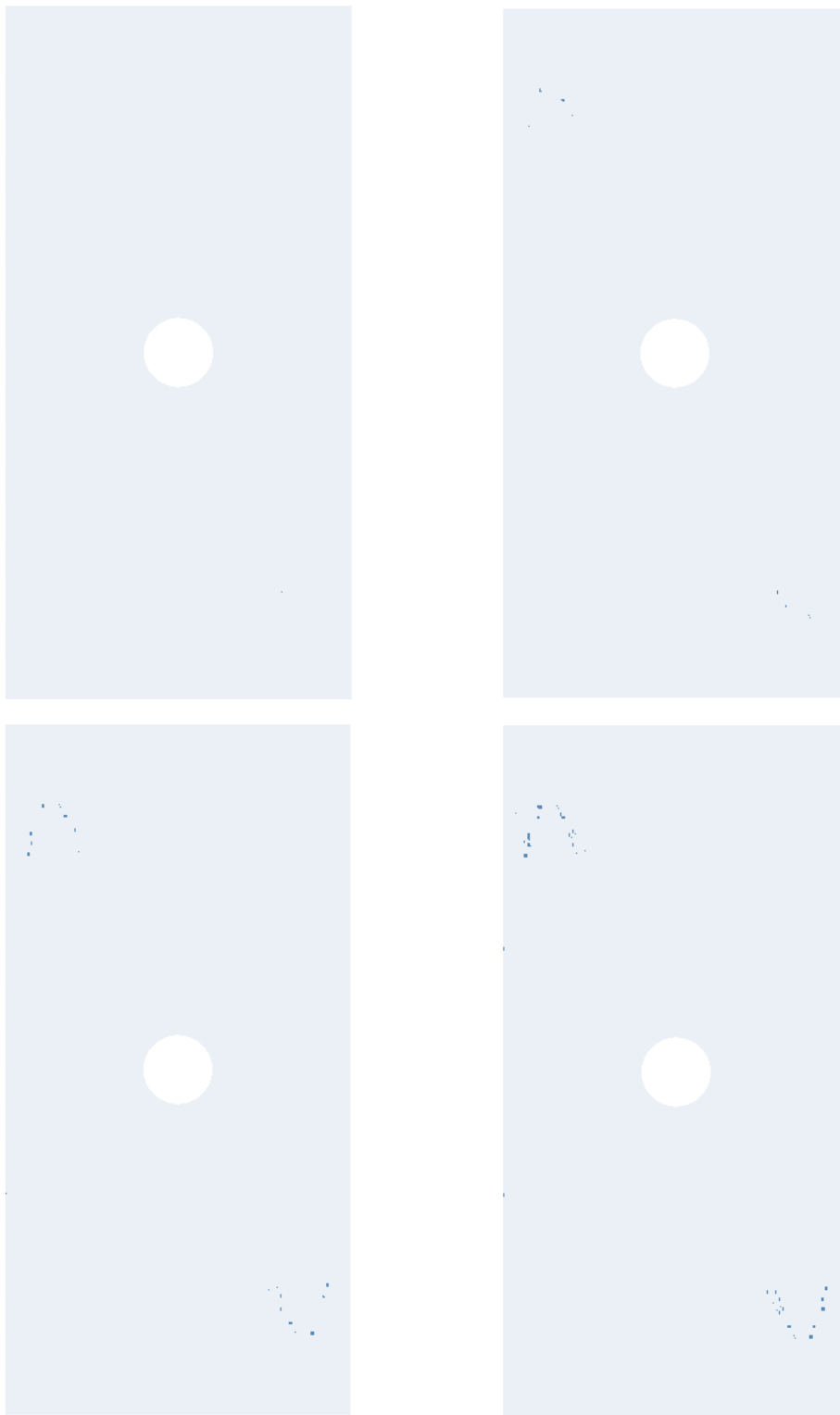Figure 6.16. Progressive Failure of Case II for $[\pm< 45|75 >]_{8s} - $ LAV

Figure 6.17. Progressive Failure of Case II for $[\pm < 45|75 >]_{8s} - \text{NAV}$

6.2.3   Case III

In this case, a rectangular plate with 300 mm x 600 mm dimensions has been analyzed by using both linear and nonlinear angle variation fiber paths. First ply failures of the plates are given in Table 6.6:

Table 6.6 First Ply Failure Loads of Case III for $[\pm< 45|75 >]_{8s}$

Case	N_{fpf} (kN)
LAV	193.0
NAV	171.8
Quasi-Isotropic	52.0

VS concept improves the post-buckling behaviour as in Case I and Case II. LAV configuration achieves a first ply failure load 3.71 times of quasi-isotropic case. For NAV, it is 3.30 times. Furthermore, LAV performs better by 12.34% than NAV. Failure of the plates for LAV and NAV are given in Figure 6.18 and Figure 6.19, respectively.

Figure 6.18. Progressive Failure of Case III for $[\pm < 45|75 >]_{8s} - \text{LAV}$
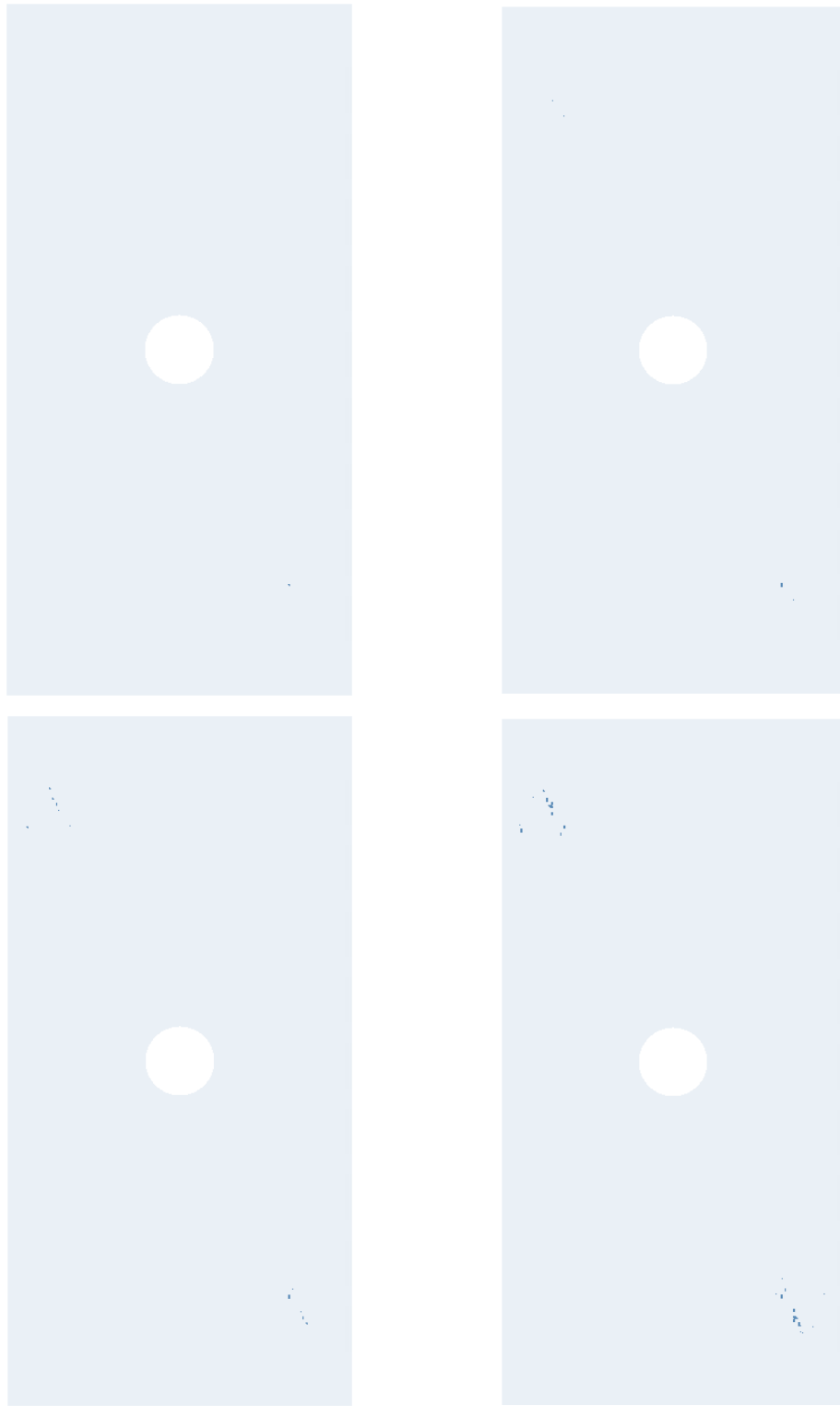
Figure 6.19. Progressive Failure of Case III for $[\pm< 45|75 >]_{8s} - \text{NAV}$

CHAPTER 7

BUCKLING AND POST-BUCKLING RESPONSE OF OPTIMUM VARIABLE STIFFNESS LAMINATE

3 different cases are investigated in this thesis to observe buckling responses of the VS laminates. Cases are defined based on the geometry of the plate as:

- Case I: $b/a = 1,$ $a = 300 \ mm, b = 300 \ mm$
- Case II: $b/a = 1.5,$ $a = 300 \ mm, b = 450 \ mm$
- Case III: $b/a = 2,$ $a = 300 \ mm, b = 600 \ mm$

where a is plate width and b is plate height. Plate has a hole at the geometric center with diameter, $D_h = a/5 = 60 \ mm$. Plate geometry can be seen in Figure 7.1.
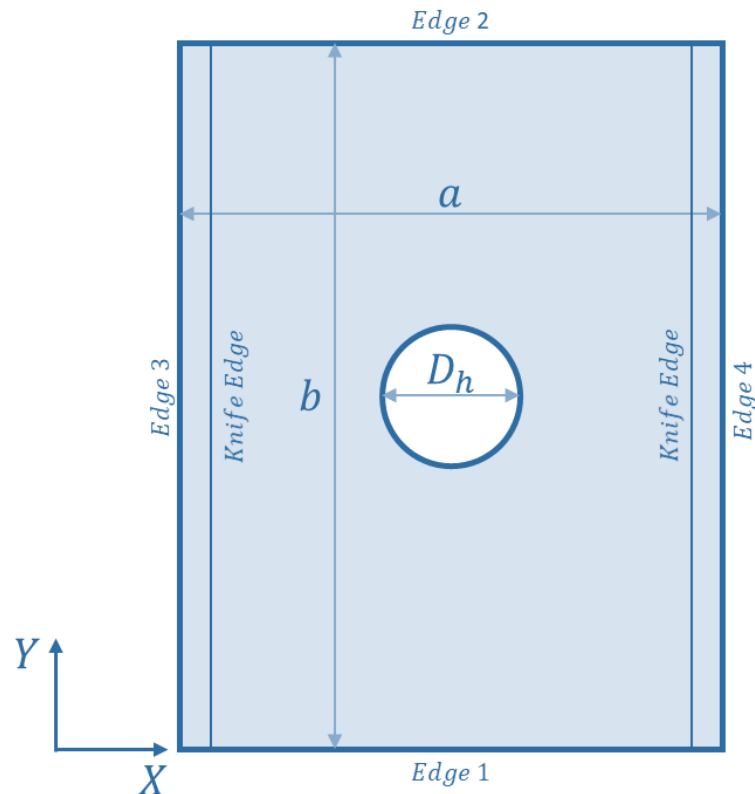

Figure 7.1. Plate Geometry

2 types of laminates have been constructed as linear angle variation and nonlinear angle variation. To model the laminates, a commercial finite element software, ANSYS Mechanical APDL, has been used with Python Script to calculate fiber paths. For the FEA, SHELL181 with Fully Integration element with 3 mm element edge size is selected.

Boundary conditions for the model are selected as considering the actual test conditions and given in Table 5.7.

To compare these two types of laminates, an optimization cycle has been run and the optimum angle configuration for these two types of angle variation type has been selected. The optimization objective is to maximize the buckling load and the performance constant mentioned below. The constraint for this optimization is the minimum curvature radius. According to [13], the minimum radius of curvature of an AFP machine is 635 mm.

The performance constant is also defined to consider the overlap differences. For example, a plate with a greater overlapped region is more likely to have greater buckling load due to increased stiffness because of increased stiffened regions. However, the mass of a plate also increases with increasing overlapped regions. Therefore, greater buckling load may not always the best solution. The main reason to use composite material is their higher strength with lower mass compared to traditional material. Therefore, mass should also be minimized to achieve the optimum design point. To achieve higher buckling load with lower mass, a constant can be defined to use as an optimization objective. It is defined as:

$$C_{perf} = \frac{N_{Buck}}{m_{plate}} \tag{7.1}$$

For the optimization, the Design Xplorer module of ANSYS Workbench has been used. Properties of the optimization is given below:

- Design of Experiment with Optimal Space Filling (OSF)
- Response Surface with Genetic Aggregation (GA)

- Multiobjective Genetic Algorithm (MOGA) utilizing Non-dominated Sorted Genetic Algorithm-II (NSGA-II)

The optimization cycle consists of two subcycles. In the first cycle, 50 design points have been created by using OSF algorithm for design of experiment. These points have been solved by using previously described finite element methodology in Chapter 5. Based on the results of these 50 design points, a response surface has been created by using Genetic Aggregation. Lastly, optimization is conducted by using this response surface with MOGA method. The software returns the optimum design point. This point is used for the second subcycle where design space is reduced to a range of 20° around the optimum point. In this subcycle, 25 design points are created by using the same procedure. Coşkun et al. [11] showed that the used number of design points satisfies the convergence of response surface. Also, quality metrics of the response surfaces are in acceptable levels. At the end of the second subcycle, the best design point is found. This point found from the response surface is also validated with FEM. The optimization procedure is illustrated in Figure 7.2.
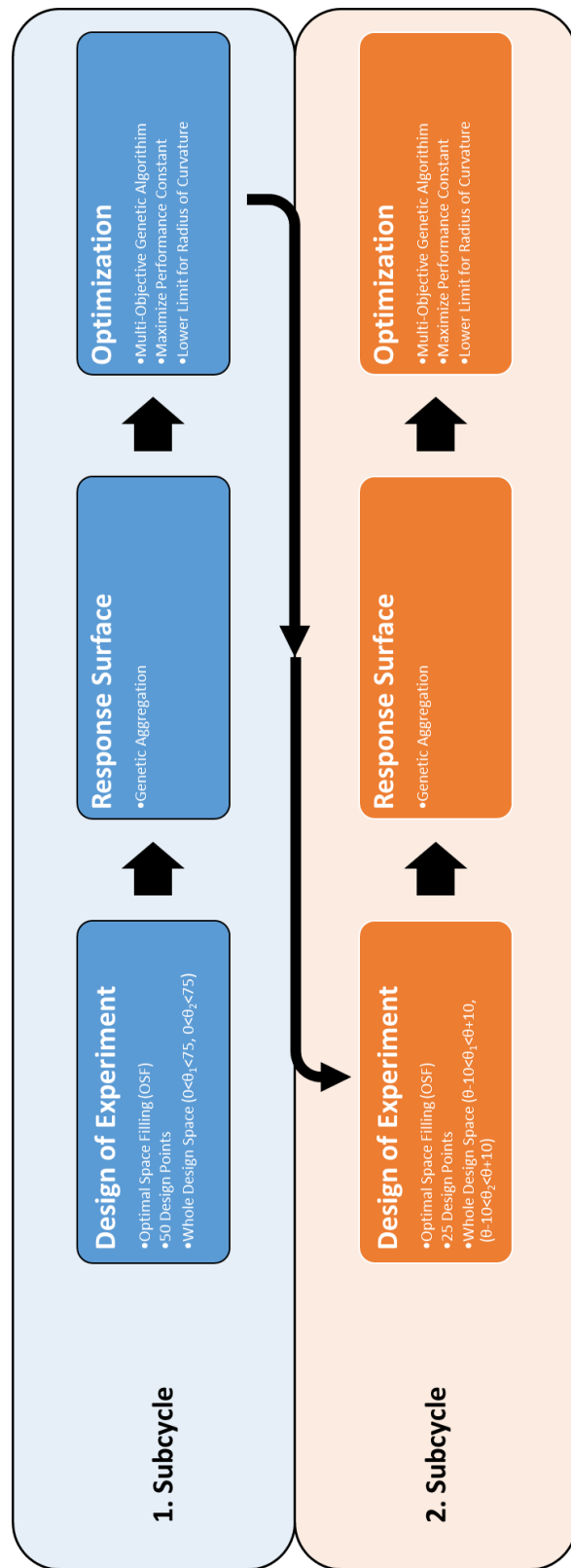
1. Subcycle

Design of Experiment
- Optimal Space Filling (OSF)
- 50 Design Points
- Whole Design Space ($0 < \theta_1 < 75$, $0 < \theta_2 < 75$)

Response Surface
- Genetic Aggregation

Optimization
- Multi-Objective Genetic Algorithim
- Maximize Performance Constant
- Lower Limit for Radius of Curvature

2. Subcycle

Design of Experiment
- Optimal Space Filling (OSF)
- 25 Design Points
- Whole Design Space ($\theta - 10 < \theta_1 < \theta + 10$, ($\theta - 10 < \theta_2 < \theta + 10$)

Response Surface
- Genetic Aggregation

Optimization
- Multi-Objective Genetic Algorithim
- Maximize Performance Constant
- Lower Limit for Radius of Curvature

Figure 7.2. Optimization Cycle

7.1 Buckling Results

7.1.1 Case I

For this case, dimensions of the plate are selected as 300 mm for both edges ($a = 300\ mm,\ \ b = 300\ mm$). Angle configuration of the plate is defined as $(\pm< T_1|T_2 >)_{8s}$. 16 plies have been used to build the laminate. It is a balanced and symmetric laminate.

The optimization cycle has been run for both linear angle variation and nonlinear angle variation (quadratic Bezier) as explained in the previous section. The optimum results for both cases and results are given in Table 7.1.

Table 7.1 Optimization Results for Case I

Case	Configuration	N_{buck} (kN)	C_{perf} (kN)	m_{plate} (g)
Buckling Load				
LAV	$[\pm< 52.625|74.99 >]_{8s}$	53.7	109.6	490
NAV	$[\pm< 47.535|74.943 >]_{8s}$	49.8	104.3	478
Performance Criteria				
LAV	$[\pm< 52.628|74.994 >]_{8s}$	53.7	109.6	490
NAV	$[\pm< 47.529|74.95 >]_{8s}$	49.9	104.4	478

As it can be seen in the table, the optimum results for the linear angle variation case performs better than the nonlinear angle variation case both in case of buckling load and performance constant. The buckling load and the performance constant are 7.6% and 5% higher, respectively for the LAV configuration. The thickness distribution and first buckling modes for both cases are given from Figure 7.3 to Figure 7.6. Also, response surfaces for optimization cycles are given in Figure 7.7 and Figure 7.8.
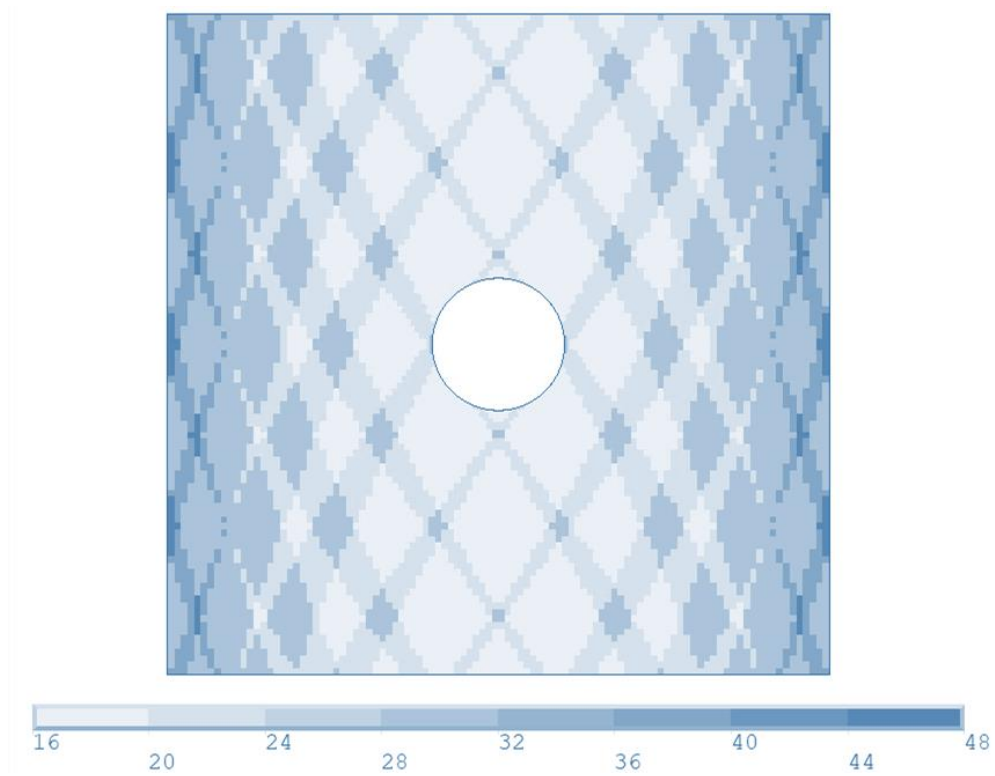
Figure 7.3. Thickness Distribution of Case I - LAV
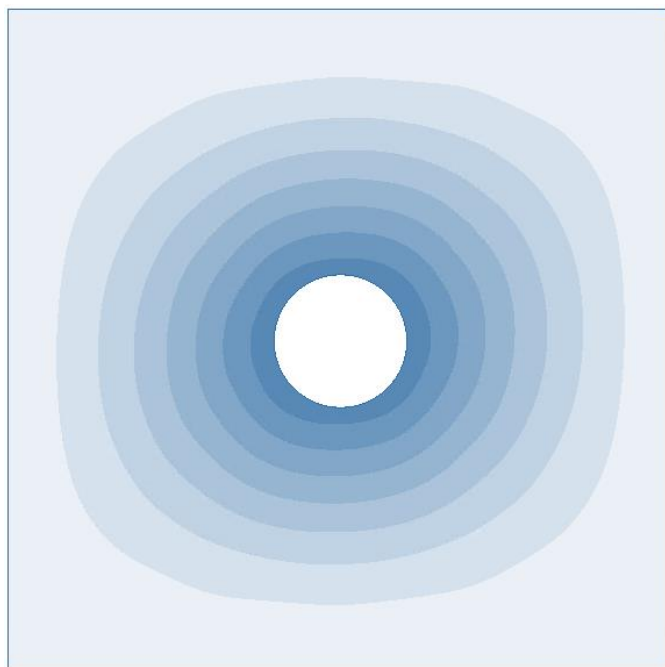
Figure 7.4. First Buckling Mode of Case I - LAV
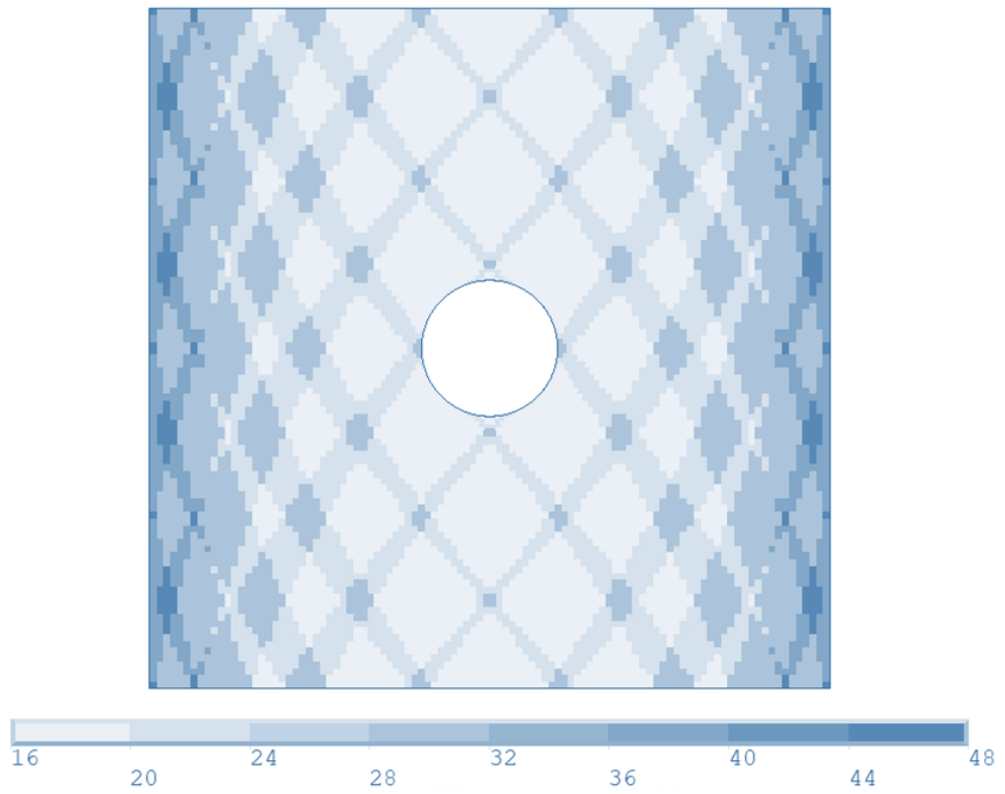
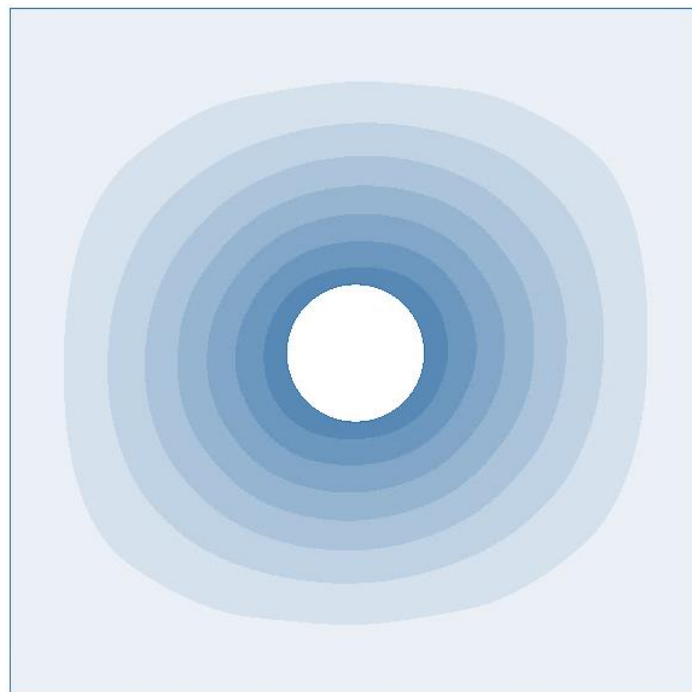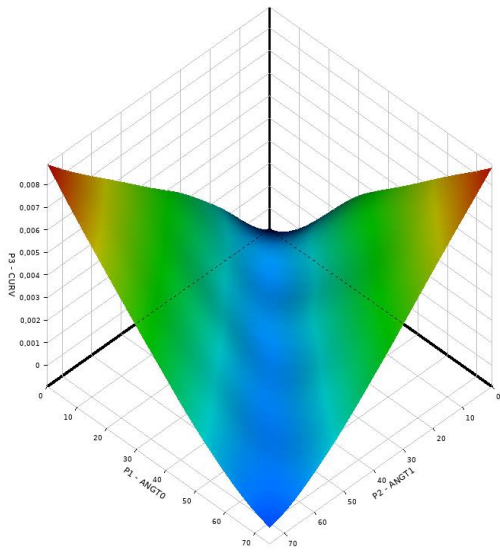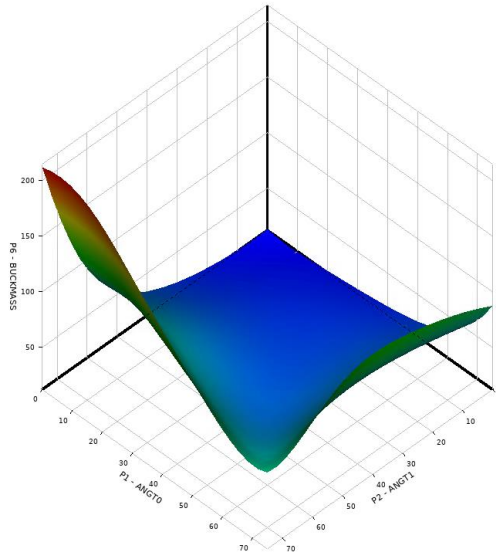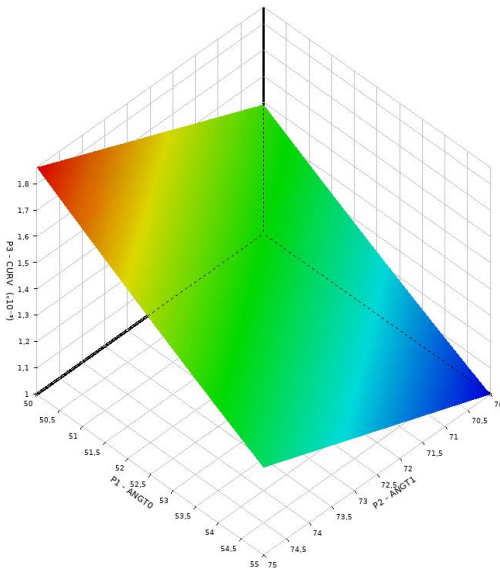Figure 7.5. Thickness Distribution of Case I - NAV

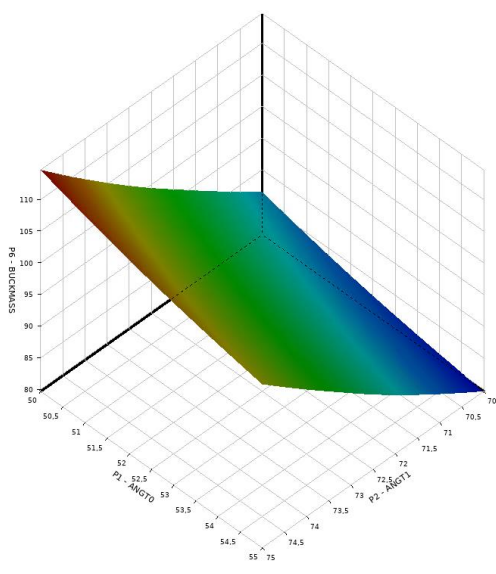Figure 7.6. First Buckling Mode of Case I – NAV

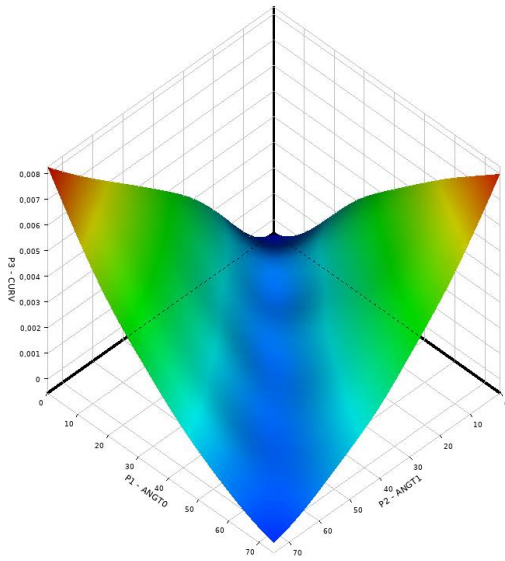a. SC1 – Curvature

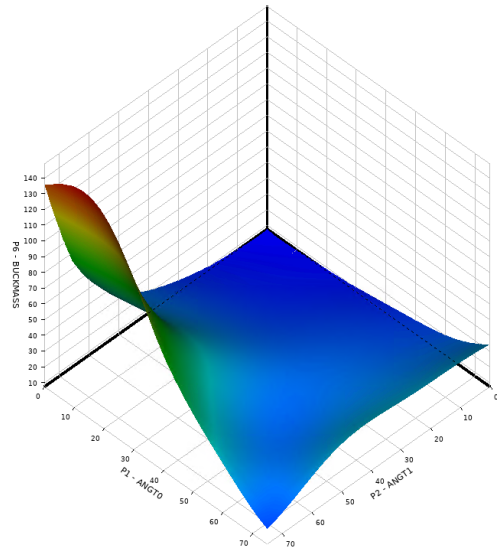b. SC1 – Performance Constant
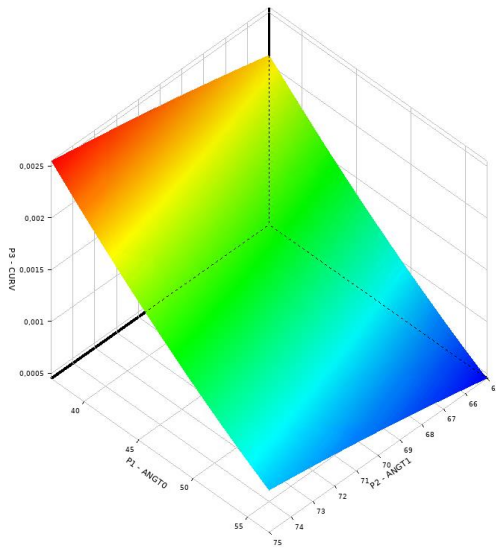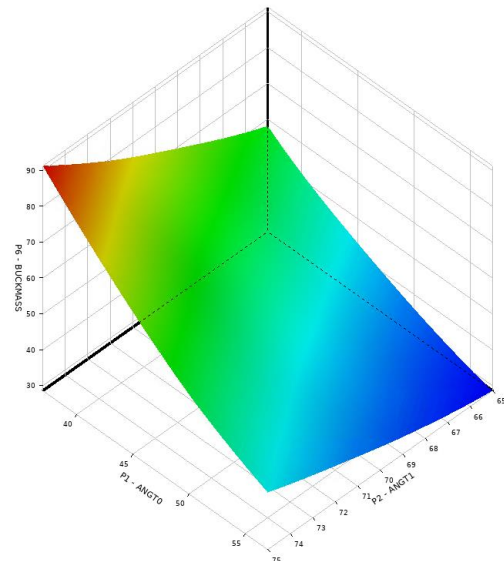
c. SC2 – Curvature

d. SC2 – Performance Constant

Figure 7.7. Response Surfaces of Optimization Cycle of Case I – LAV

a. SC1 – Curvature

b. SC1 – Performance Constant

c. SC2 – Curvature

d. SC2 – Performance Constant

Figure 7.8. Response Surfaces of Optimization Cycle of Case I – NAV

The ANOVA analysis has been conducted for the points from the response surface. As a result, the contribution of the inlet and exit angles, are found as 10% and 62.7% respectively for LAV. For NAV, the values are 6.9% and 69.5% respectively.

7.1.2   Case II

In this case, height to width ratio is taken as 1.5. Therefore, the dimensions for the plate are 300 mm x 450 mm. The procedure is the same as the Case I. Linear and nonlinear angle variation configurations are considered. There are total of 16 layers to construct the laminate. The configurations are symmetric and balanced.

After the optimization cycle, given results in Table 7.2 have been found:

Table 7.2 Optimization Results for Case II

Case	*Configuration*	N_{buck} *(kN)*	C_{perf}	m_{plate} *(g)*
Buckling Load				
LAV	$[\pm< 52.542\|74.95 >]_{8s}$	41.5	56.0	740
NAV	$[\pm< 47.51\|74.90 >]_{8s}$	44.2	61.2	722
Performance Criteria				
LAV	$[\pm< 52.597\|74.924 >]_{8s}$	41.5	56.0	740
NAV	$[\pm< 47.57\|74.952 >]_{8s}$	44.3	61.3	723

The nonlinear angle variation configuration performs better than the linear angle variation case by 6.7% for buckling load and 9.5% for performance constant. Both configurations have similar masses. First buckling modes and the thickness distribution can be seen from Figure 7.9 to Figure 7.12. Also, response surfaces for optimization cycles are given in Figure 7.13 and Figure 7.14.
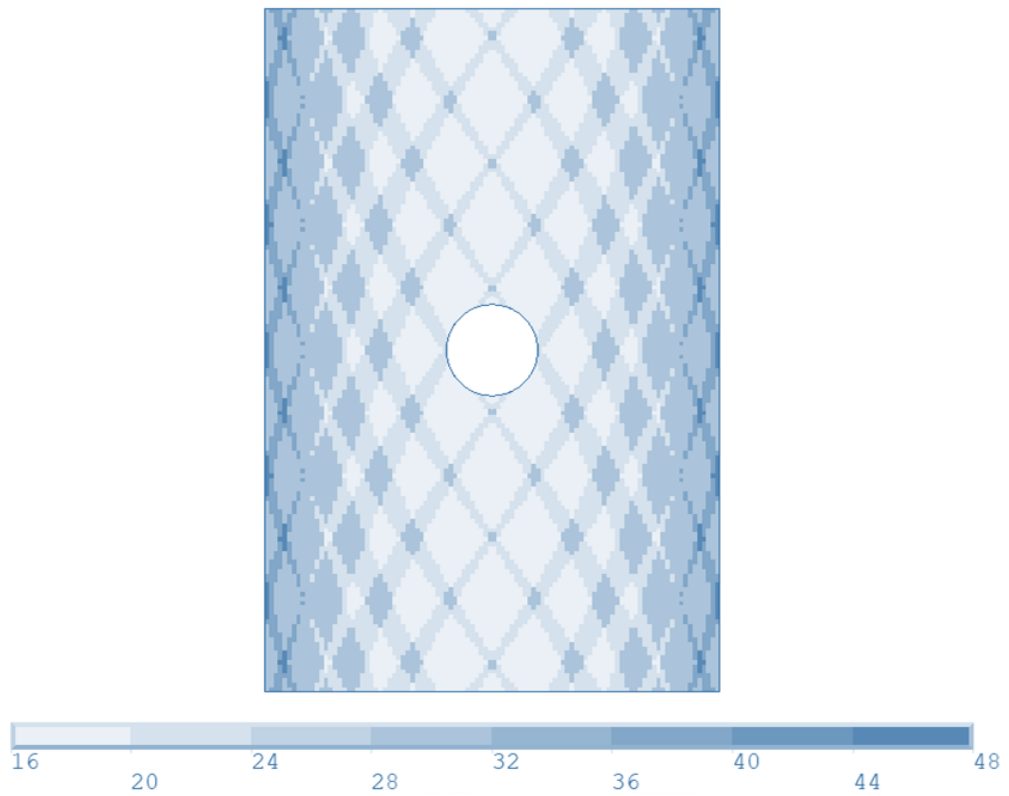
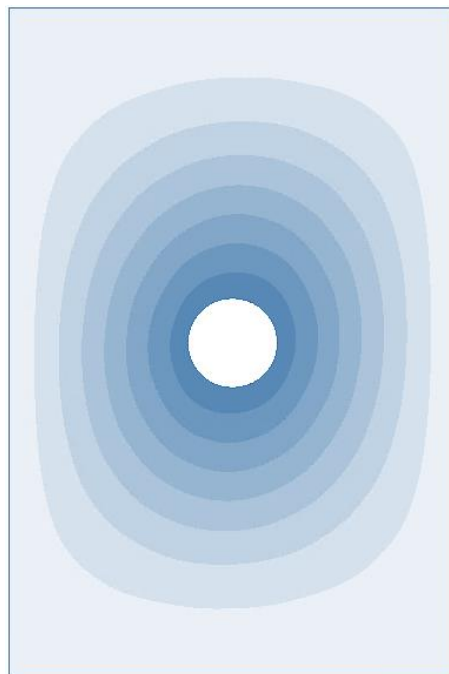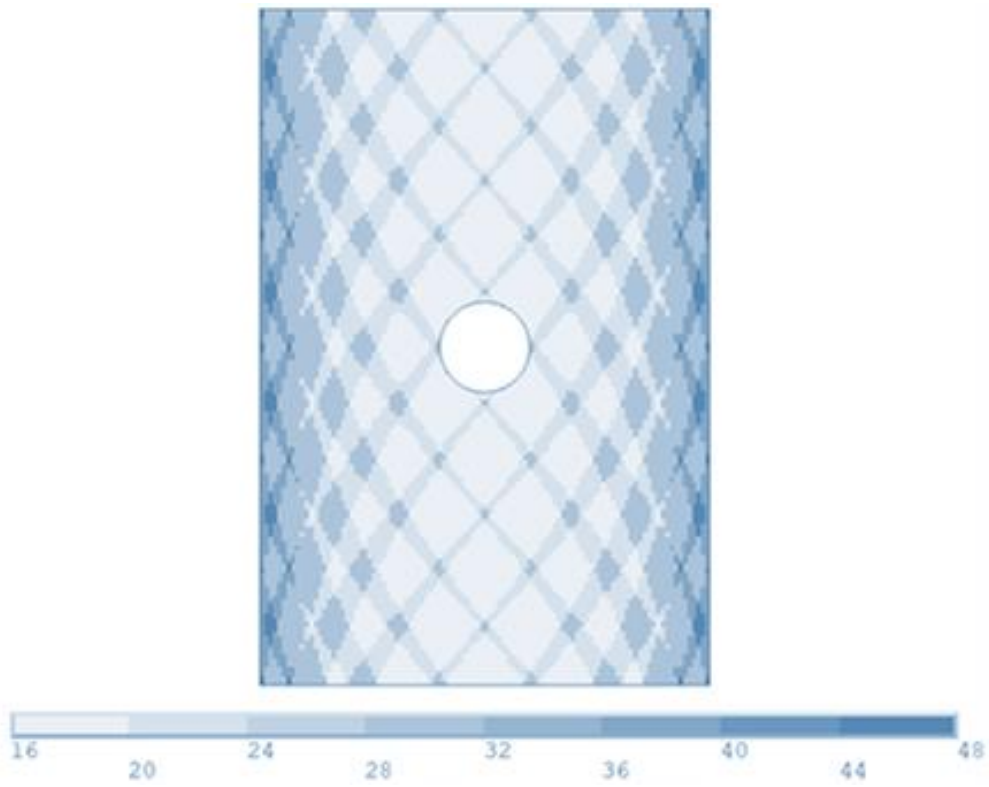Figure 7.9. Thickness Distribution of Case II – LAV

Figure 7.10. First Buckling Mode of Case II – LAV
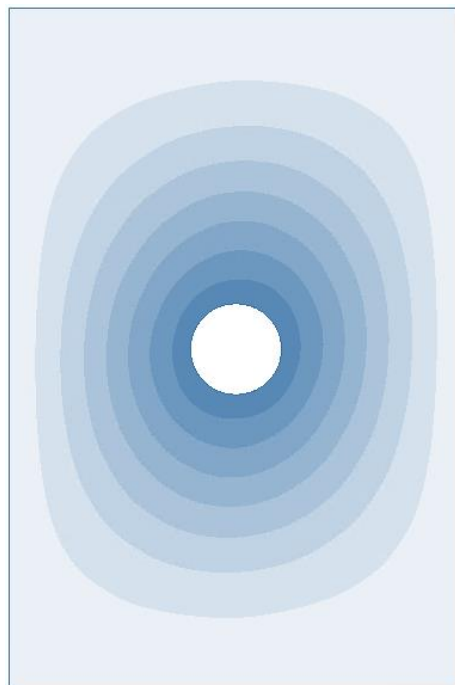
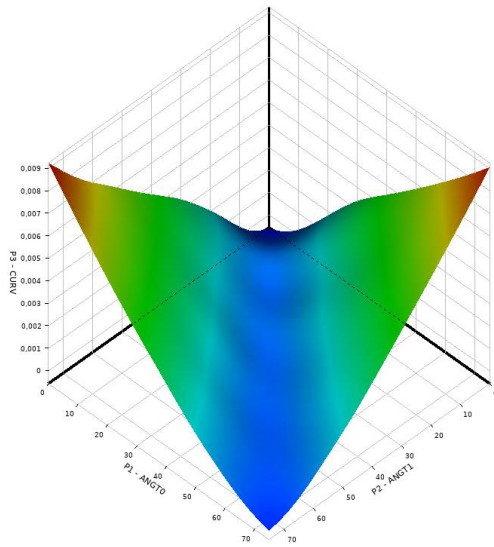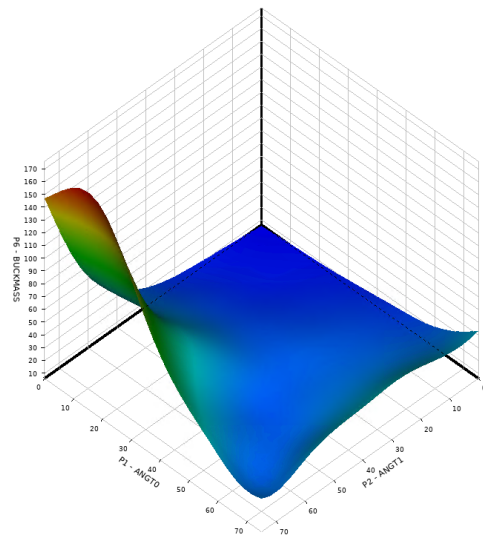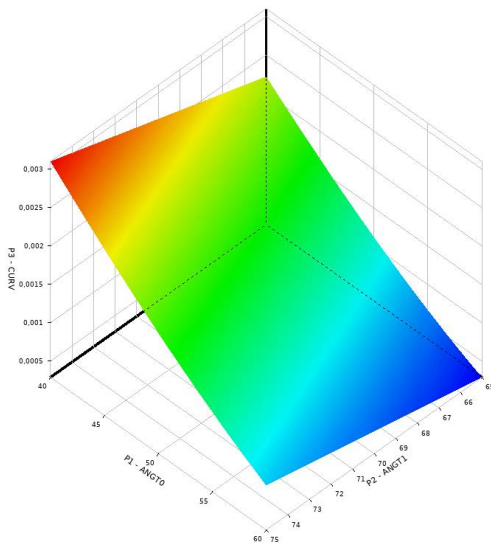Figure 7.11. Thickness Distribution of Case II – NAV

Figure 7.12. First Buckling Mode of Case II – NAV

a. SC1 – Curvature

b. SC1 – Performance Constant

c. SC2 – Curvature

d. SC2 – Performance Constant

Figure 7.13. Response Surfaces of Optimization Cycle of Case II – LAV
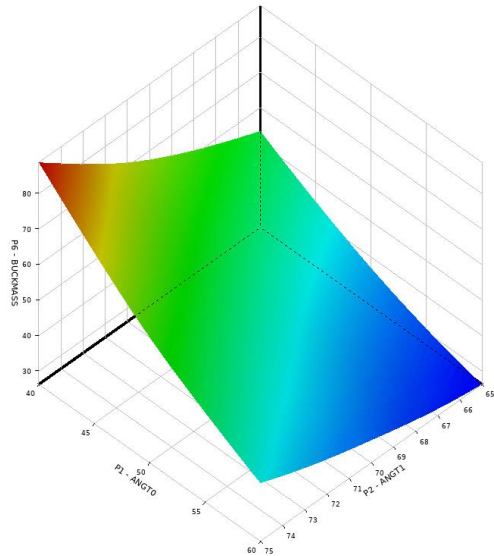
a. SC1 – Curvature

b. SC1 – Performance Constant

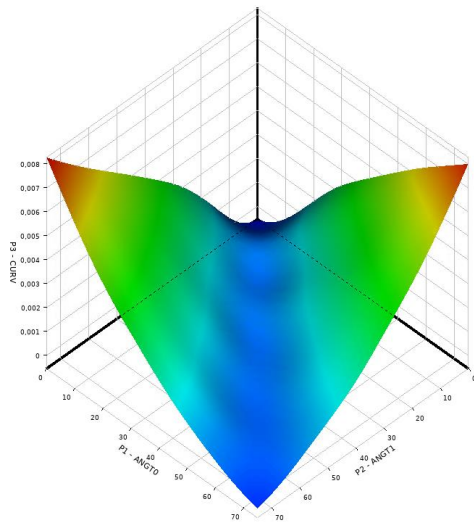c. SC2 – Curvature

d. SC2 – Performance Constant

Figure 7.14. Response Surfaces of Optimization Cycle of Case II – NAV

The ANOVA analysis of the points from the response surface has been conducted. As a result, the contribution of the inlet and exit angles, are found as 4.5% and 56% respectively for LAV. For NAV, the values are 4% and 62.3% respectively.

7.1.3   Case III

In this case, the height of the plate is increased to 600 mm. The plate geometry is 300 mm x 600mm. It is a rectangular plate. The procedure is the same as other cases. The optimization results are given in Table 7.3:

Table 7.3 Optimization Results for Case III

Case	Configuration	C_{perf}	N_{buck} (kN)	m_{plate} (g)
Buckling Load				
LAV	$[\pm< 52.471\vert74.658 >]_{8s}$	41.8	42.5	984
NAV	$[\pm< 47.592\vert74.982 >]_{8s}$	51.7	53.4	968
Performance Criteria				
LAV	$[\pm< 52.481\vert74.667 >]_{8s}$	41.9	42.5	985
NAV	$[\pm< 47.464\vert74.936 >]_{8s}$	51.9	53.6	968

As in the Case II, the nonlinear angle variation has higher performance constant than linear angle variation. As the plate's height to width ratio increases, the difference between these two configurations increases. NAV configuration performs 23.9% better than the LAV configuration in buckling load and 26% in performance constant. The thickness distribution and first buckling modes are given from Figure 7.15 to Figure 7.18. Also, response surfaces for optimization cycles are given in Figure 7.19 and Figure 7.20.

Figure 7.15. Thickness Distribution of Case III – LAV

Figure 7.16. First Buckling Mode of Case III - LAV
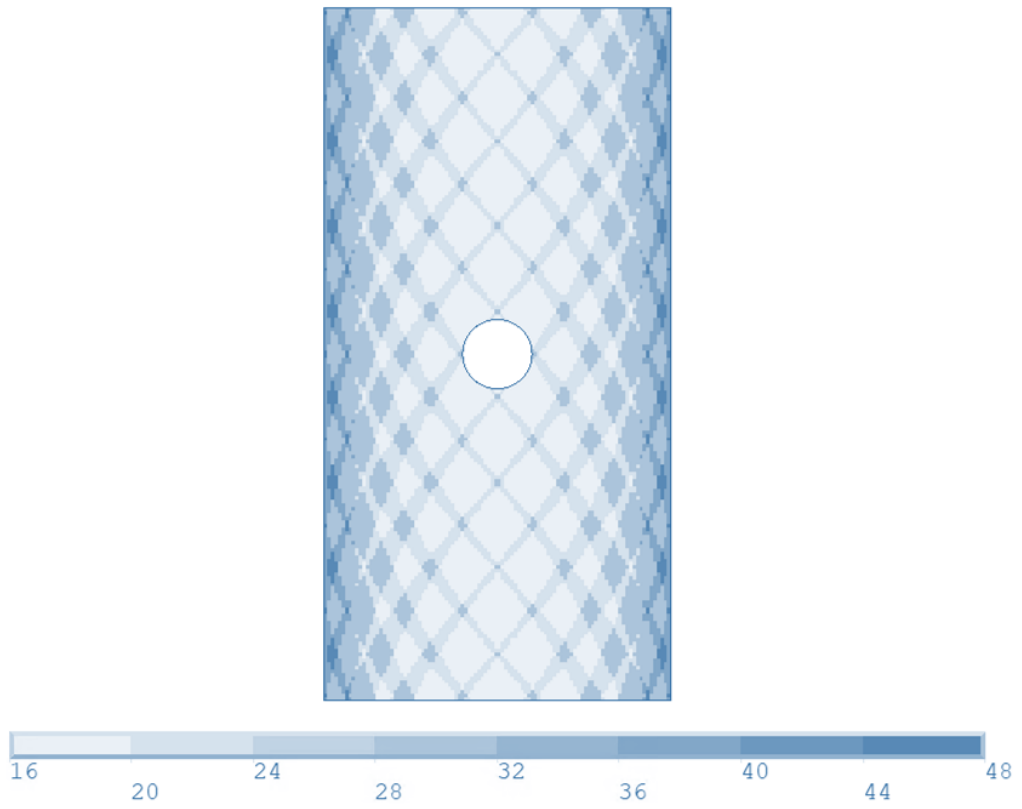
Figure 7.17. Thickness Distribution of Case III - NAV
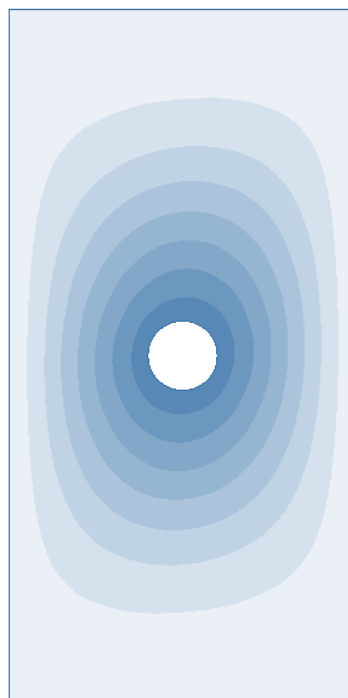
Figure 7.18. First Buckling Mode of Case III – NAV
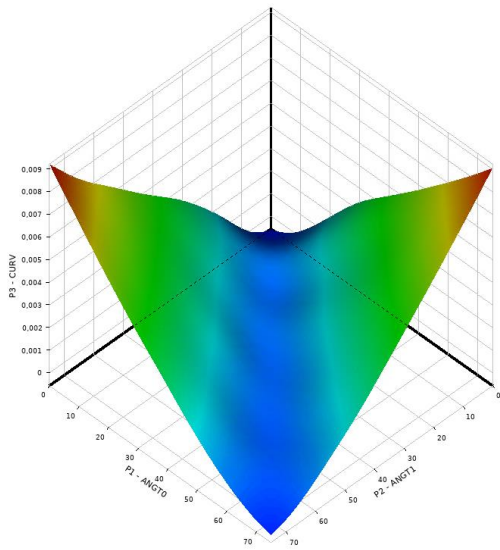
a. SC1 – Curvature
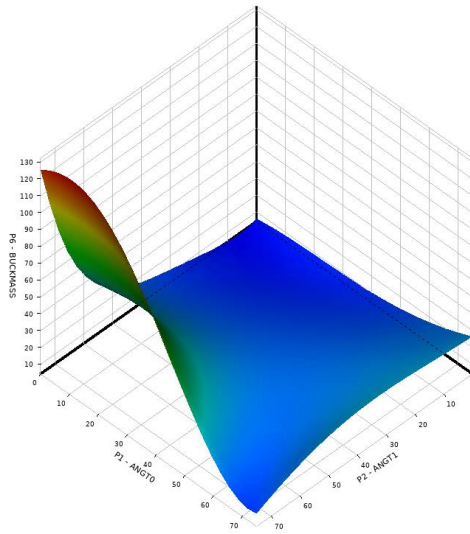
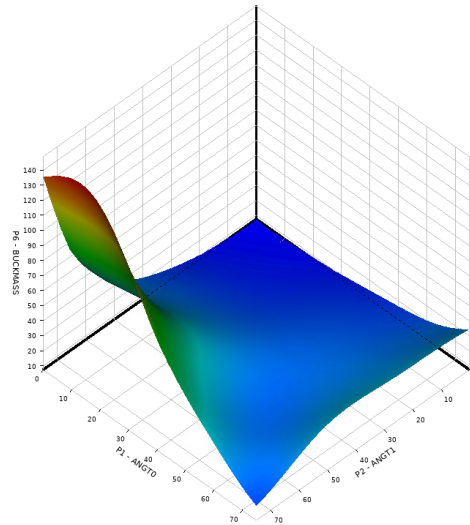b. SC1 – Performance Constant
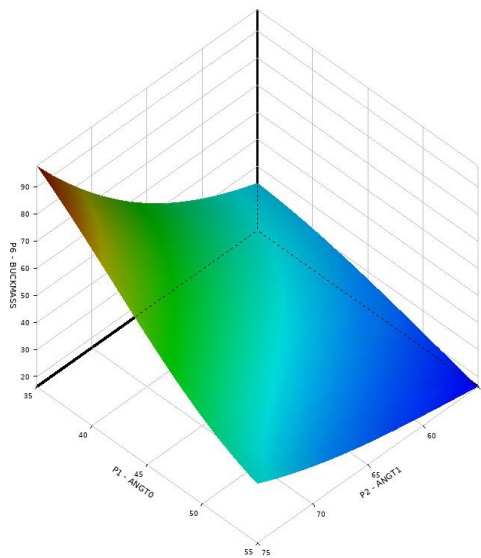
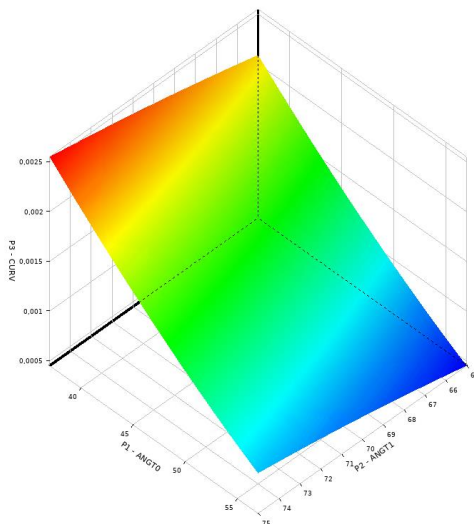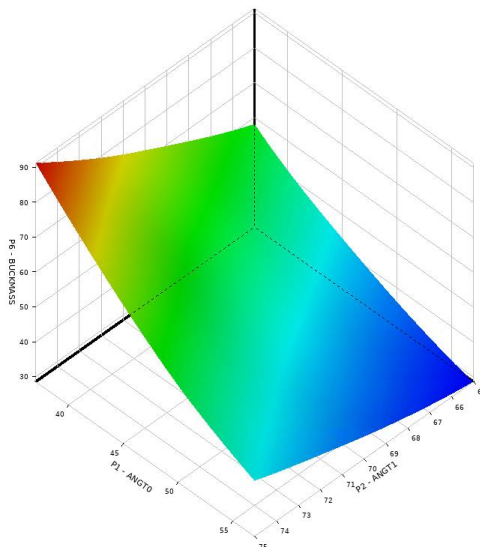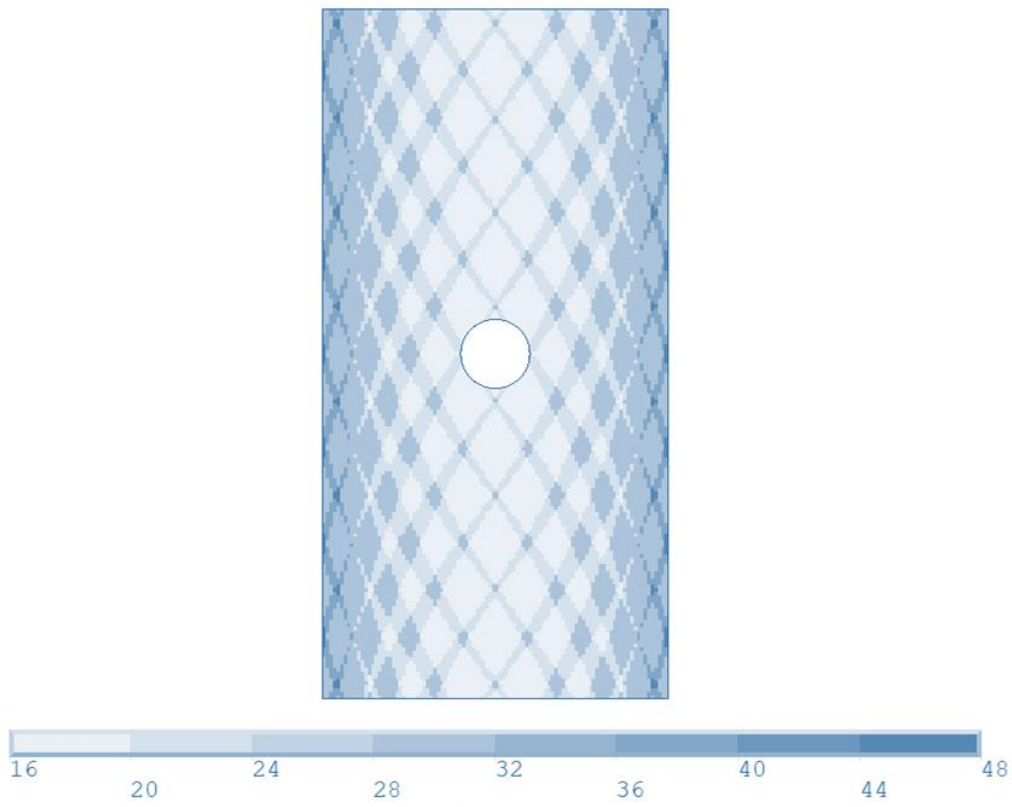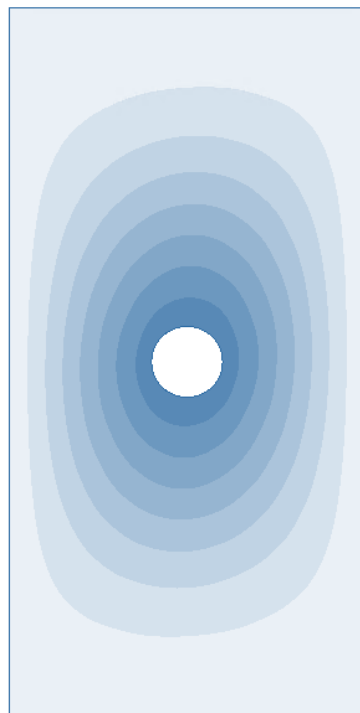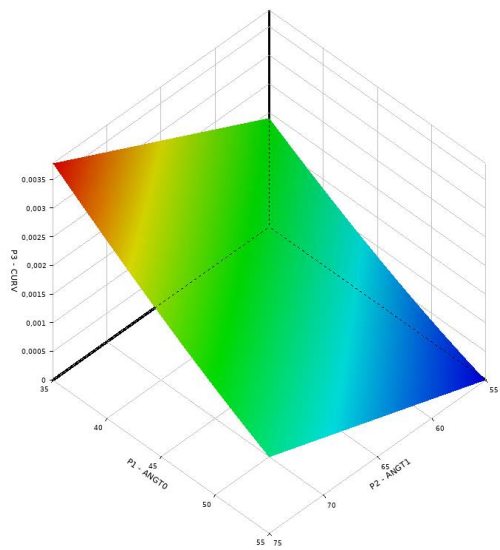

c. SC2 – Curvature

d. SC2 – Performance Constant

Figure 7.19. Response Surfaces of Optimization Cycle of Case III – LAV
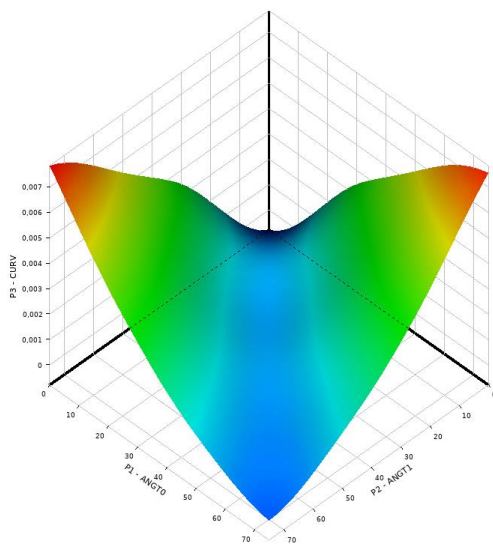
a. SC1 – Curvature
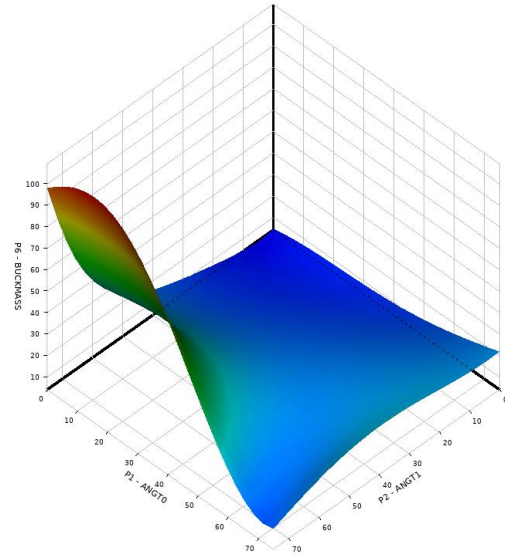
b. SC1 – Performance Constant
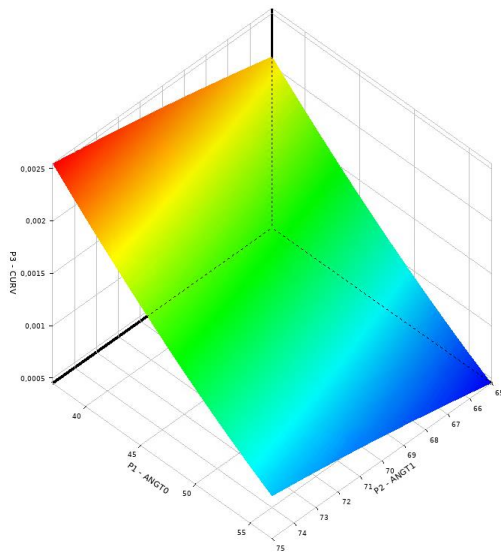
c. SC2 – Curvature
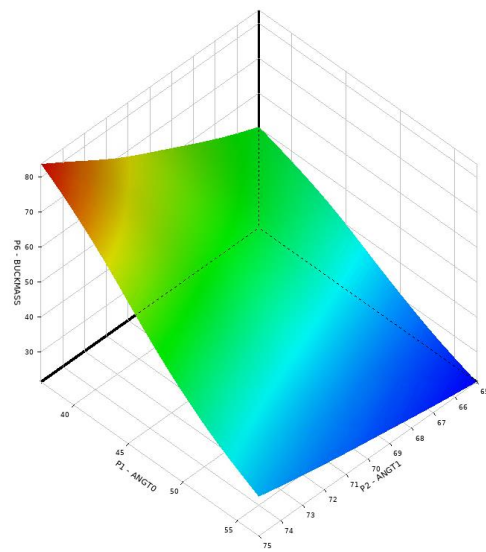
d. SC2 – Performance Constant

Figure 7.20. Response Surfaces of Optimization Cycle of Case III – NAV

The ANOVA analysis of the points from the response surface has been conducted. As a result, the contribution of the inlet and exit angles, are found as 2.6% and 60.3% respectively for LAV. For NAV, the values are 2.7% and 63.8% respectively.

7.2 Post-Buckling Results with Progressive Failure

In this section, post-buckling of previously calculated optimum variable stiffness laminates in section 7.1 are analyzed. Post-buckling analysis is run by using the same finite element model by enabling large deformation and nonlinear analysis options. Analysis method is explained in 5.2.3.2.

7.2.1 Case I

The Case I was a 300 mm x 300 mm square plate. Bucking results are presented in 7.1.1. The optimum configurations of linear angle variation and nonlinear angle variation are analyzed, and their post-buckling behaviours are investigated by considering Hashin's failure criteria.

Nonlinear static analysis has been conducted by using Newton-Raphson method. The plate has been loaded with end-displacement iteratively. In every step, stresses are calculated and checked by using Hashin's failure criteria whether the element is failed or not. When any of the elements starts to fail, it is considered as first ply failure.

Post-buckling analysis results for first case laminates are given in Table 7.4.

Table 7.4 First Ply Failure Loads of Case I

Case	First Ply Failure Load (kN)
Linear Angle Variation	184.2
Nonlinear Angle Variation	178.1

The failure load for the optimum results of buckling optimization is close to each other. Linear angle variation configuration performs 3.4% better than the nonlinear angle variation case. The progressive failure of LAV and NAV plates are given in Figure 7.21 and Figure 7.22, respectively.
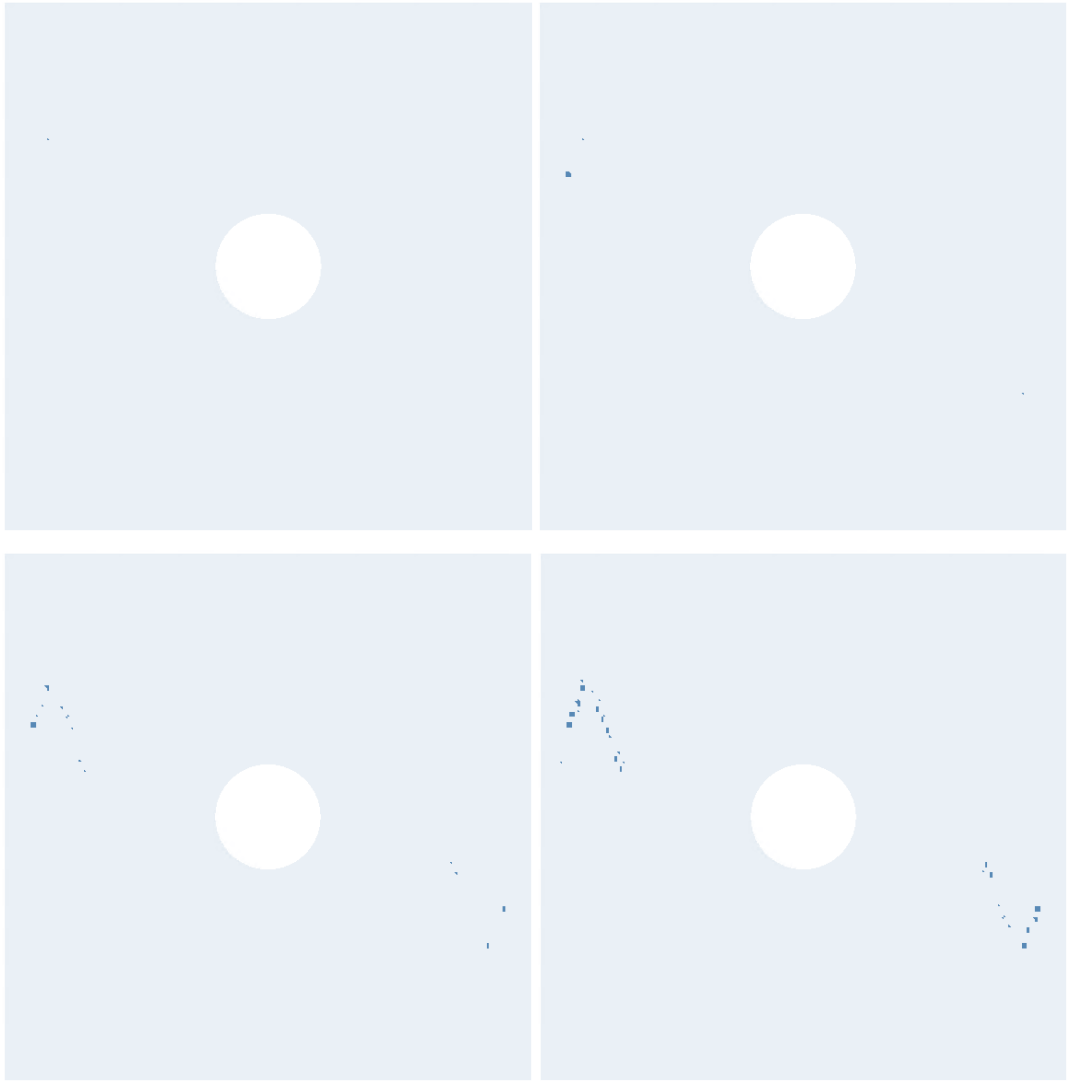
Figure 7.21. Progressive Failure of Case I – LAV

Figure 7.22. Progressive Failure of Case I – NAV

7.2.2   Case II

This section covers the post-buckling response of the Case II. The plate is a rectangular plate with a dimensions of 300 mm x 450 mm. The optimum configuration for both curve types is analyzed and their failure results are determined. These results are given in Table 7.5.

Table 7.5 First Ply Failure Loads of Case II

Case	First Ply Failure Load (kN)
Linear Angle Variation	179.7
Nonlinear Angle Variation	185.6

For this case, nonlinear angle variation configuration achieves higher first ply failure load than the linear angle variation configuration. It is 3.3% higher. It can be said that the nonlinear angle variation configuration performs better at the plate with higher aspect ratio. Failure and its progress can be seen in Figure 7.23 and Figure 7.24.
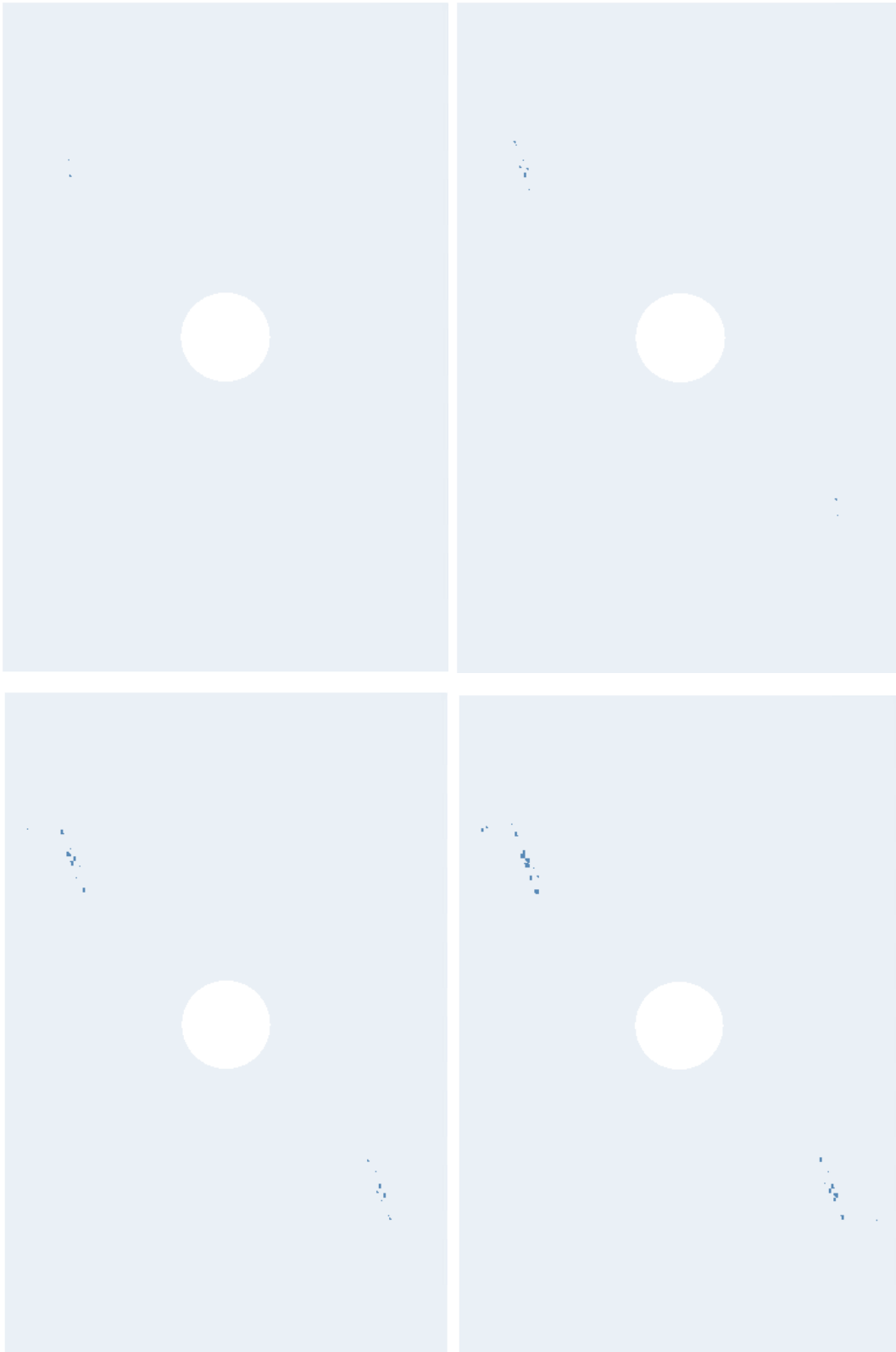
Figure 7.23. Progressive Failure of Case II – LAV
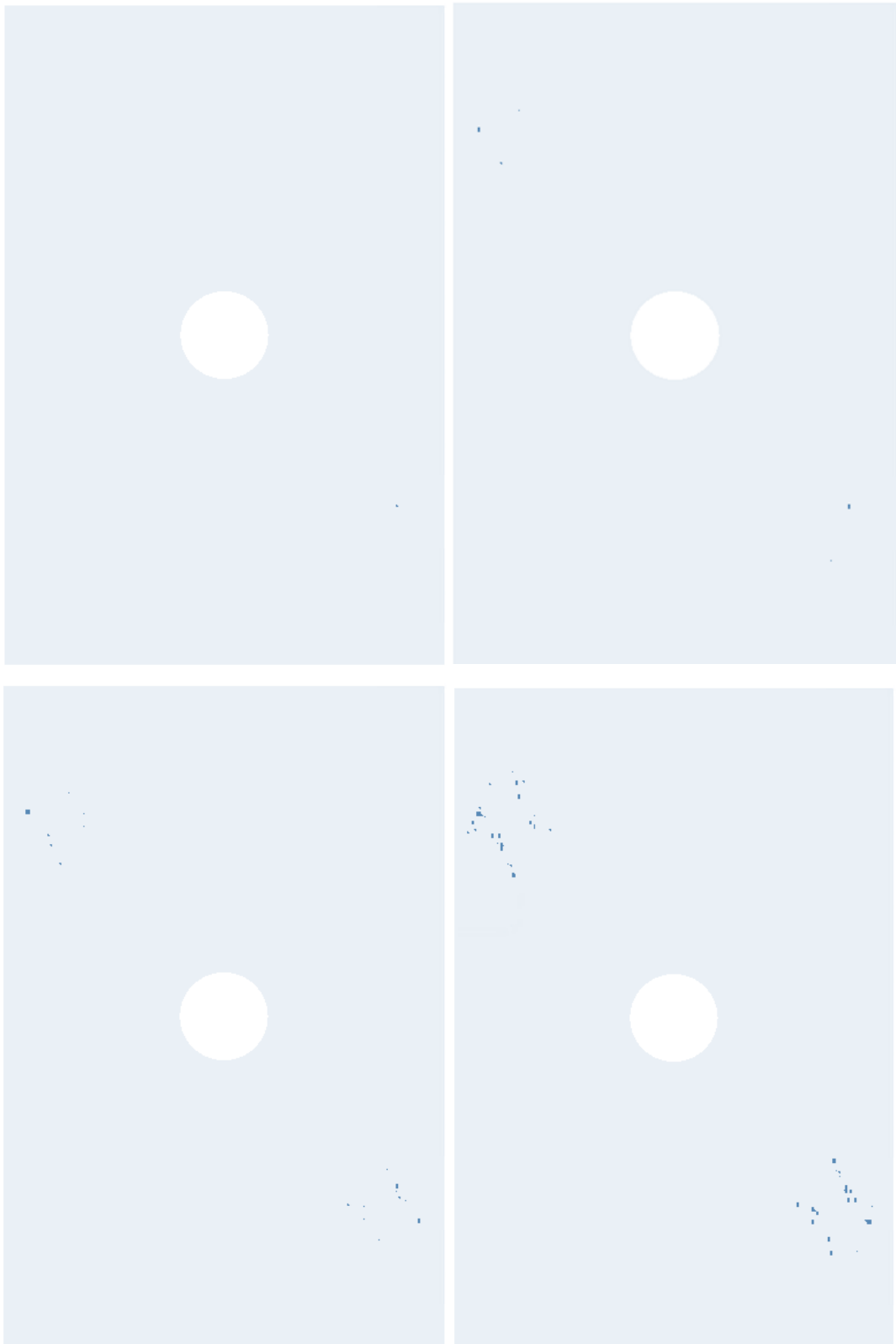
Figure 7.24. Progressive Failure of Case II – NAV

7.2.3   Case III

In this case, a rectangular plate with 300 mm x 600 mm dimensions has been optimized for buckling strength by using both linear and nonlinear angle variation fiber paths. The optimum configurations of both variations have been analyzed for post-buckling with progressive failure. The procedure is the same as in 7.2.1. The selected configurations are given in 7.1.3. The post-buckling analysis with progressive failure results are given in Table 7.6:

Table 7.6 First Ply Failure Loads of Case III

Case	First Ply Failure Load (kN)
Linear Angle Variation	145.7
Nonlinear Angle Variation	166.5

In this case, the first ply failure load of nonlinear angle variation configuration performs better compared to the linear angle variation case unlike the Case I. First ply failure for the NAV configuration is 14.3% higher. With increasing slenderness, nonlinear angle variation can improve failure due to buckling. The progressive failure of LAV and NAV plates are given in Figure 7.25 and Figure 7.26, respectively.

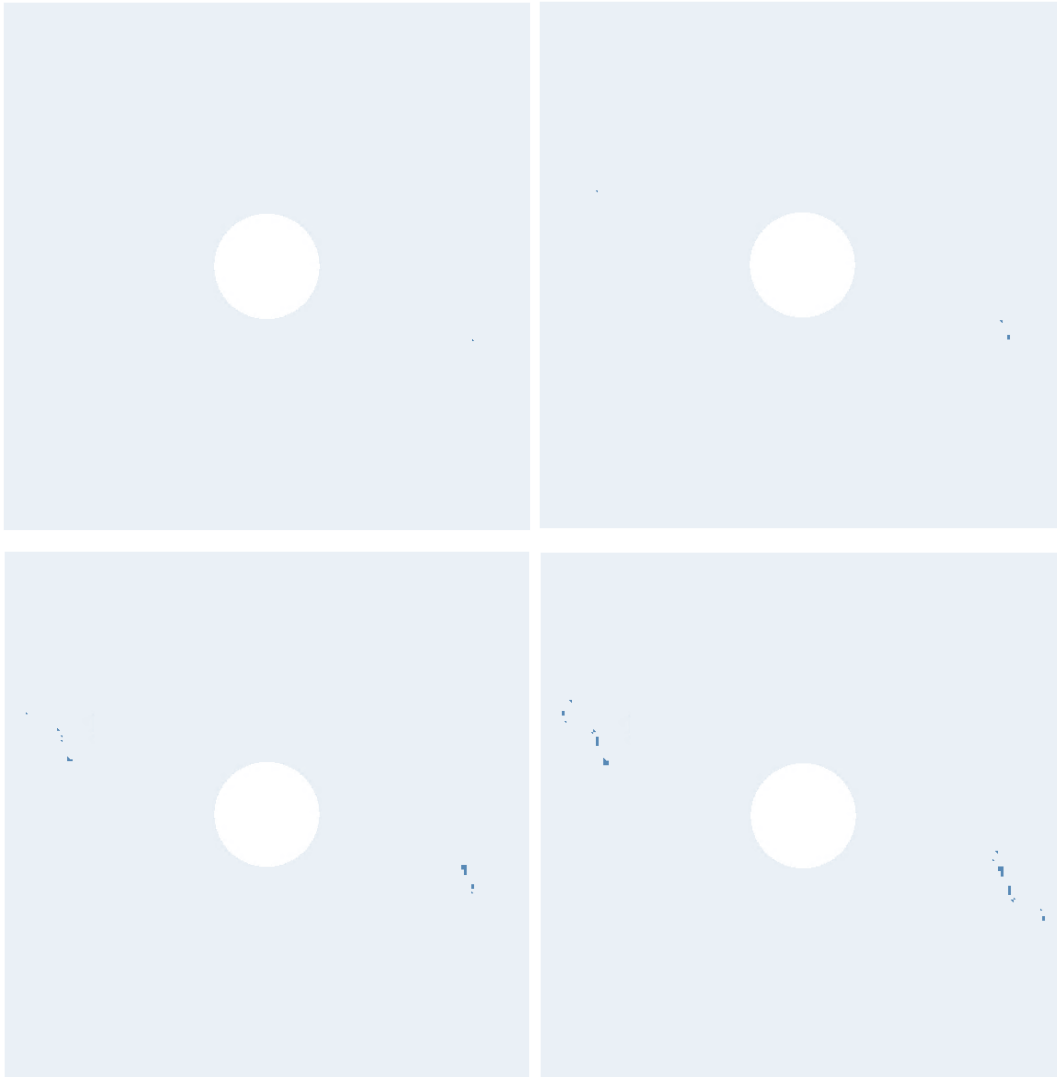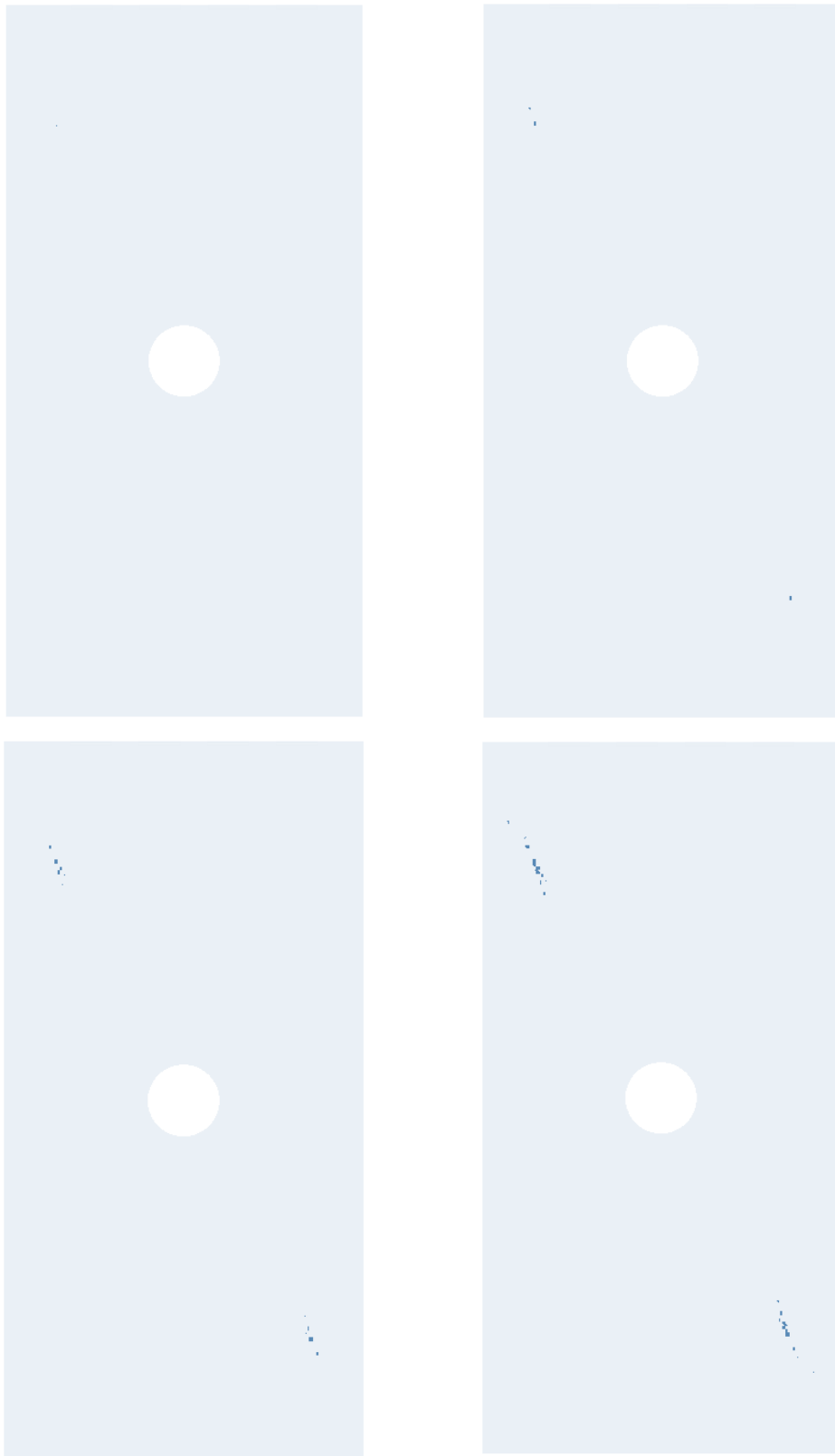Figure 7.25. Progressive Failure of Case III – LAV
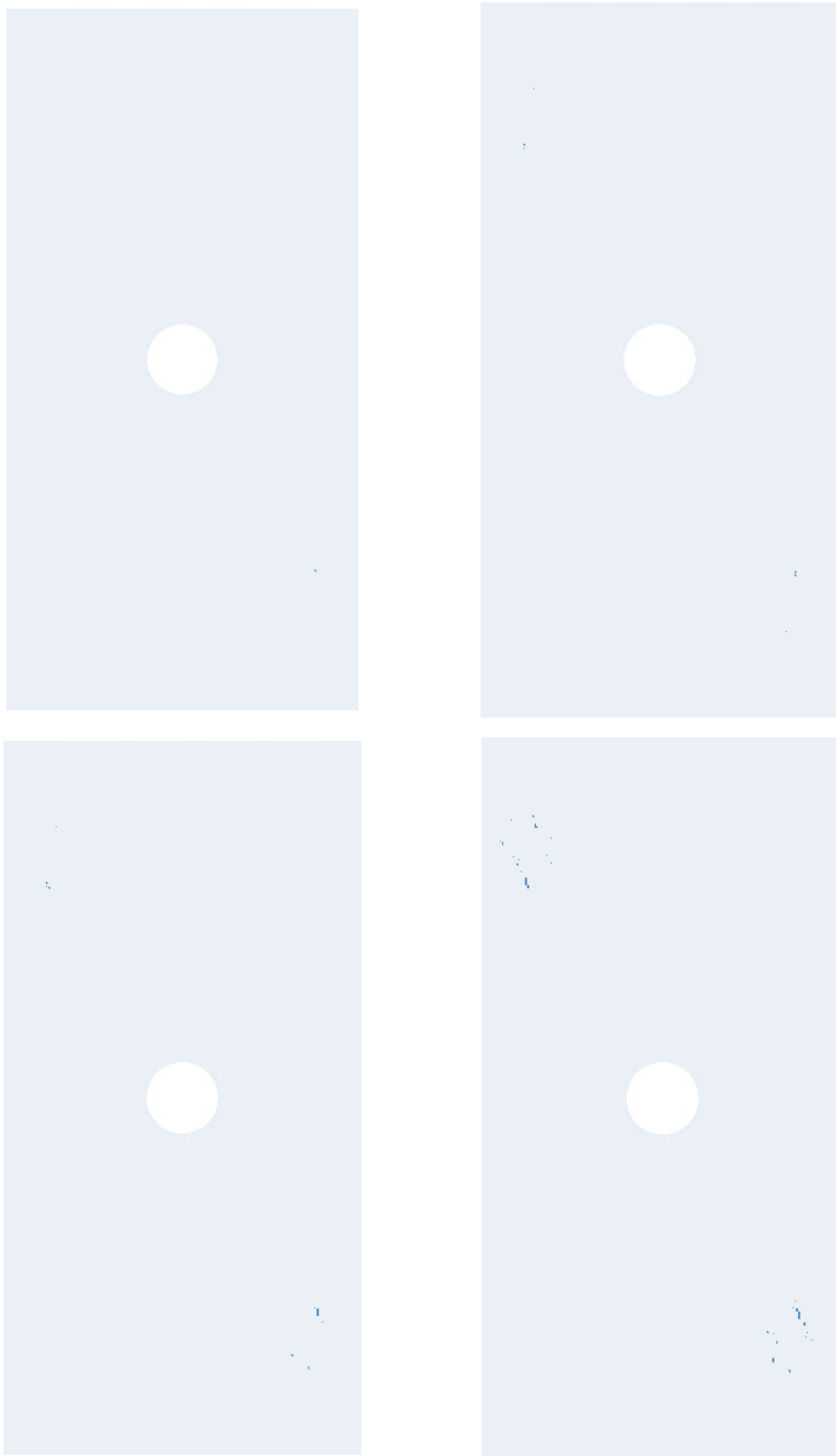
Figure 7.26. Progressive Failure of Case III – NAV

CHAPTER 8

CONCLUSION

8.1   Results

In this thesis, buckling and post-buckling of variable stiffness composite plates are investigated by carrying out progressive failure analyses. The parameters of variable stiffness are determined through an optimization procedure to obtain the highest buckling load. Test cases have been used to validate the developed method for further analyses. As a result, following conclusion have been withdrawn:

a) Test Cases:

1. First buckling load for the test cases are calculated via numerical methods and the results are compared with experiments. It is found that numerical methods are close to experimental ones.

2. Experimental results found for first ply failure loads of variable stiffness plates were compared with the results of numerical methods. The numerical results well agree with the experimental results.

3. The discrepancies of the results for the test case can be attributed to unknowns about the test and the specimen such as curing process, manufacturing defects, calibration of the test bench etc.

b) Plates with same selected inlet and exit angles:

4. Buckling results of the analyzed configurations for the same arbitrarily selected inlet and exit angles for linear and nonlinear angle variation, and quasi-isotropic case showed that, VS configurations improve the buckling load of the structure compared to quasi-isotropic plates for 3 different aspect ratios (1, 1.5, 2).

5. With increasing aspect ratio, buckling capability of quasi-isotropic plate decreases faster than VS plates. This can be explained with the better

distribution of the load over the plate in variable stiffness angle configurations. Also, overlapped regions create stiffer regions which lead to increase in buckling load.

6. Comparison between linear angle variation and nonlinear angle variation configuration showed that plates with linear angle variation achieves higher buckling critical loads. This situation may occur due to higher curvature fiber paths of the linear angle variation which leads to more overlapped regions that create stiffened regions.

7. Post-buckling with progressive failure analysis of these configurations showed that VS configuration achieves higher first ply failure loads than the quasi-isotropic plate.

8. Plate with linear angle variation achieves higher first ply failure loads than the nonlinear angle variation case. As for the buckling load, higher curvature and higher overlapped regions cause stiffer regions to build up which lead to higher strength.

c) Plates with optimized on inlet and exit angles:

9. Optimization study has been conducted to find the angle configuration for higher buckling load and higher buckling load to mass ratio objectives for linear and nonlinear angle variation. The analyses are carried out for plates with 3 different aspect ratios; 1, 1.5, 2. The results of these studies showed that the nonlinear angle variation configuration performs better for the plates with the aspect ratios 1.5 and 2 for buckling load and buckling load to mass ratio. However, for aspect ratio 1 linear angle variation configuration outperforms the nonlinear angle variation for both objectives.

10. With increasing aspect ratio, higher buckling performance is achieved by the nonlinear angle variation configuration. The nonlinear angle variation configuration is built by minimizing the curvature. Therefore, this configuration can reach fiber angles where linear angle variation cannot achieve since linear angle variation configuration can only offer a single type of curve where nonlinear angle variation enlarges the design space and

allowing better configurations to be built by benefiting the flexibility of Bezier curves.

11. Post-buckling with progressive failure analysis for both linear and nonlinear angle variation fiber paths showed similar phenomena. Plate with linear angle variation fiber path achieves higher first ply failure load than the nonlinear angle variation configuration for plate with aspect ratio 1 where nonlinear angle variation configuration outperforms the linear angle variation for aspect ratios 1.5 and 2.

8.2   Future Works

For the future works, experimental studies can be conducted to investigate behaviour of optimized plates realistically and as a result the analysis models can be improved.

REFERENCES

[1]   R. M. Jones, *Mechanics of Composite Materials*, 2nd ed. CRC Press, 1999.

[2]   R. A. Olmedo, "Compression and Buckling of Composite Panels with Curvilinear Fibers," 1992.

[3]   D. M. J. Peeters, F. X. Irisarri, C. Groenendijk, and R. Růžek, "Optimal design, manufacturing and testing of non-conventional laminates," *Compos. Struct.*, vol. 210, no. July 2018, pp. 29–40, 2019, doi: 10.1016/j.compstruct.2018.10.062.

[4]   S. B. Biggers and S. Srinivasan, "Compression Buckling Response of Tailored Rectangular Composite Plates," *AIAA J.*, vol. 31, no. 3, pp. 590–596, Mar. 1993, doi: 10.2514/3.61543.

[5]   P. J. Crothers, K. Drechsler, D. Feltin, I. Herszberg, and T. Kruckenberg, "Tailored fibre placement to minimise stress concentrations," *Compos. Part A Appl. Sci. Manuf.*, vol. 28, no. 7, pp. 619–625, Jan. 1997, doi: 10.1016/S1359-835X(97)00022-5.

[6]   M. W. Hyer and H. H. Lee, "The use of curvilinear fiber format to improve buckling resistance of composite plates with central circular holes," *Compos. Struct.*, vol. 18, no. 3, pp. 239–261, Jan. 1991, doi: 10.1016/0263-8223(91)90035-W.

[7]   B. F. Tatting, Z. Gurdal, and D. Jegley, "Design and Manufacture Tow Placed Plates of Elastically Tailored," 2002. [Online]. Available: https://ntrs.nasa.gov/citations/20020073162.

[8]   J. Huang and R. T. Haftka, "Optimization of fiber orientations near a hole for increased load-carrying capacity of composite laminates," *Struct. Multidiscip. Optim.*, vol. 30, no. 5, pp. 335–341, Nov. 2005, doi: 10.1007/s00158-005-

0519-z.

[9] Z. Wu, G. Raju, and P. M. Weaver, "Postbuckling analysis of variable angle tow composite plates," *Int. J. Solids Struct.*, vol. 50, no. 10, pp. 1770–1780, May 2013, doi: 10.1016/j.ijsolstr.2013.02.001.

[10] S. Arranz, A. Sohouli, and A. Suleman, "Buckling Optimization of Variable Stiffness Composite Panels for Curvilinear Fibers and Grid Stiffeners," *J. Compos. Sci.*, vol. 5, no. 12, p. 324, Dec. 2021, doi: 10.3390/jcs5120324.

[11] O. Coşkun and H. S. Türkmen, "Multi-objective optimization of variable stiffness laminated plates modeled using Bézier curves," *Compos. Struct.*, vol. 279, no. October 2021, p. 114814, Jan. 2022, doi: 10.1016/j.compstruct.2021.114814.

[12] Z. Wu, P. M. Weaver, G. Raju, and B. Chul Kim, "Buckling analysis and optimisation of variable angle tow composite plates," *Thin-Walled Struct.*, vol. 60, pp. 163–172, Nov. 2012, doi: 10.1016/j.tws.2012.07.008.

[13] S. Nagendra, S. Kodiyalam, J. Davis, and V. Parthasarathy, "Optimization of tow fiber paths for composite design," Apr. 1995, doi: 10.2514/6.1995-1275.

[14] L. Parnas, S. Oral, and Ü. Ceyhan, "Optimum design of composite structures with curved fiber courses," *Compos. Sci. Technol.*, vol. 63, no. 7, pp. 1071–1082, May 2003, doi: 10.1016/S0266-3538(02)00312-3.

[15] A. W. Blom, C. S. Lopes, P. J. Kromwijk, Z. Gurdal, and P. P. Camanho, "A Theoretical Model to Study the Influence of Tow-drop Areas on the Stiffness and Strength of Variable-stiffness Laminates," *J. Compos. Mater.*, vol. 43, no. 5, pp. 403–425, Mar. 2009, doi: 10.1177/0021998308097675.

[16] A. Alhajahmad, M. M. Abdalla, and Z. Gürdal, "Design Tailoring for Pressure Pillowing Using Tow-Placed Steered Fibers," *J. Aircr.*, vol. 45, no. 2, pp. 630–640, Mar. 2008, doi: 10.2514/1.32676.

[17] J. N. Reddy, *Laminated Composite Plates and Shells*. London: Springer

London, 2003.

[18] ANSYS Inc., "Element Reference," 2020.

[19] ANSYS Inc., "Theory Reference." 2020.

[20] V. Mishra, "A methodology to predict the stiffness properties and buckling load of manufacturable variable stiffness panels," Delft University of Technology, 2017.

[21] Ö. Namdar and H. Darendeliler, "Buckling, postbuckling and progressive failure analyses of composite laminated plates under compressive loading," *Compos. Part B Eng.*, vol. 120, pp. 143–151, Jul. 2017, doi: 10.1016/j.compositesb.2017.03.066.

[22] C. Kassapoglou, *Design and Analysis of Composite Structures with Applications to Aerospace Structures*. 2013.

[23] G. H. Staab, *Laminar Composites*. Elsevier, 1999.

[24] C. S. Lopes, "Damage and Failure of Non-Conventional Composite Laminates," 2009.

[25] Z. Gurdal and R. Olmedo, "In-plane response of laminates with spatially varying fiber orientations - Variable stiffness concept," *AIAA J.*, vol. 31, no. 4, pp. 751–758, Apr. 1993, doi: 10.2514/3.11613.

[26] D. H. J. A. Lukaszewicz, C. Ward, and K. D. Potter, "The engineering aspects of automated prepreg layup: History, present and future," *Compos. Part B Eng.*, vol. 43, no. 3, pp. 997–1009, 2012, doi: 10.1016/j.compositesb.2011.12.003.

[27] R. Postier, "Factory automation for composite structures manufacturing," *Sampe Q.*, vol. 16, no. 3, pp. 45–49, 1985.

[28] P. V. E. William B. Goldsworthy, "Geodesic path length compensator for composite-tape placement head," 1974.

[29] A. Brasington, C. Sacco, J. Halbritter, R. Wehbe, and R. Harik, "Automated fiber placement: A review of history, current technologies, and future paths forward," *Compos. Part C Open Access*, vol. 6, no. August, p. 100182, Oct. 2021, doi: 10.1016/j.jcomc.2021.100182.

[30] D. O. Evans, "Fiber Placement," in *Composites*, ASM International, 2001, pp. 477–479.

[31] M. N. Grimshaw, C. G. Grant, and J. M. L. Diaz, "Advanced technology tape laying for affordable manufacturing of large composite structures," *Int. SAMPE Symp. Exhib.*, vol. 46 II, no. 4, pp. 2484–2494, 2001.

[32] F. Bullock, S. Kowalski, and R. Young, "Automated prepreg tow placement for composite structures," in *Advanced Materials: The Challenge for the Next Decade*, 1990, pp. 734–754.

[33] C. S. Lopes, Z. Gürdal, and P. P. Camanho, "Variable-stiffness composite panels: Buckling and first-ply failure improvements over straight-fibre laminates," *Comput. Struct.*, vol. 86, no. 9, pp. 897–907, May 2008, doi: 10.1016/j.compstruc.2007.04.016.

[34] "Automatic Fiberplacement Machine." https://mtorres.es/en/equipment/manufacturing-systems/lamination/automatic-machine-of-fiberplacement-torresfiberlayup (accessed Aug. 18, 2022).

[35] D. Peeters, "Design Optimisation of Practical Variable Stiffness and Thickness Laminates," Delft University of Technology, 2017.

[36] D. Jegley, B. Tatting, and Z. Gurdal, "Optimization of Elastically Tailored Tow-Placed Plates with Holes," in *44th AIAA/ASME/ASCE/AHS/ASC Structures, Structural Dynamics, and Materials Conference*, Apr. 2003, no. April, doi: 10.2514/6.2003-1420.

[37] A. W. Blom, P. B. Stickler, and Z. Gürdal, "Design and Manufacture of a

Variable-Stiffness Cylindrical Shell," in *Proceedings of the SAMPE Europe 30th International Conference*, 2009, pp. 1–8.

[38]   C. S. Lopes, P. P. Camanho, Z. Gürdal, and B. F. Tatting, "Progressive failure analysis of tow-placed, variable-stiffness composite panels," *Int. J. Solids Struct.*, vol. 44, no. 25–26, pp. 8493–8516, Dec. 2007, doi: 10.1016/j.ijsolstr.2007.06.029.

[39]   A. W. Blom, "Structural Performance of Fiber-Placed, Variable-Stiffness Composite Conical and Cylindrical Shells," Delft University of Technology, 2010.

[40]   J. R. Reeder, "Nasa Technical Memorandum an Evaluation of Mixed-Mode Delamination," VA, United States, 1992.

[41]   P. P. Camanho, P. Maimí, and C. G. Dávila, "Prediction of size effects in notched laminates using continuum damage mechanics," *Compos. Sci. Technol.*, vol. 67, no. 13, pp. 2715–2727, Oct. 2007, doi: 10.1016/j.compscitech.2007.02.005.